

**FRACTURED WELL TEST DESIGN AND ANALYSIS IN THE PRESENCE
OF NON-DARCY FLOW**

by

Jamir A. Gil

ProQuest Number: 10794593

All rights reserved

INFORMATION TO ALL USERS

The quality of this reproduction is dependent upon the quality of the copy submitted.

In the unlikely event that the author did not send a complete manuscript and there are missing pages, these will be noted. Also, if material had to be removed, a note will indicate the deletion.



ProQuest 10794593

Published by ProQuest LLC (2018). Copyright of the Dissertation is held by the Author.

All rights reserved.

This work is protected against unauthorized copying under Title 17, United States Code
Microform Edition © ProQuest LLC.

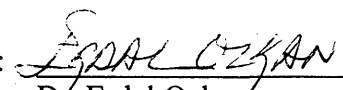
ProQuest LLC.
789 East Eisenhower Parkway
P.O. Box 1346
Ann Arbor, MI 48106 – 1346

A thesis submitted to the Faculty and Board of Trustees of the Colorado School of Mines in partial fulfillment of the requirements for the degree of Master of Science (Petroleum Engineering).

Golden, Colorado

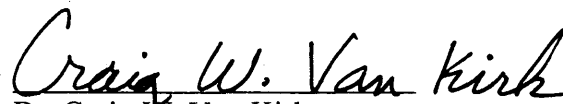
Date 08/31/01

Signed: 
James A. Gil

Approved: 
Dr. Erdal Ozkan
Thesis Advisor

Golden, Colorado

Date August 31, 2001


Dr. Craig W. Van Kirk
Professor and Head,
Department of Petroleum
Engineering

ABSTRACT

Non-Darcy flow in fractures complicates the pressure transient analysis of fractured well tests and leads to erroneous estimates of fracture properties such as conductivity and fracture half-length. Although several studies have been presented in the literature to discuss this phenomenon, none of them has provided an easy and practical tool for the design and analysis of fractured well tests under the influence of fracture non-Darcy flow. They have shown, however, that should the effects of non-Darcy flow be ignored, lower estimates of fracture conductivity and fracture half-length would be obtained from the well test interpretation.

The overall objective of this thesis is to improve the design and analysis of fractured well tests in the presence of non-Darcy flow in the fracture. Because non-Darcy flow in the reservoir is outside the scope of this thesis, Darcy flow is assumed in the reservoir under all conditions and non-Darcy flow is limited to the fracture. A semi-analytical model is used to generate the theoretical transient pressure responses under fracture non-Darcy flow effects. From the analysis of the data generated, a practical correlation is developed to enhance the design of the fractured well tests. The correlation provides the conditions under which non-Darcy flow in the fracture does not have a significant influence on the transient pressure responses and thus the interpretation of the data is relatively simplified.

This study also provides a new analysis technique for fractured well tests in the presence of fracture non-Darcy flow. This technique is applicable in the existence of bilinear and linear flow regimes and is shown to work even when the wellbore storage effects mask the bilinear flow. The new technique is advantageous over the conventional analysis

techniques because it requires only one test to estimate the fracture properties and the non-Darcy flow coefficient. The new technique also overcomes the non-uniqueness problem encountered in the application of the regression techniques when fracture non-Darcy flow is effective.

TABLE OF CONTENTS

	Pages
ABSTRACT	iii
LIST OF FIGURES	viii
LIST OF TABLES	xi
ACKNOWLEDGEMENTS	xii
Chapter 1. INTRODUCTION	
1.1 Objective	1
1.2 Organization	2
1.3 Literature Review	3
Chapter 2. RATE DEPENDENT SKIN AND THE EFFECT OF NON-DARCY FLOW	
2.1 Objectives	6
2.2 Non-Darcy Flow in the Reservoir	7
2.3 Non-Darcy Flow in Fractures	8
2.4 System Definitions and Dimensionless Variables	9
2.5 Semi-Analytical Model	11
2.6 Ranges of Reservoir, Fluid, and Fracture Properties Investigated in this study	12
2.7 Non-Darcy Flow on Transient Pressure Responses	14
2.8 Fracture Non-Darcy Flow Skin	15
2.9 Methodology	17

2.9.1 General Procedure	18
2.9.2 Effect of Non-Darcy Flow Coefficient, β	20
2.9.3 Effect of Fracture Width, w_f	21
2.9.4 Effect of Reservoir Permeability, k	21
2.9.5 Effect of Fracture Permeability, k_f	25
2.9.6 Effect of the Other Properties	25
2.9.7 Effect of Initial Reservoir Pressure, p_I	33
 Chapter 3. NON-DARCY FLOW AND PRODUCTIVITY	
3.1 Objectives	67
3.2 Productivity Index in gas Wells.....	67
3.3 Discussion of Productivity Ratio, PR	70
 Chapter 4. ANALYSIS OF FRACTURED WELL TEST DATA IN THE PRESENCE OF NON-DARCY FLOW	
4.1 Objectives	80
4.2 Theoretical Basis.....	80
4.2.1 Bilinear Flow Regime	81
4.2.1.1 Combination of Guppy <i>et al.</i> and Cinco-L <i>et al.</i> Theories ...	81
4.2.1.2 Combination of Gidley, Guppy <i>et al.</i> , and Cinco-L. <i>et al.</i> Theories	83
4.2.2 Reservoir Linear Flow Regime	85
4.3 Summary of the New Analysis Technique	86

4.4 Application Examples.....	87
Chapter 5. CONCLUSIONS.....	98
REFERENCES	100
LIST OF SYMBOLS	102

LIST OF FIGURES

		Pages
Figure 2-1	Reservoir, fracture and well system.....	36
2-2	Non-Darcy flow effect on transient pressure responses	37
2-3	Non-Darcy flow skin.....	38
2-4	Non-Darcy flow skin vs. conductivity	39
2-5	Non-Darcy flow skin vs. fracture half-length	40
2-6	Non-Darcy flow skin vs. fracture half-length for different β values	41
2-7	Flow rate vs. fracture half-length for different β values	42
2-8	Incorporating β to the correlation: q vs. $x_f \beta$	43
2-9	q vs. $x_f \beta$ for different initial reservoir pressures.....	44
2-10	q vs. $x_f \beta$ for different β coefficients and fracture widths	45
2-11	q vs. $x_f \beta$ for different fracture widths.....	46
2-12	Non-Darcy flow correlation correlation: q/w_f vs. $x_f \beta /w_f$	47
2-13	Non-Darcy flow skin vs. fracture half-length for $k = 1$ md	48
2-14	Non-Darcy flow skin for $k = 10$ md.....	49
2-15	Non-Darcy flow skin vs. fracture half-length for $k = 10$ md	50
2-16	Non-Darcy flow skin vs. fracture half-length for $k = 20$ md	51
2-17	Non-Darcy flow skin vs. fracture half-length for $k = 30$ md	52

Figure 2-18	q/w_f vs. $x_f \beta /w_f$ for different k values.....	53
2-19	Non-Darcy flow correlation: $(q k^{1/2})/w_f$ vs. $(x_f \beta k^{1/2})/w_f$	54
2-20	$(q k^{1/2})/w_f$ vs. $(x_f \beta k^{1/2})/w_f$ for $k_f = 360000$ md	55
2-21	$(q k^{1/2})/w_f$ vs. $(x_f \beta k^{1/2})/w_f$ for all k_f values.....	56
2-22	Non-Darcy flow correlation after considering the effect of k_f . $(q k^{1/2})/w_f$ vs. $(x_f \beta k^{1/2})/w_f$	57
2-23	S_{ND} vs. x_f plot for the test cases	58
2-24	Test points plotted on partial correlation	59
2-25	Incorporating h to the correlation	60
2-26	Incorporating γ_g to the correlation.....	61
2-27	Testing the correlation for different values of γ_g	62
2-28	S_{ND} vs. x_f for different p_i values	63
2-29	Effect of p_i on the correlation	64
2-30	Correlating initial reservoir pressure	65
2-31	Final correlation.....	66
3-1	Effective wellbore radius as a function of dimensionless conductivity.....	73
3-2	Effect of reservoir permeability on the productivity ratio	74
3-3	Effect of flow rate on the productivity ratio	75
3-4	Effect of non-Darcy flow coefficient on the productivity ratio	76
3-5	Effect of fracture width on the productivity ratio	77

Figure 3-6	Effect of initial reservoir pressure on the productivity ratio.....	78
3-7	Effect of fracture permeability on the productivity ratio	79
4-1	Non-Darcy response and type curve	91
4-2	Bilinear and linear flow corrections.....	92
4-3	Demonstration of the uniqueness of the results	93
4-4	Data for Example 2 without wellbore storage effects.....	94
4-5	Data for Example 2 with wellbore storage effects.....	95
4-6	Match of the corrected responses with the type curve under wellbore storage effects	96
4-7	Match with the derivative type curve under wellbore storage effects.....	97

LIST OF TABLES

	Pages
Table 2-1	Ranges of Reservoir, Fluid, and Fracture Properties 13
2-2	Data Used to Generate Fig 2-3..... 17
2-3	Base Case Data 18
2-4	Data Used to Generate Fig 2-14..... 23
2-5	Data Used for Test Point 1 26
2-6	Data Used for Test Point 2..... 27
2-7	Data Used for Test Point 3..... 28
2-8	Data Used for Test Point 4..... 29
2-9	Data Used for Test Point 5..... 30
2-10	Data Used for Test Point 6..... 32
2-11	Data Used for Test Point 7..... 33
2-12	Influence of p_i on S_{ND} 34

ACKNOWLEDGEMENTS

I would like to express my sincere gratitude to my advisor, Dr. Erdal Ozkan, for his invaluable support during my stay at Colorado School of Mines (CSM). His advice and dedication, especially during the course of this research, were unequalled. He teaches excellence that motivates the hard work.

I must also thank the Petroleum Engineering Department at CSM, for the financial support provided during this last year and for the opportunity to work for the school.

This work is dedicated to my family: Leonardo for your patience and encouragement, David Arturo because you are my inspiration and light of my life, my parents for your guidance and motivation, my brother and sisters because we are always close in spirit. Thank you God for this opportunity!

Jamir A. Gil

CHAPTER 1

INTRODUCTION

1.1 Objective

The general objective of this work is to improve the design and analysis of fractured well tests in the presence of non-Darcy flow within the fracture. Even in the absence of non-Darcy flow, the analysis of transient pressure responses of finite-conductivity fractures is a challenging problem. Non-Darcy flow further complicates the analysis and usually leads to erroneous or non-unique interpretations of the transient pressure data.

Many formation, fracture, and fluid parameters are responsible for the deviation from Darcy's Law and this complicates the understanding and control of the non-Darcy flow effects. Several numerical, analytical, or semi-analytical models have been proposed in the literature¹⁻⁵ to understand and predict the effects of non-Darcy flow but because of the complexity of these models, they have not attracted much attention. Therefore, one of the objectives of this study is to develop a simple and practical correlation that can be used to design fractured well tests with negligible influence of non-Darcy flow in the fracture. The semi-analytical model discussed in Refs. 4 – 6 provides the data that are the basis of the correlation. For simplicity, it is assumed that the flow in the reservoir always obeys Darcy's Law and non-Darcy flow only takes place in the fracture. This assumption is in line with the prediction of Ref. 2 that non-Darcy flow in the reservoir should be negligible compared to that in the fracture.

In some cases, the effect of non-Darcy flow in the fracture may not be completely eliminated by simple design considerations or the data may have already been affected by fracture non-Darcy flow because of poor test design. In these cases, the well-test analyst is challenged by two fundamental problems. The first one of these problems is the

requirement of two tests at different flow rates as proposed by Guppy *et al.*⁴ and Guppy *et al.*⁵ to determine the non-Darcy flow effects and to obtain accurate estimates of fracture conductivity and half-length. Running two tests at different rates, however, is usually not a practical proposition. When the data are only available from a single test, then the analyst faces the non-uniqueness problem in the conventional analysis of the data (regression or type-curve matching with the theoretical responses). This is because of the fact that infinitely many combinations of the fracture conductivity and non-Darcy flow coefficient may generate the same pressure transient response.⁶ Each combination of these parameters corresponds to a different fracture half-length and unless one of the three parameters, non-Darcy flow coefficient, fracture conductivity, and fracture half-length, is known by independent means, the conventional analysis does not yield accurate estimates. Therefore, the second objective of this thesis is to develop a new analysis technique that should overcome the non-uniqueness problem without requiring multiple tests.

1.2 Organization

This thesis is divided into five chapters. The introduction of the thesis is presented in Chapter 1. This chapter presents the objectives and the organization of the thesis. A section on literature review is also included in Chapter 1.

Chapter 2 presents the definition of non-Darcy flow and its effect on transient pressure responses. Here, the pseudo skin concept is used for the development of a correlation that can be used to minimize the non-Darcy flow effects during a well test.

Chapter 3 briefly discusses the productivity reduction resulting from non-Darcy flow effects in fractures by using the productivity ratio concept. Because the focus of this

thesis is the analysis of the transient pressure responses, the discussion on productivity reduction is brief and introductory.

Chapter 4 is devoted to the analysis of fractured-well-tests in the presence of non-Darcy flow in the fracture. A new analysis technique is presented that has two advantages over the conventional analyses: i) uniqueness of the solutions and ii) the need for only one well test to complete the analysis. The validity of the new technique is demonstrated by two example applications.

Chapter 5 presents a general discussion of the results. The most important conclusions drawn from the research presented are also highlighted in this chapter.

1.3 Literature Review

It is a common practice to hydraulically fracture low permeability gas reservoirs to increase production. The hydraulic fracture, however, complicates the transient flow behavior of the well. If non-Darcy flow also prevails in the fracture, the transient flow behavior becomes even more complex.

Many authors have conducted research to determine the effects of hydraulic fractures on well performance and transient pressure behavior. In 1968 Millheim and Cichowicz¹ presented one of the first transient pressure solutions for vertically fractured gas wells. They assumed ideal gas flow and included the effects of formation damage and non-Darcy flow in the reservoir. One year later, Wattenbarger and Ramey² extended the previous work to real gases using the pseudo-pressure function concept. As in Ref. 1, they considered non-Darcy flow only in the reservoir. They demonstrated that for short fractures, the non-Darcy flow affects the linear and pseudo-radial flow regimes and from the linear flow period, a low estimate of fracture half-length results. Wattenbarger and

Ramey also discussed that the non-Darcy flow effects within the fracture could have more significant influence on the transient flow behavior than non-Darcy flow in the reservoir.

Holditch and Morse³ used a numerical model to study non-Darcy flow effects both in the fracture and reservoir. They concluded that non-Darcy flow in the fracture causes lower estimates of fracture length, reduces the apparent fracture conductivity near the wellbore, and affects the shape of the pressure buildup responses.

In 1982 Guppy *et al.*⁴ developed a semi-analytical model to analyze post-fracturing drawdown data. This work showed the changes in the flux distribution along the fracture in the presence of non-Darcy flow and demonstrated the resulting reduction in the apparent fracture conductivity. They found that the apparent conductivity is a function of the non-Darcy dimensionless flow rate, q_{DND} , and the true conductivity, C_{fD} . They developed a method to compute the true conductivity based on the identification of the bilinear flow period and using two well tests at different flow rates. These authors further extended the method to analyze buildup responses⁵.

In 2000, Umnuyponwiwat *et al.*⁶ used the semi-analytical model explained in Refs. 4 and 5 to study the effects of fracture non-Darcy flow on drawdown and buildup responses. They showed that non-Darcy flow effects increase the pressure drop in the fracture, change the flux distribution, and affect the fracture performance. They explained that ignoring the non-Darcy flow in the fracture would result in significantly lower estimates of fracture length and conductivity. These authors further concluded that non-Darcy flow responses could be matched with the Darcy flow responses for infinitely many combinations of q_{DND} and C_{fD} .

Settari *et al.*⁷ analyzed the non-Darcy flow effects on fractured wells in high permeability gas reservoirs. They demonstrated that by fracturing the well, the reservoir non-Darcy flow effects could be removed. Correlations were provided to compute the required fracture half-lengths to remove non-Darcy flow effects in the reservoir and to remove the mechanical skin. Unfortunately, these correlations are not general to be used for all practical applications.

In this study, the semi-analytical model discussed in Refs. 4-6 was used to study the fractured-well-test design and analysis in the presence of fracture non-Darcy flow. Following the lines of Wattenbarger and Ramey², the non-Darcy flow effects in the reservoir are assumed negligible compared to those in the fracture. A more general correlation than that presented in Ref. 7 is developed to provide guidelines for the design of fractured well tests if fracture non-Darcy flow is of concern. A new analysis technique was also developed for fractured-well-tests that requires only one test and provides accurate and unique estimates of fracture half-length and fracture conductivity.

CHAPTER 2

RATE DEPENDENT SKIN AND THE EFFECT OF NON-DARCY FLOW

2.1 Objectives

This chapter discusses the non-Darcy flow skin (or rate dependent skin) concept and presents a non-Darcy flow correlation that can be used to limit the fracture non-Darcy flow skin to 0.1. This correlation is useful to design fractured well tests that are not significantly influenced by fracture non-Darcy flow. The envelope of the formation, fluid, and fracture properties to assure a non-Darcy flow skin less than or equal to 0.1 is defined as a “safe region” for fractured well tests. When the well test is designed and run in the safe region, the additional pressure drop that may be due to non-Darcy flow should be within 10% of the drawdown for the corresponding Darcy flow pressure drop. This ensures that fracture non-Darcy flow does not significantly interfere with the interpretation of the pressure transient data.

The chapter starts with discussing non-Darcy flow in reservoirs and fractures. As explained in section 1.3, because the effects of non-Darcy flow in the reservoir is usually negligible compared to those in the fracture, only the effect of non-Darcy flow in the fracture is considered in this study. The assumptions about the reservoir-fracture-well system follows. The definitions of the dimensionless variables used are provided. After introducing the base case used in the investigations, the effect of non-Darcy flow on transient pressure responses is discussed. The non-Darcy flow skin concept is explained. This is followed by the methodology used to develop the non-Darcy flow correlation for the “safe region”. Finally, this chapter concludes by highlighting the benefits of the non-Darcy flow correlation.

2.2 Non-Darcy Flow in Reservoirs

In 1856, Henry Darcy, a French engineer, conducted a series of experiments measuring the flow of water through unconsolidated sand filters. He proposed an equation, known as Darcy's law, which described the flow of water through porous media. In a more general form applicable to all fluids, this equation states that the velocity of the fluid is proportional to the pressure gradient in the medium. Neglecting the gravitational effects, Darcy's Law is mathematically expressed as

$$\overline{\nabla p} = \overline{v} \frac{\mu}{k}, \quad \text{Eq. 2-1}$$

where

- $\overline{\nabla p}$ = pressure gradient, atm/cm,
- \overline{v} = superficial fluid velocity vector, cm/s,
- μ = viscosity, cp,
- k = formation permeability, darcy.

Darcy's experiments were conducted at relatively low velocities. However, it is known that the high pressure gradients around the wellbore may cause higher velocities than those considered by the Darcy's law. This may cause the fluid flow to deviate from Darcy's law especially in gas reservoirs where the flow velocities are usually higher.

In 1901, Forchheimer established the following relationship to account for the additional pressure drop because of non-Darcy flow effects

$$\overline{\nabla p} = \overline{v} \frac{\mu}{k} + \beta \rho |\overline{v}|^2, \quad \text{Eq. 2-2}$$

where

- β = non-Darcy flow coefficient, atm-s²/g,
- ρ = density, gr/cm³.

Forchheimer's equation states that the total pressure gradient corresponds to the sum of the pressure gradients due to viscous forces (the first term in the right hand side of Eq. 2-2) and the inertial forces (the second term in the right hand side of Eq. 2-2). At low velocities, the pressure gradient is controlled by the viscous drag of the fluid molecules on the grain⁸ and Darcy's law is valid. As mentioned by Geertsma⁹, the non-Darcy inertial forces are mainly created by the acceleration and deceleration of the fluid particles moving through the porous medium.

It is evident that for the same velocity and properties, the pressure drop for the non-Darcy flow case will be higher than that for the Darcy flow case. If non-Darcy flow is present and it is desired to keep the same pressure drop as in the Darcy flow case, a productivity reduction would occur.

2.3 Non-Darcy Flow in Fractures

It is a common practice to create hydraulic fractures to improve the productivity of wells producing from low-permeability-gas reservoirs. The fracture provides a higher conductivity medium around the wellbore that eases the flow into the well.

The presence of a (generally vertical) fracture complicates the mathematical and physical description of flow towards the wellbore. Several authors^{4-6,10} agree that the transient pressure responses of finite-conductivity fractures with non-Darcy flow is governed by the following two dimensionless parameters

$$C_{fD} = \frac{k_f w_f}{k x_f}, \quad \text{Eq. 2-3}$$

where C_{fD} = dimensionless conductivity,

k_f = fracture permeability, md,

w_f = fracture width, ft,

x_f = fracture half-length, ft,

and

$$q_{DND} = \frac{4.64 \times 10^{-16} k_f \beta M q}{w_f h \mu_i}, \quad \text{Eq. 2-4}$$

where

- q_{DND} = non-Darcy dimensionless flow rate,
- β = non-Darcy flow coefficient, ft^{-1} ,
- M = gas molecular weight, lbm/lbmole,
- q = constant surface flow rate, MSCF/D,
- h = formation thickness, ft,
- μ_i = initial gas viscosity, cp.

The β term defines the non-Darcy flow characteristics of a given medium and is determined by laboratory measurements.

As mentioned in Chapter 1, following the discussion of Wattenbarger and Ramey,² it is assumed in this study that flow always obeys Darcy's law in the reservoir and only non-Darcy flow in the fracture is considered. Therefore, the objective of this chapter is to provide tools to minimize the fracture non-Darcy flow effects in the analysis of pressure transient responses.

2.4 System Definitions and Dimensionless Variables

For the purpose of this study, the following considerations were made: A real gas is flowing through a laterally infinite, isotropic, and homogeneous reservoir of permeability, k , and uniform thickness, h . A vertical well has been hydraulically fractured and the fracture fully penetrates the pay zone. The vertical, finite-conductivity fracture has a half-length of x_f , permeability of k_f , and width of w_f . Fig. 2-1 shows a sketch of the

system. Production is at a constant rate at the sandface (this chapter does not examine wellbore storage effects).

Because real gas flow is considered in this study, the results are presented in terms of pseudo-pressure, $m(p)$, defined by

$$m(p) = 2 \int_0^p \frac{p'}{Z(p')\mu(p')} dp' , \quad \text{Eq. 2-5}$$

where p = pressure, psi,
 Z = gas compressibility factor.

The dimensionless form of the previous equation is

$$m_D(t_D) = \frac{kh}{1422 q T} [m(p_i) - m(p_{wf})] , \quad \text{Eq. 2-6}$$

where p_i = initial pressure, psi,
 p_{wf} = flowing bottomhole pressure, psi,
 T = reservoir temperature, °R.
 q = gas flow rate, MSCF/D.

In Eq. 2-6 the dimensionless time, t_D , is defined in field units by

$$t_D = \frac{2.637 \times 10^{-4} k}{\phi(\mu c)_i x_f^2} t , \quad \text{Eq. 2-7}$$

where $(\mu c)_i$ = viscosity-compressibility product at initial conditions.

The dimensionless flux is defined as

$$q_D(x_D) = \frac{2 x_f q_f(x)}{q} , \quad \text{Eq. 2-8}$$

where q_f = flux at the fracture surface at a distance x from the well,
MSCF/D/ft.

The dimensionless length represents the point within the fracture where the solution is obtained and is defined by

$$x_D = \frac{x}{x_f} . \quad \text{Eq. 2-9}$$

2.5 The Semi-Analytical Model

The data used in this study was generated by using a semi-analytical model discussed in Refs. 4 - 6. Because the objective of this work is to study the effects of non-Darcy flow in fractures, the development of the model is not discussed here. The basic equations of the model, however, are briefly introduced below.

The equation used to describe the flow in the fracture is

$$m_D(0, t_D) - m_D(x_D, t_D) = \frac{2\pi}{C_{fD}} \left[\int_0^{x_D} q_{cD} dx_D + q_{DND} \int_0^{x_D} q_{cD}^2 dx_D \right] , \quad \text{Eq. 2-10}$$

where $m_D(0, t_D)$ = dimensionless pseudo-pressure at the wellbore ($x_D = 0$)
at time t_D ,

$m_D(x_D, t_D)$ = pseudo-pressure at some distance x_D from the well at time t_D ,

q_{cD} = dimensionless flow rate at some point x_D in the fracture,

and

$$q_{cD}(x_D) = \int_{x_D}^{x_f} q_{fD}(t) dt . \quad \text{Eq. 2-11}$$

The dimensionless time, t_D , is defined by Eq. 2-7 and the dimensionless length, x_D , is given by Eq. 2-9.

The dimensionless pseudo-pressure $m_D(x_D, t_D)$ in Eq. 2-10 is given by

$$m_D(x_D, t_D) = \frac{1}{4} \int_0^{t_D} \int_0^1 \frac{q_{jD}(t, \tau)}{(t_D - \tau)} \left\{ \exp\left[-\frac{(x_D - t)^2}{4(t_D - \tau)}\right] + \exp\left[-\frac{(x_D + t)^2}{4(t_D - \tau)}\right] \right\} dt d\tau .$$

Eq. 2-12

Although this summary of the model is presented for drawdown solutions, the model can also be used for buildup. Note that the computation of Eq. 2-10 requires discretization of time and fracture length. Also, due to the non-linearity condition of the expression, an iterative scheme is used to obtain the solution. The numerical evaluation of the solution given in Eq. 2-10 is discussed in Ref. 4 and will not be explained here because it is out of the scope of this thesis.

2.6 Ranges of Reservoir, Fluid, and Fracture Properties Investigated in this Study

Several parameters were investigated to obtain a correlation for the region that is safe from non-Darcy flow effects in the fracture. Table 2-1 presents the ranges of the iteration parameters for the reservoir, fluid, and fracture properties. They were selected to cover the most practical ranges for gas reservoirs and fractured wells.

TABLE 2-1. Ranges of Reservoir, Fluid, and Fracture Properties

Parameter	1	2	3	4	5	Units
Formation Porosity, ϕ	0.1	0.2	---	---	---	fraction
Formation Thickness, h	60	100	120	---	---	ft.
Initial Gas Viscosity, μ_i	0.015	0.018	---	---	---	cp.
Gas Density, ρ	8.23	9.96	11.83	13.84	---	lbm/ft ³
Total Compressibility, c_t	1.E-05	2.E-04	---	---	---	psi ⁻¹
Specific Gravity of Gas, γ_g	0.6	0.7	0.8	0.9	---	---
Gas Molecular Weight, M	17.382	20.279	23.176	26.073	---	lbm/lbmole
Reservoir Pressure, p_i	1000	2000	3000	5000	6000	psia
Formation Permeability, k	0.1	1	10	20	30	md
Fracture Permeability, k_f	10000	50000	360000	720000	---	md
Fracture Width, w_f	0.15	0.25	0.45	---	---	in.
Gas Flow Rate, q	1000	5000	7000	10000	20000	MSCF/D
Non-Darcy Flow Coefficient, β	0	0.98x10 ⁹	1.29x10 ⁹	1.79x10 ⁹	---	ft ⁻¹
Fracture Half Length, x_f	50	100	200	300	---	ft.

The values presented in Table 2-1 were mostly taken from the works by Vincent *et al.*⁸, Guppy *et al.*⁴, and Settari *et al.*⁷ Some comments on the values shown in Table 2-1 should be useful:

Settari *et al.*⁷ considered three values for the initial reservoir pressure: 1000, 3000 and 5000 psia. In this work, pressures up to 6000 psia were investigated.

The maximum reservoir permeability value considered in this work was 30 md. Settari *et al.*⁷ examined the effects of non-Darcy flow for moderate to high reservoir permeability

(from 5 to 500 md.) with short fracture half-lengths, x_f , (up to 64 ft.) In this study, the values of x_f were up to 300 ft.

Fracture permeability and width, being the critical fracture properties governing non-Darcy flow, are of great interest in this study. Their range is very wide, covering almost all possibilities in the design of fractures. Note that these parameters appear in both, the dimensionless conductivity (Eq. 2-3) and dimensionless non-Darcy flow rate (Eq. 2-4) equations. As the fracture permeability approaches the reservoir permeability value, the conductivity decreases and the system acts like no fracture is present (ineffective fracture). Also, an increase in the fracture width should decrease the fluid velocity, causing less deviation from Darcy's law.

The influence of the flow rate is also studied in detail. Working from low to high values, this crucial parameter is also correlated to cover most practical possibilities.

Four values for the non-Darcy flow coefficient, β , are considered, including the Darcy flow case ($\beta = 0$). This parameter is usually presented in atm-s²/g, however, to be consistent, the β coefficient is used in ft⁻¹ in this work (the following conversion factor can be used: 1 atm-s²/g is equivalent to 30.8917959×10^6 ft⁻¹). The β -factors are taken from Vincent *et al.*⁸ which correspond to the common values for propping agents. It must be noted that some correlations exist in the literature to compute the β -factors as a function of system properties. For the purposes of this study, we only used a range of β -factors independent of the system properties.

2.7 Non-Darcy Flow on Transient Pressure Responses

The transient pressure response of a fractured well may be affected by the presence of non-Darcy flow in the fracture. It has been discussed in the literature¹⁻⁶ that if the non-

Darcy flow effects are neglected, the fracture conductivity and half-length may be grossly under-estimated from the analysis of pressure responses. These errors are also reflected on the estimation of formation properties by well tests. This will be discussed in detail in Chapter 4. This section intends to document and correlate the effect of non-Darcy flow on transient pressure behavior.

As explained above, non-Darcy flow increases the pressure drop in the fracture. Fig. 2-2 shows the log-log plot of dimensionless pseudo-pressure versus dimensionless time for a fracture half-length of 200 ft and a value of non-Darcy flow coefficient of $\beta = 0.98 \times 10^5$ ft⁻¹. The pressure responses shown in Fig. 2-2 were obtained for three different flow rates: 1000, 5000, and 10000 MSCF/D with the corresponding dimensionless non-Darcy flow rates $q_{DND} = 12.62, 63.12, \text{ and } 126.24$, respectively. The formation and fracture properties are the same for all three cases. The dimensionless fracture conductivity is $C_{fD} = 375$, which is considered as infinite conductivity.

The Darcy-flow case ($\beta = 0$) is also shown in Fig. 2-2 for comparison (as discussed in Chapter 4, this is usually used as type curve for transient pressure analysis). The dimensionless pseudo-pressure for the Darcy-flow case is not a function of the flow rate. For the non-Darcy flow cases, however, it is apparent that the higher the q_{DND} , the higher the pressure drop and therefore the more the influence of non-Darcy flow effects.

2.8 Fracture Non-Darcy Flow Skin

The difference between the dimensionless pseudo-pressures of a fracture with non-Darcy and Darcy flow ($\beta = 0$) in the fracture is called the fracture non-Darcy flow pseudo-skin. This is expressed as

$$\Delta m(p)_D = m(p)_{D,ND} - m(p)_{D,D} . \quad \text{Eq. 2-13}$$

Because the non-Darcy pseudo-skin depends on the value of q_{DND} , it is also known as the rate dependant skin. If everything else is constant, non-Darcy pseudo-skin varies with flow rate. For a fixed value of flow rate, however, it will change with time until stabilized flow is reached (pseudo-radial flow). After stabilized flow begins, the pseudo-skin becomes constant. Fig. 2-3 illustrates this behavior. Note that at the onset of the pseudo-radial flow ($t_D \approx 20$) the curves for Darcy and non-Darcy flow become parallel. This means that the non-Darcy pseudo-skin is no longer rate dependant and, therefore, it becomes a constant value. This is referred to as fracture non-Darcy flow skin and denoted hereafter as S_{ND} .

In Fig. 2-4, fracture non-Darcy flow skin, S_{ND} , has been plotted against $C_{\mathcal{D}}$. It is apparent that the higher the dimensionless conductivity, the lower the non-Darcy flow skin (and therefore, the lower the productivity reduction caused by non-Darcy flow effects). Because S_{ND} can be used to measure the reduction on productivity of the well, this parameter was adopted as the main tool to correlate the fracture performance.

In order to explain the procedure used to determine the fracture non-Darcy flow pseudo-skin, Table 2-2 shows the Darcy and non-Darcy flow data used to generate the curves in Fig. 2-3. The non-Darcy pseudo-skin was calculated as shown in Eq. 2-13. At the onset of the pseudo-radial flow it can be seen that S_{ND} is constant and approximately equal to 0.168.

In this study, it was arbitrarily chosen that a difference of 10% between the non-Darcy and Darcy flow dimensionless pressure responses might be taken as the limit of tolerable non-Darcy flow effects. As mentioned before, however, fracture non-Darcy flow pseudo-skin, $S_{ND} = 0.1$, was used to develop the correlation for the effect of non-Darcy flow. Note that for the example presented in Table 2-2, $S_{ND} = 0.1$ represents 3.4% of the total

Darcy flow pressure drop. For the other cases, this percentage could be higher or lower, but never exceeds 10%.

TABLE 2-2. Data Used to Generate Fig. 2-3

t_D	Darcy Flow m_{wD}	Non-Darcy Flow m_{wD}	S_{ND}
1.00E-05	0.0082	0.0441	0.0360
1.00E-04	0.0204	0.0828	0.0624
1.00E-03	0.0583	0.1499	0.0916
1.00E-02	0.1731	0.2896	0.1165
1.00E-01	0.4949	0.6319	0.1370
1.00E+00	1.2143	1.3734	0.1591
2.00E+00	1.5099	1.6731	0.1632
3.00E+00	1.6942	1.8591	0.1649
4.00E+00	1.8284	1.9943	0.1658
5.00E+00	1.9341	2.1005	0.1664
6.00E+00	2.0213	2.1881	0.1668
7.00E+00	2.0955	2.2626	0.1671
8.00E+00	2.1601	2.3274	0.1673
9.00E+00	2.2173	2.3848	0.1674
1.00E+01	2.2687	2.4362	0.1676
2.00E+01	2.6091	2.7773	0.1682
3.00E+01	2.8098	2.9782	0.1684
4.00E+01	2.9526	3.1211	0.1685

2.9 Methodology

In this work, a correlation is proposed to improve the design of fractured well tests to minimize the non-Darcy flow effects in the fracture. This section describes the steps

taken to arrive at the final form of the correlation and helps the reader appreciate the importance of each parameter in the correlation.

First, reservoir, fluid, and fracture properties are set to constitute a base case. These properties are modified when necessary to study the effect of the change on non-Darcy flow characteristics. Table 2-3 presents the data for the base case.

TABLE 2-3. Base Case Data

Property	Value	Units
Reservoir Pressure, p_i	3000	psia
Formation Permeability, k	0.1	md
Formation Porosity, ϕ	0.1	fraction
Formation Thickness, h	60	ft
Initial Gas Viscosity, μ_i	0.018	cp
Gas Density, ρ	8.23	lbm/ft ³
Total Compressibility, c_t	1.00E-05	psi ⁻¹
Non-Darcy Flow Coefficient, β	0.98x10 ⁵	ft ⁻¹
Fracture Half Length, x_f	200	ft
Fracture Permeability, k_f	360000	md
Fracture Width, w_f	0.02083	ft
Reservoir Temperature, T	190	°F
Specific Gravity of Gas, γ_g	0.6	---
Gas Molecular Weight, M	17.382	lbm/lb mole

2.9.1 General Procedure

In this study, more than 1200 combinations of the properties shown in Table 2-3 were considered. To calculate S_{ND} , the transient pseudo-pressure responses of fractured wells

for both Darcy and non-Darcy flow cases were generated by using the semi-analytical model discussed in Refs. 4 - 6.

To examine the effects of fracture, reservoir, and fluid properties, non-Darcy flow skin, S_{ND} , was plotted as a function of fracture half-length, x_f , and production rate, q (or q_{DND}). The other system properties were then changed to observe the influence on S_{ND} . In this process, the system property being changed is called the *iteration parameter*.

Fig. 2-5 shows a plot of S_{ND} vs. x_f for the base case shown in Table 2-3. Four different flow rates are considered in this figure. The intersection points of the curves for different flow rates with the line $S_{ND} = 0.1$ indicate the pairs of fracture half-length and production rate to have less than 10% pressure drop due to non-Darcy flow. This figure can be used for design purposes. For example, if 10000 MSCF/D is the desired q , the maximum x_f allowed in order to limit the fracture non-Darcy flow effects to $S_{ND} = 0.1$ is about 110 ft. For production purposes, assuming that a 200-ft. long fracture exists, considerable pressure drop due to non-Darcy flow ($\geq 10\%$) should be expected for flow rates higher than 5000 MSCF/D.

As mentioned earlier, the main objective of this work is to develop a correlation to determine the system properties that would limit the additional pressure drop due to non-Darcy flow to 10% of the drawdown for the Darcy flow case. The intersection points of the curves in Fig. 2-5 with $S_{ND} = 0.1$ provide the data to be used in the correlation. To obtain a correlation, the properties used in Fig. 2-5 were changed within the ranges shown in Table 2-1, and the intersection point of the curves with the $S_{ND} = 0.1$ line was noted for each case. It must be emphasized that $S_{ND} = 0.1$ is rather an arbitrary value chosen in this work for tolerable non-Darcy flow effects. At $S_{ND} = 0.1$, the pressure drop due to non-Darcy flow corresponds to different percentiles of the total drawdown for different cases. As will be shown later, however, for all the cases considered in this study,

$S_{ND} = 0.1$ represents a non-Darcy flow pressure drop less than 10% of the total Darcy flow drawdown. In the following sections, the influence of the system properties on the fracture non-Darcy flow skin, S_{ND} , is investigated.

2.9.2 Effect of Non-Darcy Flow Coefficient, β .

The first iteration parameter is the non-Darcy flow coefficient, β . Fig. 2-6 presents the same cases shown in Fig. 2-5, except that two other β values have been added. The pairs of the flow rate and fracture half-length at the intersection points of the curves in Fig. 2-6 with $S_{ND} = 0.1$ were plotted in Fig. 2-7 for three values of β . In this plot, the region to the left of each curve represents the “safe region”, where the non-Darcy flow effects have tolerable influence for well testing purposes.

The trend of the three curves in Fig. 2-7, suggests that they may be combined to obtain a single curve by a lateral shift. It was found that the curves for different β values collapse into one single curve on a plot of q vs. $x_f \beta$. Fig. 2-8 illustrates this behavior and represents the first step toward obtaining a correlation for the fracture non-Darcy flow effects.

The correlation shown in Fig. 2-8 was tested for several values of initial reservoir pressure and fracture width. Although the effects of these parameters will be discussed later, Figs. 2-9 and 2-10 verify that the correlation obtained at this stage is valid for all property ranges. Due to the results obtained so far, β will not be considered as a parameter in the following sections and the values of β used to develop the correlation will not be given.

2.9.3 Effect of Fracture Width, w_f .

The fracture width, w_f , affects the flow velocities and thus it is an important property for the presence of non-Darcy flow. The three different w_f values used in Fig. 2-11 cover a wide range of practical fracture widths. Examination of Fig. 2-11 reveals parallel nature of the curves for different values of w_f . Because q and w_f appear, respectively, in the nominator and denominator of the dimensionless non-Darcy flow rate equation (Eq. 2-4), it was reasonable to construct a new ordinate axis as q / w_f . Also from the definition of dimensionless conductivity (Eq. 2-3), the abscissa was scaled by w_f to yield $x_f \beta / w_f$. Fig. 2-12 shows the final form of the correlation at this stage that incorporates β and w_f . Note that all the curves in Fig. 2-12 overlap indicating an excellent correlation.

2.9.4 Effect of Reservoir Permeability, k .

The results obtained in Sections 2.9.2 and 2.9.3 were for $k = 0.1$ md. Figs. 2-5 and 2-6 present the behavior of S_{ND} vs. x_f for $k = 0.1$ md where $S_{ND} = 0.1$ is the threshold value. The same plot is shown on Fig. 2-13 for $k = 1$ md. As expected, the non-Darcy flow effects become significant at lower flow rates or for shorter fracture half-lengths for $k = 1$ md. This may be better explained with an example. Consider the case $k = 0.1$ md and $q = 10000$ MSCF/D for $\beta = 0.98 \times 10^5$ ft⁻¹. Note on Fig. 2-6 that the maximum x_f allowed to minimize non-Darcy flow effects is about 125 ft. For the $k = 1$ md case (see Fig. 2-13), however, the fracture half-length is only a few feet for the same conditions. Now assume that the fracture is already created and $x_f = 125$ ft. To produce the well under tolerable non-Darcy flow effects, the maximum producing rate should be 1000 MSCF/D, which represents 10% of the flow rate initially considered.

To add confidence to these observations, the case for $k = 10$ md was also examined. Table 2-4 shows the Darcy and non-Darcy flow dimensionless pseudo-pressures and fracture non-Darcy flow pseudo-skin for the data used in Table 2-2 ($q = 10000$ MSCF/D,

$q_{DND} = 126.24$, $\beta = 0.98 \times 10^5 \text{ ft}^{-1}$, $x_f = 200 \text{ ft.}$) except for $k = 10 \text{ md.}$ The same data are also presented graphically in Fig. 2-14. Comparing Tables 2-2 and 2-4, or graphically, Figs. 2-3 and 2-14, it is apparent that the non-Darcy flow skin increases as the permeability increases. (The pressure drop because of Darcy and non-Darcy flow become higher as the permeability increases. However, while the Darcy flow pressure drop increases by 40%, the non-Darcy flow pressure drop increases by 100%.)

The fact that the dimensionless pressure drop increases as the reservoir permeability increases may be contrary to our expectations and deserves comment. As discussed in Section 2.3, as the reservoir permeability increases, the dimensionless conductivity decreases and the flow diverts to the regions closer to the wellbore. In other words, the efficiency of the fracture decreases and the efficiency of the reservoir increases as k increases. The interplay between these two effects and the fact that k is a scaling parameter in the definition of the dimensionless pseudo-pressure (Eq. 2-6) determines the final dimensionless pressure drop. The S_{ND} value for the example presented in Table 2-4 where $x_f = 200 \text{ ft.}$ is approximately 2.2, which represents 54.8% of the Darcy flow pseudo-pressure drop. Computations indicate that for $k = 10 \text{ md}$ the threshold value of $S_{ND} = 0.1$ no longer represents 10% of the dimensionless pressure for the corresponding Darcy flow case, but a much lower percentage.

TABLE 2-4. Data Used to Generate Fig. 2-14

t_D	Darcy Flow m_{wD}	Non-Darcy Flow m_{wD}	S_{ND}
1.00E-04	0.1211	0.6284	0.5074
1.00E-03	0.2227	1.1652	0.9425
1.00E-02	0.3996	1.8506	1.4510
1.00E-01	0.7699	2.6987	1.9287
7.00E-01	1.3849	3.5396	2.1547
1.00E+00	1.5303	3.7072	2.1768
1.00E+01	2.5989	4.8333	2.2344
1.00E+02	3.7410	5.9820	2.2411
2.00E+02	4.0870	6.3284	2.2414

Fig. 2-15 presents the S_{ND} vs. x_f plot for $k = 10$ md. Note that if $S_{ND} = 0.1$ is kept as the threshold value, the corresponding fracture half-lengths approach zero. Computations not shown here also indicate that the additional pressure drop due to non-Darcy flow is well in excess of 10% of the drawdown for practical fracture half-lengths in Fig. 2-15. This indicates that for the data shown in this example, non-Darcy flow effects may not be avoided by simple design considerations.

In Figs. 2-16 and 2-17 S_{ND} vs. x_f has been plotted for $k = 20$ and 30 md respectively. From Figs. 2-15 through 2-17, it is evident that as the permeability increases, the non-Darcy flow effects in the fracture increase in such a way that practically nothing can be done to avoid it. (To minimize non-Darcy flow, very low flow rates or extremely short fracture half-lengths would be required.) The results thus far lead to the conclusion that

up to $k = 1$ md, the non-Darcy flow effects can be effectively controlled. For $k = 10$ md, however, productivity loss due to non-Darcy flow may not be avoided.

Exploring more on Figs. 2-16 and 2-17, it can be seen that S_{ND} becomes almost constant as x_f increases. An explanation for this behavior is necessary: As x_f increases, C_{fD} decreases (see Eq. 2-3) and more fluid enters the fracture from the region closer to the wellbore. There is, however, a limit at which further increase in the fracture half-length does not contribute with additional production and the fracture is considered ineffective. As a consequence, the non-Darcy pressure drop becomes constant and hence the non-Darcy flow skin.

In light of the above discussion, the effect of reservoir permeability was incorporated into the correlation for non-Darcy flow effects considering a threshold value of $S_{ND} = 0.1$. Fig. 2-18 shows the correlation for $k = 0.1$ and $k = 1$ md. As in the case of β and w_f , many permutations of the axes were examined to collapse the two curves in Fig. 2-18. Fig. 2-19 presents the new correlation where the reservoir permeability was incorporated by multiplying the abscissa and ordinate of Fig. 2-18 by $k^{1/2}$. This yielded one single curve for both values of the permeability. As in the previous form of the correlation, this single curve indicates that the region to the left of the curve corresponds to the area where non-Darcy flow effects are insignificant.

The intersection points of the constant flow rate curves with $S_{ND} = 0.1$ for the case $k = 10$ md (see Fig. 2-15) were tested on Fig. 2-19 and all the points fell on the curve. However, because no practical values of fracture half-lengths result from the intersection ($x_f < 3$ ft.), the cases $k = 20$ and $k = 30$ md were not considered in the correlation (as discussed before, it is almost impossible to avoid the non-Darcy flow effects as the reservoir permeability increases).

2.9.5 Effect of Fracture Permeability, k_f .

A wide range of fracture permeabilities was considered in this work (see Table 2-1). Fig. 2-20 shows the correlation for the base case (Table 2-3), except for $\beta = 0.98 \times 10^5$ and $1.79 \times 10^5 \text{ ft}^{-1}$. Note that the curves for the two β values overlap verifying the correlation obtained so far. The same behavior was observed for $k_f = 720000$ and 50000 md (results not shown here) but not for $k_f = 10000$ md.

Fig. 2-21 shows the correlation for non-Darcy flow effects for the base case and the four different k_f values. Note that only the case for $k_f = 10000$ md does not follow the trend. However, it is important to note that the curve for $k_f = 10000$ md is located up and to the right of the general trend or correlation. This indicates that the correlation developed here provides conservative estimates of the properties for which non-Darcy flow is of concern and by using this correlation, it is assured that the non-Darcy flow effects would be limited to tolerable ranges for all fracture permeabilities.

Based on the results discussed so far, Fig. 2-22 shows the non-Darcy flow correlation developed. Below, the influence of the other physical properties is discussed.

2.9.6 Effect of the Other Properties

This section discusses the influence of some formation and fluid properties, such as: specific gravity, γ_g , initial gas viscosity, μ_i , total compressibility, c_t , formation thickness, h , and formation porosity, ϕ , on the non-Darcy flow correlation developed above.

To conduct the analyses, the properties set on Table 2-3 were changed and the effects on the correlation were observed. Seven test cases shown in Tables 2-5 through 2-11 were examined. The same procedure explained in Section 2.9.1 was followed but only one flow rate was considered. Therefore, the intercept of the S_{ND} vs. x_f curve with $S_{ND} = 0.1$ is a single point for each test case and yields a test point (seven test points in total).

Fig. 2-23 shows the S_{ND} vs. x_f plot for the test cases and the intercepts at $S_{ND} = 0.1$. The intercepts were then plotted on the correlation chart and checked for agreement. This is shown in Fig. 2-24 and discussed below.

Test Point 1

Table 2-5 shows the data used to obtain Test Point 1. Comparing this table with the base case (Table 2-3), we note that the following properties has been changed: k , β , and w_f .

TABLE 2-5. Data Used for Test Point 1

Property		Value	Unit
Reservoir Pressure	p_i	3000	psia
Formation Permeability	k	1	md
Formation Porosity	ϕ	0.1	fraction
Formation Thickness	h	60	ft
Initial Gas Viscosity	μ_i	0.018	cp
Gas Density	ρ	8.23	lbm/ft ³
Total Compressibility	c_t	1.00E-05	psi ⁻¹
Non-Darcy Flow Coefficient	β	1.79E+05	ft ⁻¹
Fracture Permeability	k_f	360000	md
Fracture Width	w_f	0.45	in.
Reservoir Temperature	T	190	°F
Specific Gravity of Gas	γ_g	0.6	---
Gas Molecular Weight	M	17.382	lbm/lb mole
Gas Flow Rate	q	7000	MSCF/D

These changes were already studied and incorporated to the correlation in earlier sections, but they are presented here for reference. Note from Fig. 2-24 that Test Point 1 falls on the correlation curve as expected.

Test Point 2

To obtain Test Point 2, all the values except p_i were changed from the base case (k was kept as 1 md). The new values are presented on Table 2-6.

TABLE 2-6. Data Used for Test Point 2

Property		Value	Unit
Reservoir Pressure	p_i	3000	psia
Formation Permeability	k	1	md
Formation Porosity	ϕ	0.2	fraction
Formation Thickness	h	100	ft
Initial Gas Viscosity	μ_i	0.015	cp
Gas Density	ρ	11.83	lbm/ft ³
Total Compressibility	c_t	2.00E-04	psi ⁻¹
Non-Darcy Flow Coefficient	β	1.297E+05	ft ⁻¹
Fracture Permeability	k_f	250000	md
Fracture Width	w_f	0.35	in.
Reservoir Temperature	T	190	°F
Specific Gravity of Gas	γ_g	0.8	---
Gas Molecular Weight	M	23.176	lbm/lb mole
Gas Flow Rate	q	7000	MSCF/D

Test Point 2 does not fall on the correlation curve (Fig. 2-24), which indicates that some of the modified parameters have influence on non-Darcy flow. To find and incorporate the individual effects of these properties, Test Points 3-7 were examined.

Test Point 3

This data set is basically the same as that used for Test Point 2, except that the specific gravity, γ_g , has been changed back to 0.6. Table 2-7 presents the data used for this case.

TABLE 2-7. Data Used for Test Point 3

Property		Value	Unit
Reservoir Pressure	p_i	3000	psia
Formation Permeability	k	1	md
Formation Porosity	ϕ	0.2	fraction
Formation Thickness	h	100	ft
Initial Gas Viscosity	μ_i	0.015	cp
Gas Density	ρ	8.23	lbm/ft ³
Total Compressibility	c_t	2.00E-04	psi ⁻¹
Non-Darcy Flow Coefficient	β	1.297E+05	ft ⁻¹
Fracture Permeability	k_f	250000	md
Fracture Width	w_f	0.35	in.
Reservoir Temperature	T	190	°F
Specific Gravity of Gas	γ_g	0.6	---
Gas Molecular Weight	M	17.382	lbm/lb mole
Gas Flow Rate	q	7000	MSCF/D

Note from Test Points 2 and 3 in Fig. 2-24 that changing the specific gravity to the original value ($\gamma_g = 0.6$) used to develop the correlation, caused further deviation, thus indicating that γ_g has influence on the non-Darcy flow effects.

Test Point 4

Test Point 4 corresponds to the same properties as in Test Point 3 but the initial viscosity, μ_i , was changed to the original value ($\mu_i = 0.018$ cp). The data for this case is shown on Table 2-8.

TABLE 2-8. Data Used for Test Point 4

Property		Value	Unit
Reservoir Pressure	p_i	3000	psia
Formation Permeability	k	1	md
Formation Porosity	ϕ	0.2	fraction
Formation Thickness	h	100	ft
Initial Gas Viscosity	μ_i	0.018	cp
Gas Density	ρ	8.23	lbm/ft ³
Total Compressibility	c_t	2.00E-04	psi ⁻¹
Non-Darcy Flow Coefficient	β	1.297E+05	ft ⁻¹
Fracture Permeability	k_f	250000	md
Fracture Width	w_f	0.35	in.
Reservoir Temperature	T	190	°F
Specific Gravity of Gas	γ_g	0.6	---
Gas Molecular Weight	M	17.382	lbm/lb mole
Gas Flow Rate	q	7000	MSCF/D

Surprisingly, Test Point 4 fell on top of Test Point 3 (see Fig. 2-24). This indicates that viscosity is not a sensitive parameter for the correlation for non-Darcy flow effects.

Test Point 5

The data used to generate Test Point 5 preserves the earlier changes in Test Point 3 and 4 but set the formation thickness, h , back to 60 ft., which was the original value used to develop the correlation. Table 2-9 shows the data for this case.

TABLE 2-9. Data Used for Test Point 5

Property		Value	Unit
Reservoir Pressure	p_i	3000	psia
Formation Permeability	k	1	md
Formation Porosity	ϕ	0.2	fraction
Formation Thickness	h	60	ft
Initial Gas Viscosity	μ_i	0.018	cp
Gas Density	ρ	8.23	lbm/ft ³
Total Compressibility	c_t	2.00E-04	psi ⁻¹
Non-Darcy Flow Coefficient	β	1.297E+05	ft ⁻¹
Fracture Permeability	k_f	250000	md
Fracture Width	w_f	0.35	in.
Reservoir Temperature	T	190	°F
Specific Gravity of Gas	γ_g	0.6	---
Gas Molecular Weight	M	17.382	lbm/lb mole
Gas Flow Rate	q	7000	MSCF/D

As can be seen on Fig. 2-24, the modification to h caused the test point to overlap with the correlation curve. The significant influence of h on the non-Darcy flow effects can be easily understood if the fracture is seen as tri-dimensional. As explained earlier in this

chapter, the model used to generate the data assumes that the fracture fully penetrates the reservoir. This means that the fracture height is equal to the formation thickness. As the fracture height decreases, flow velocities within the fracture for a fixed flow rate increases and this results in higher non-Darcy flow pressure drops.

It was possible to incorporate the effect of formation thickness into the correlation by dividing the vertical axis by h . As shown in Fig. 2-25 this modification made all the test points fall on the same curve, except for Test Point 2. Because the difference between Test Point 2 and the rest of the test points is the specific gravity, γ_g , the effect of this parameter is incorporated into the correlation as discussed below.

Specific Gravity

After several combinations of this fluid property with the x and y axes, a new form of the correlation was found. The result is presented in Fig. 2-26. To gain more confidence, some other γ_g values were also tested.

Fig. 2-27 shows the new values used to validate the correlation. Table 2-10 shows the data used to generate the point for $\gamma_g = 0.9$ (Test Point 6). The data are exactly the same as that used for Test Point 5, except for γ_g . Note that the test point falls perfectly on the curve.

TABLE 2-10. Data Used for Test Point 6

Property		Value	Unit
Reservoir Pressure	p_i	3000	psia
Formation Permeability	k	1	md
Formation Porosity	ϕ	0.2	fraction
Formation Thickness	h	60	ft
Initial Gas Viscosity	μ_i	0.018	cp
Gas Density	ρ	13.84	lbm/ft ³
Total Compressibility	c_t	2.00E-04	psi ⁻¹
Non-Darcy Flow Coefficient	β	1.297E+05	ft ⁻¹
Fracture Permeability	k_f	250000	md
Fracture Width	w_f	0.35	in.
Reservoir Temperature	T	190	°F
Specific Gravity of Gas	γ_g	0.9	---
Gas Molecular Weight	M	26.073	lbm/lb mole
Gas Flow Rate	q	2000	MSCF/D

To generate Test Point 7 for $\gamma_g = 0.7$, the data presented in Table 2-11 was used. Here, not only γ_g , but also h and c_t were modified. The points $\gamma_g = 0.6$ and 0.8 were taken from the base case and Test Point 2, respectively. Note that the match with the correlation is perfect.

Fig. 2-27, therefore, represents the refined correlation. The final property to be tested is the initial reservoir pressure and it is discussed below.

TABLE 2-11. Data Used for Test Point 7

Property		Value	Unit
Reservoir Pressure	p_i	3000	psia
Formation Permeability	k	1	md
Formation Porosity	ϕ	0.2	fraction
Formation Thickness	h	120	ft
Initial Gas Viscosity	μ_i	0.018	cp
Gas Density	ρ	9.96	lbm/ft ³
Total Compressibility	c_t	1.00E-05	psi ⁻¹
Non-Darcy Flow Coefficient	β	1.297E+05	ft ⁻¹
Fracture Permeability	k_f	250000	md
Fracture Width	w_f	0.35	in.
Reservoir Temperature	T	190	°F
Specific Gravity of Gas	γ_g	0.7	---
Gas Molecular Weight	M	20.279	lbm/lb mole
Gas Flow Rate	q	2000	MSCF/D

2.9.7 Effect of Initial Reservoir Pressure, p_i .

The correlation developed thus far assumes that $p_i = 3000$ psia. To understand the effect of p_i on the correlation, five different values of pressure were considered: $p_i = 1000$, 2000, 3000, 5000, and 6000 psia (note that Settari *et al.*⁷ worked with three p_i values: 1000, 3000, and 5000 psia).

From Fig. 2-28 it can be seen that, as the initial pressure increases the non-Darcy flow skin, S_{ND} , decreases. Table 2-12 shows the change in S_{ND} as a function of p_i for a fixed fracture half-length of $x_f = 300$ ft for reference.

TABLE 2-12. Influence of p_i on S_{ND}

p_i (psia)	1000	2000	3000	5000	6000
S_{ND}	0.27	0.25	0.22	0.18	0.16

These results indicate that p_i has considerable influence on non-Darcy flow effects. Fig. 2-29 displays the influence of initial pressure on the correlation developed here. The results in this figure indicate a predictable pattern: as p_i increases, the region where non-Darcy flow should be of concern is reduced.

In an effort to incorporate the effect of p_i into the correlation, several combinations of the axes were tested. Fig. 2-30 shows the best correlation found. Note that except for $p_i = 1000$ psia, all the points fall on one curve. As in the case of fracture permeability, the case for $p_i = 1000$ psia is close to the general curve and shifted right. This indicates that using the correlation for $p_i < 2000$ psia provides conservative estimates of the properties for which non-Darcy flow is of concern and assures that the non-Darcy flow effects will be insignificant.

The final form of the correlation is presented in Fig. 2-31. This correlation is a convenient tool for the design of fractured-well-tests when non-Darcy flow is of concern. By using this correlation, it is possible to determine the well flow rate before the test to improve the analysis and thus the results. It is important to recall that, as explained in Section 2.9.4, it is not always possible to avoid the non-Darcy flow effects. In these cases, the figures for S_{ND} presented in this work can be used to determine the non-Darcy flow skin, S_{ND} , and the productivity reduction caused by it. Also, if the pressure transient data are already influenced by the fracture non-Darcy flow, the analysis technique suggested in Chapter 4 may be used.

As a final remark, the units used in the correlation are shown below:

$$q = \text{MSCF/D}$$

$$k = \text{md}$$

$$\gamma_g = \text{dimensionless}$$

$$w_f = \text{ft}$$

$$p_i = \text{psia}$$

$$x_f = \text{ft}$$

$$\beta = \text{ft}^{-1}$$

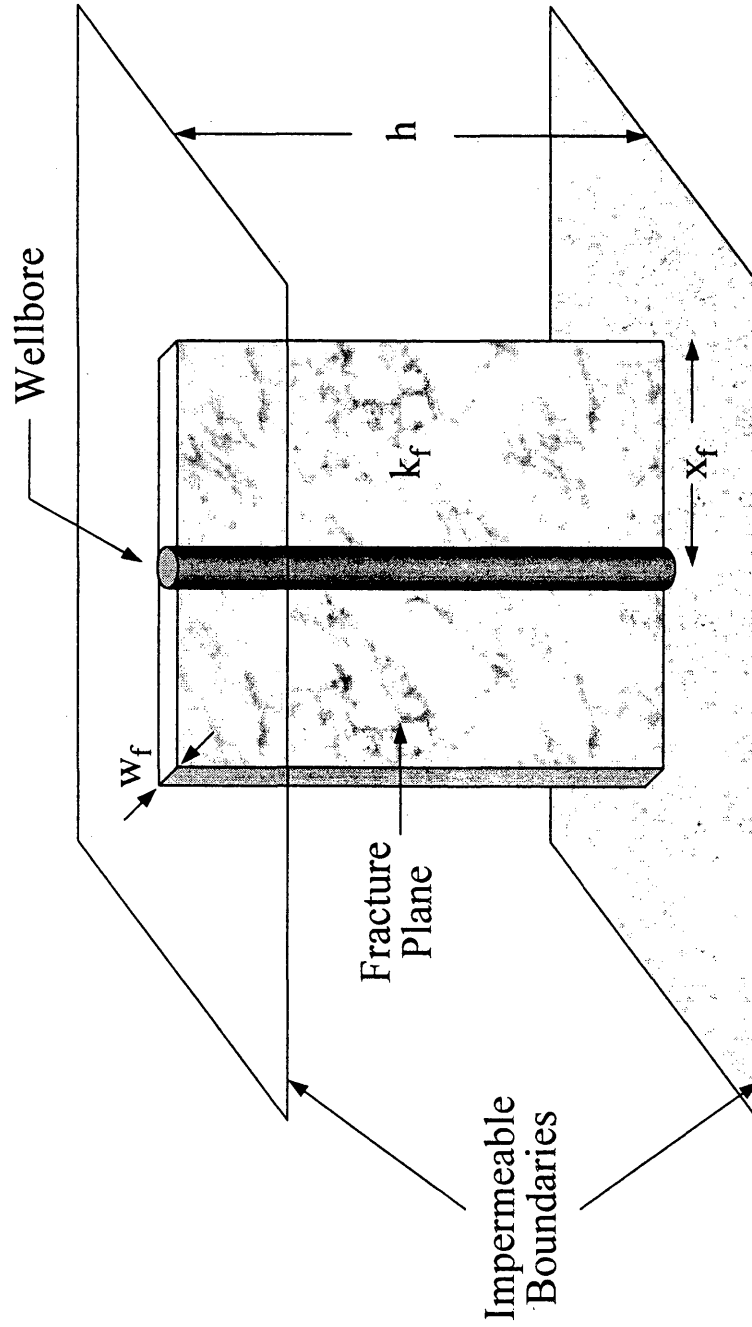


Fig. 2-1. Reservoir, fracture and well system

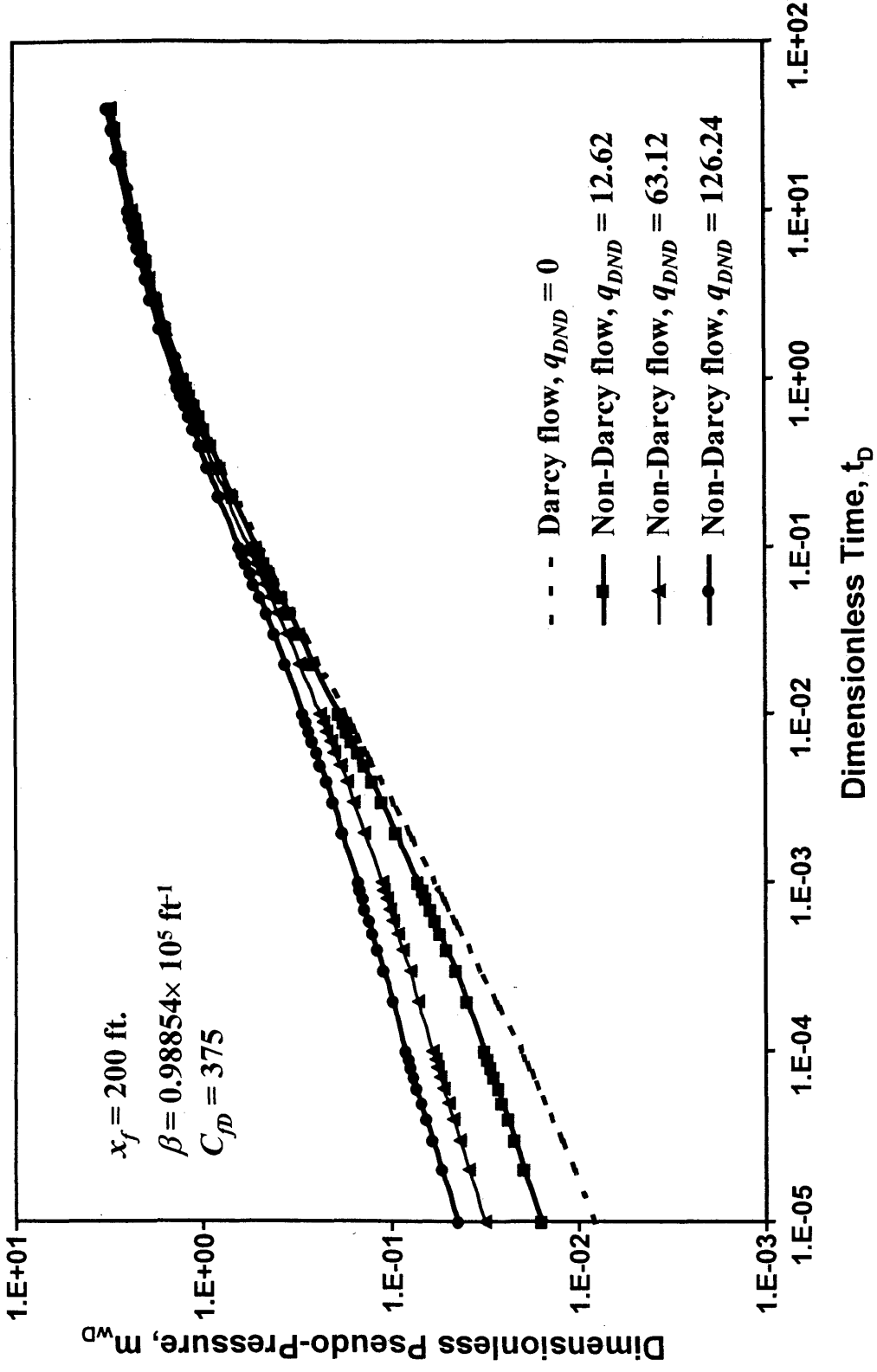


Fig. 2-2. Non-Darcy flow effect on transient pressure responses

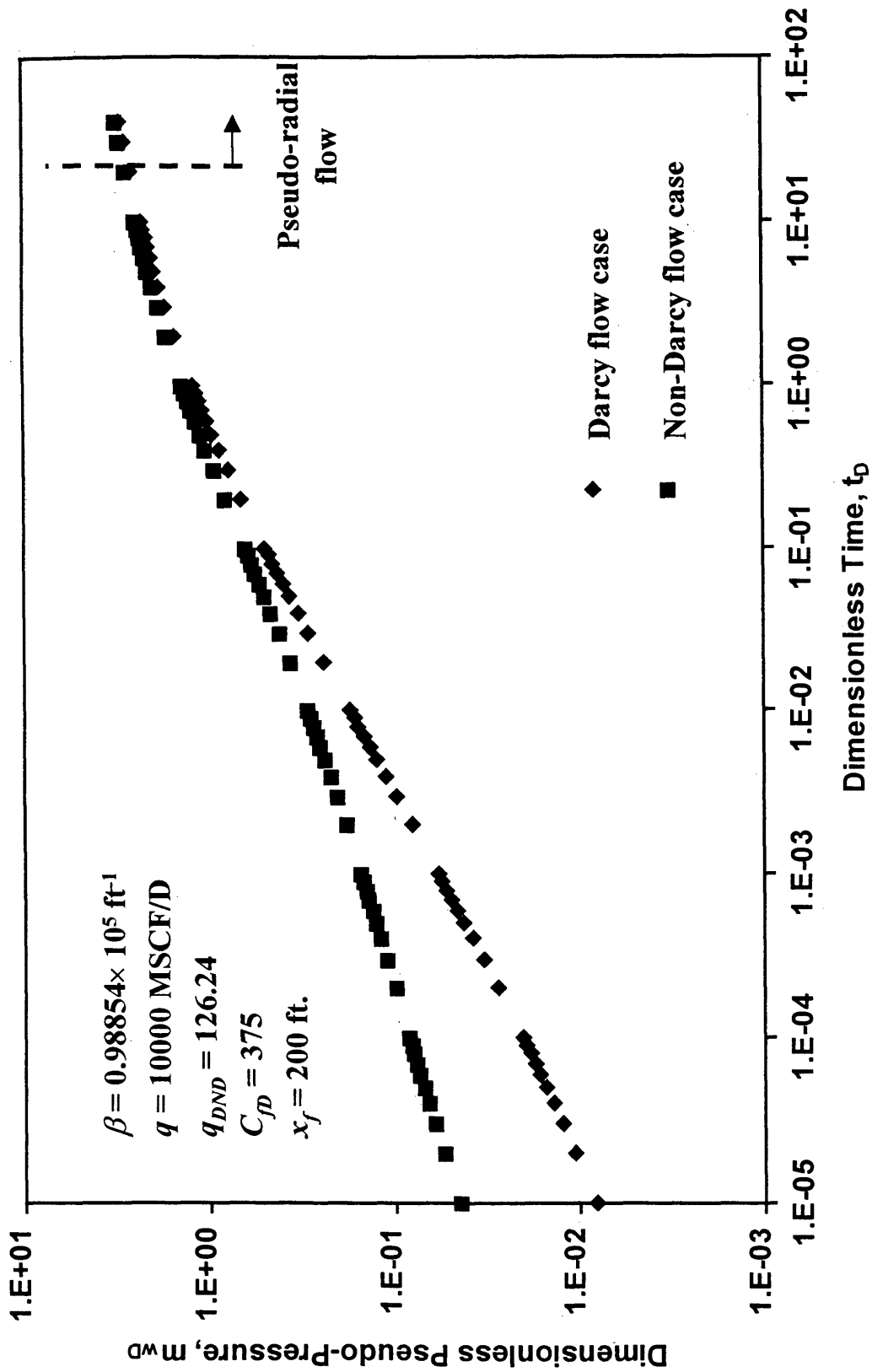


Fig. 2-3. Non-Darcy flow skin

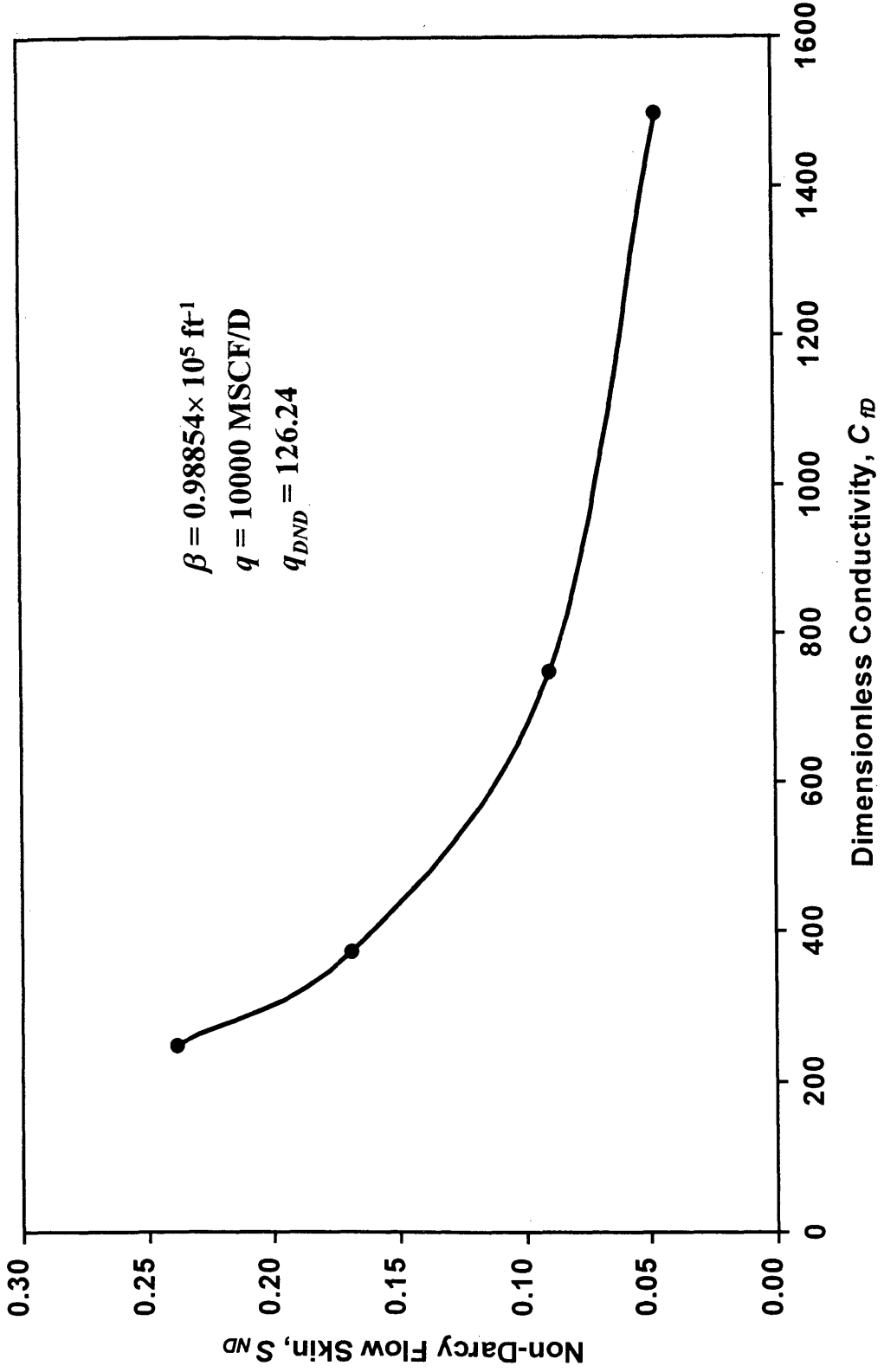


Fig. 2-4. Non-Darcy flow skin vs. conductivity

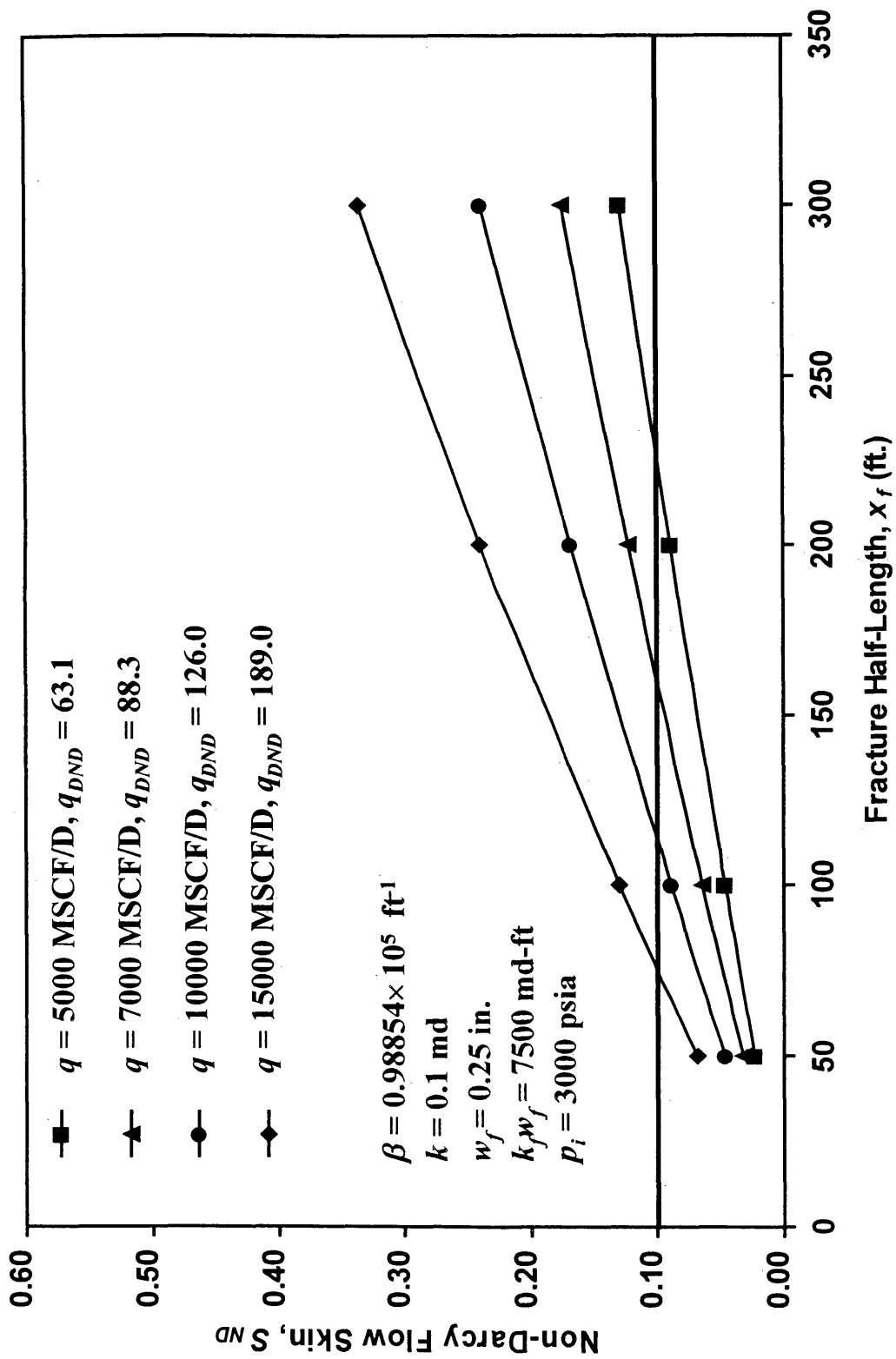


Fig. 2-5. Non-Darcy flow skin vs. fracture half-length

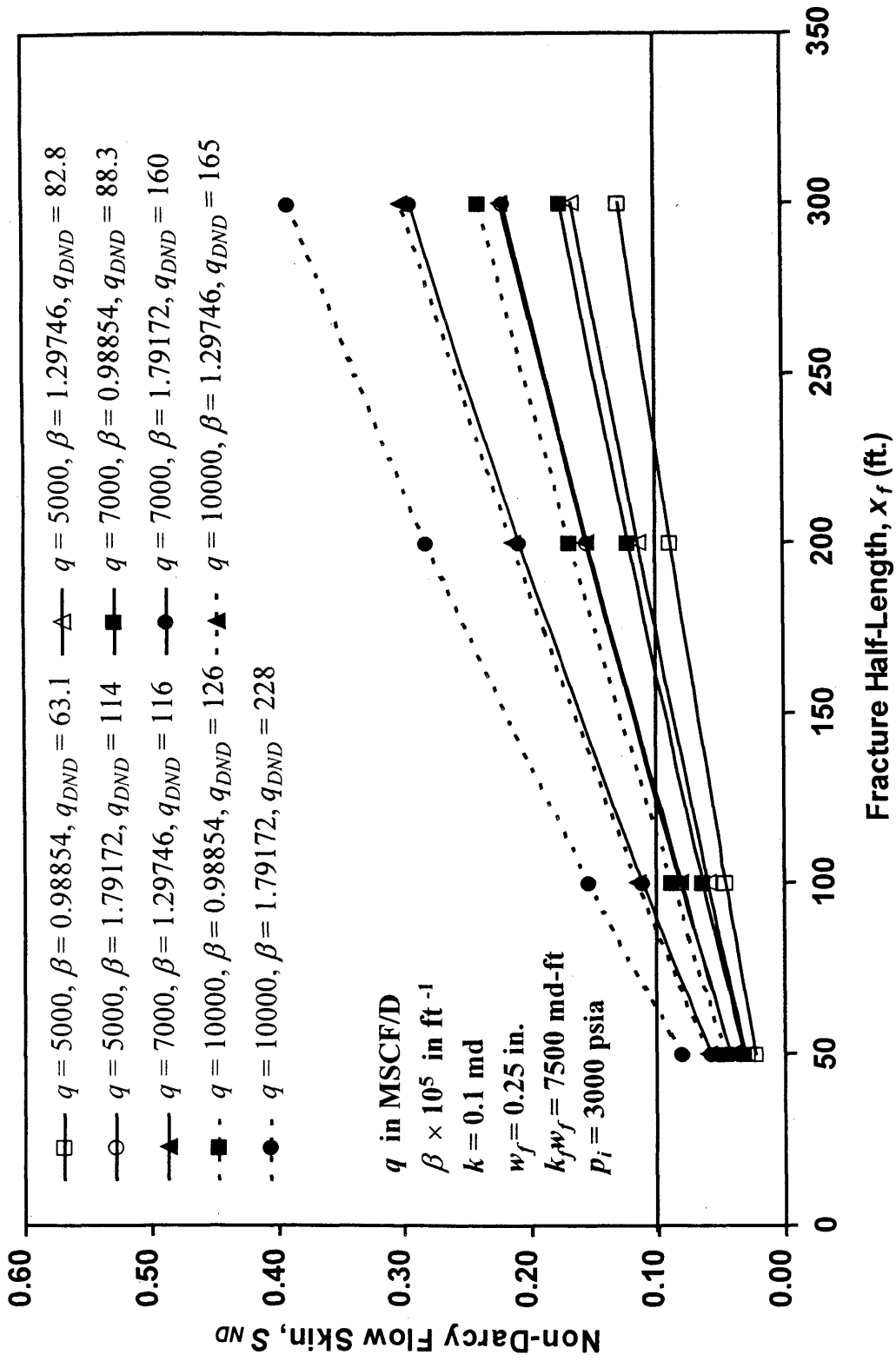


Fig. 2-6. Non-Darcy flow skin vs. fracture half-length for different β values

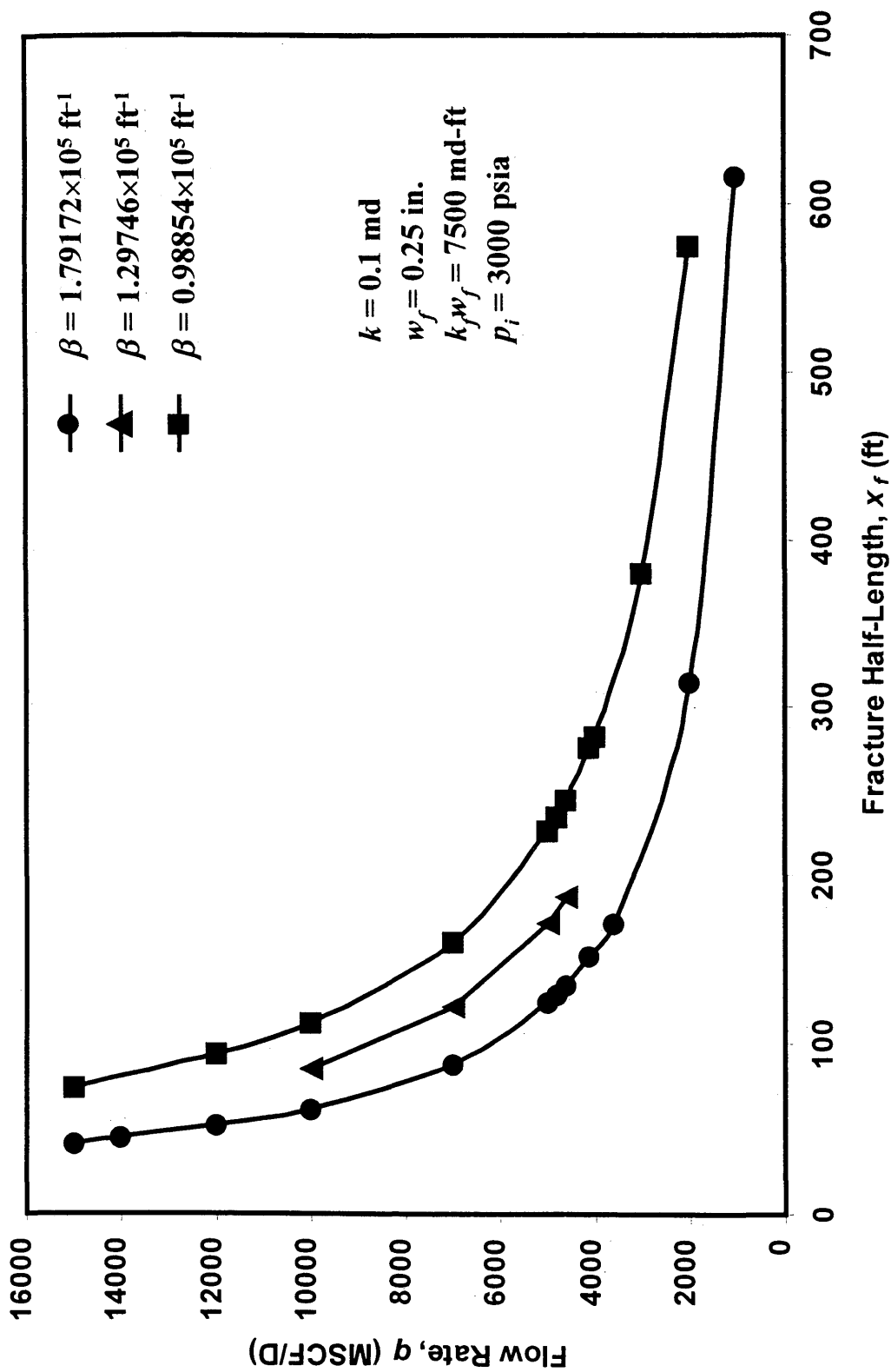


Fig. 2-7. Flow rate vs. fracture half-length for different β values

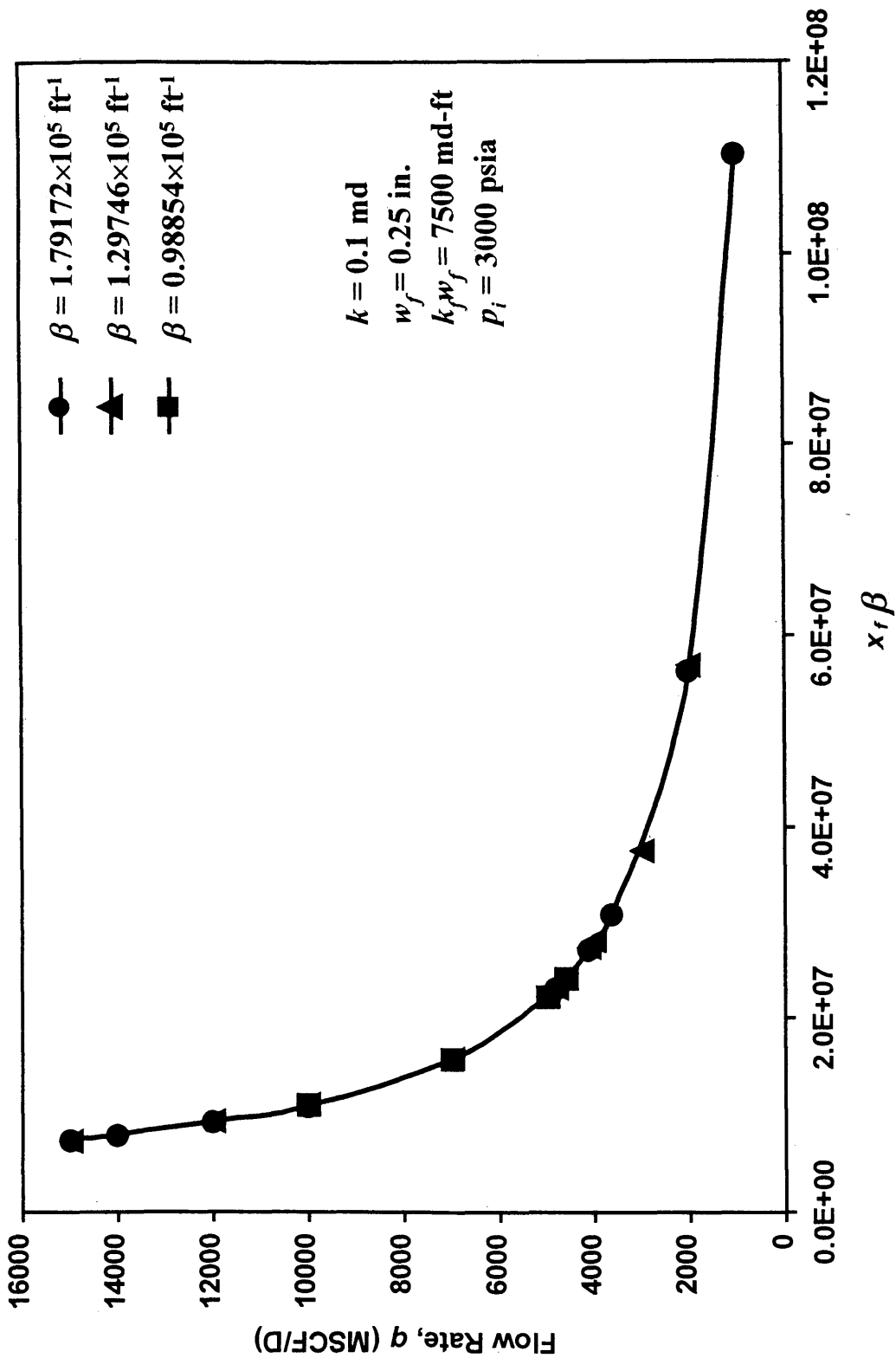


Fig. 2-8. Incorporating β to the correlation: q vs. $x_r * \beta$

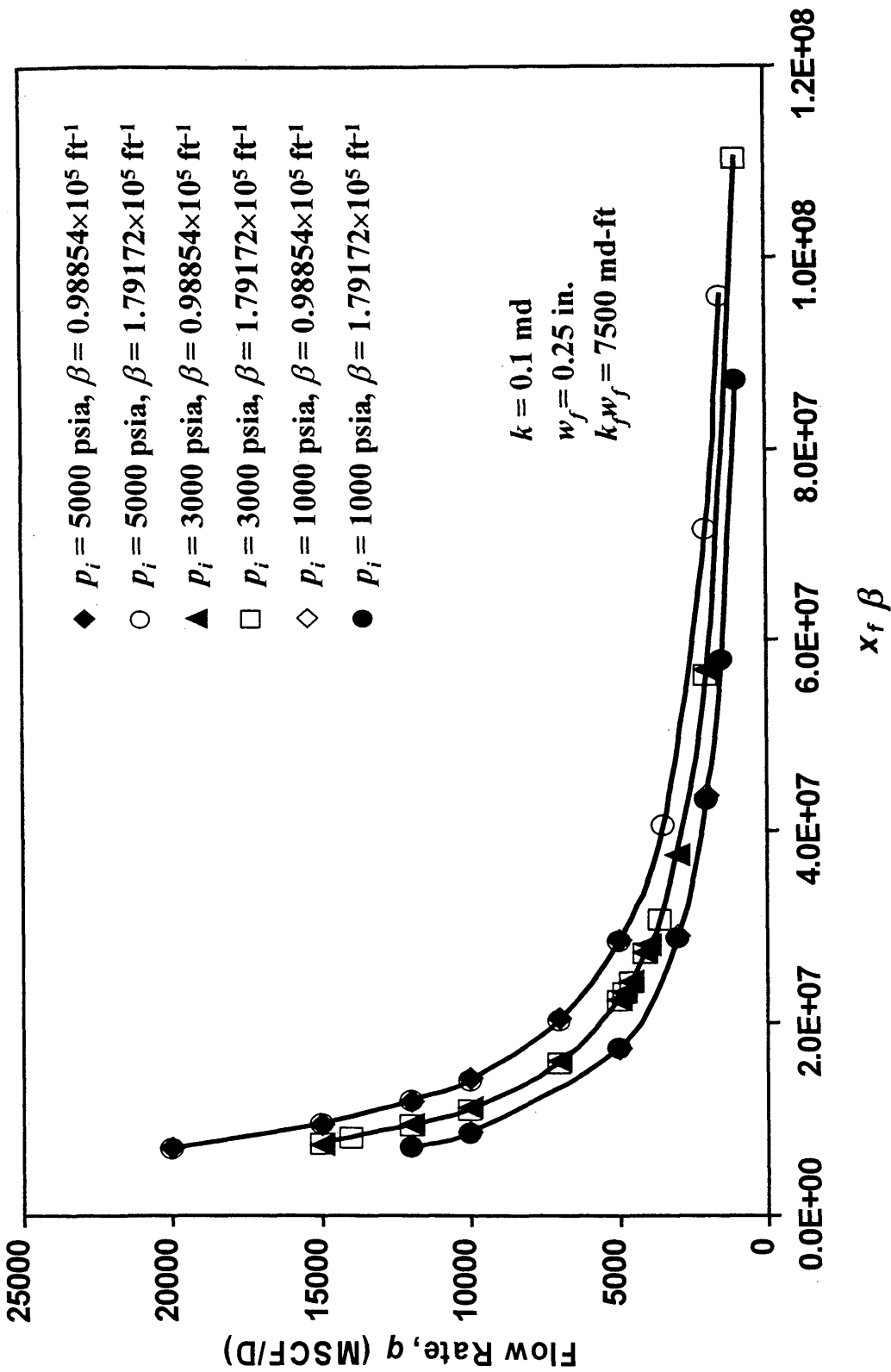


Fig. 2-9. q vs. $x_r \beta$ for different initial reservoir pressures

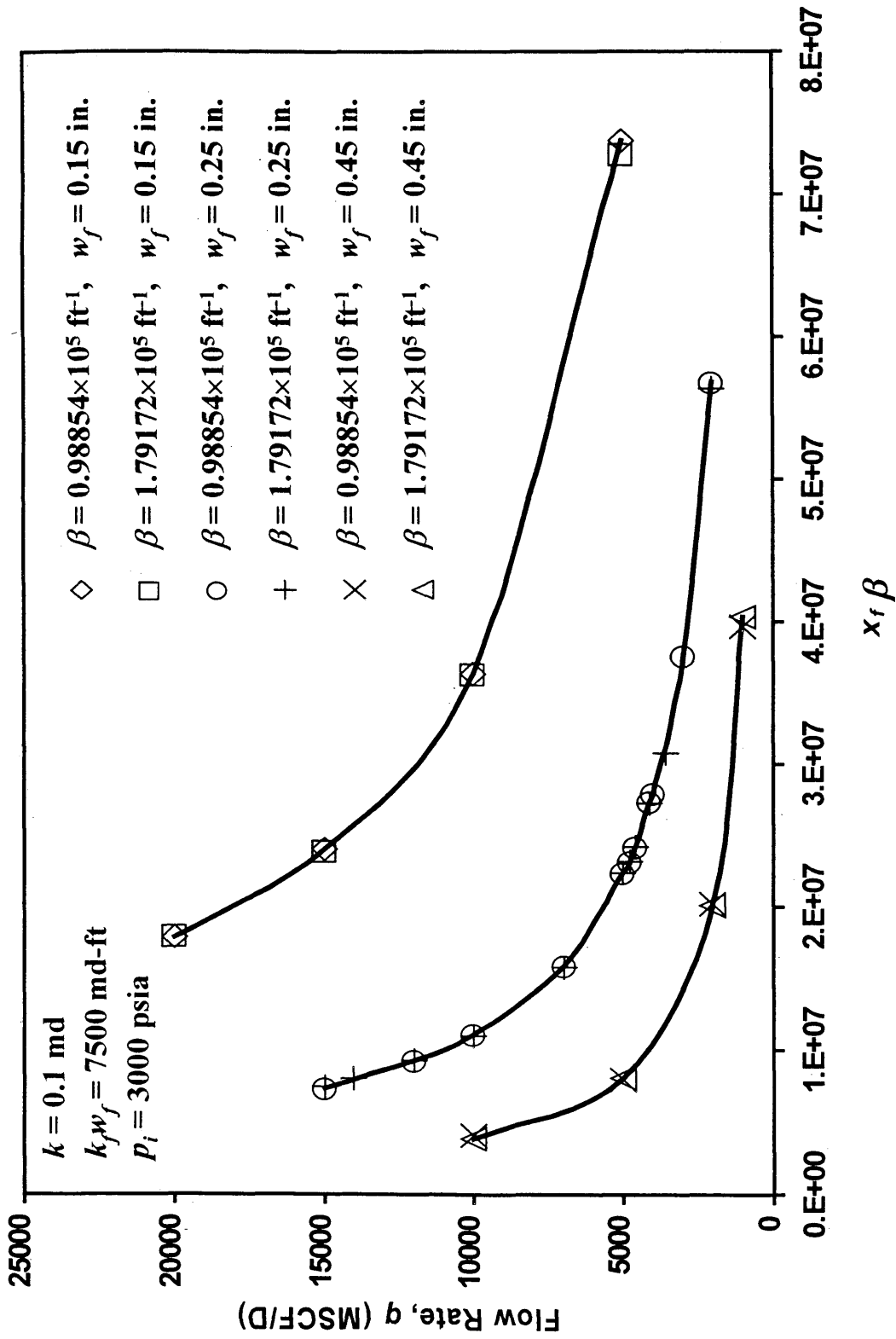


Fig. 2-10. q vs. $x_r \beta$ for different β coefficients and fracture widths

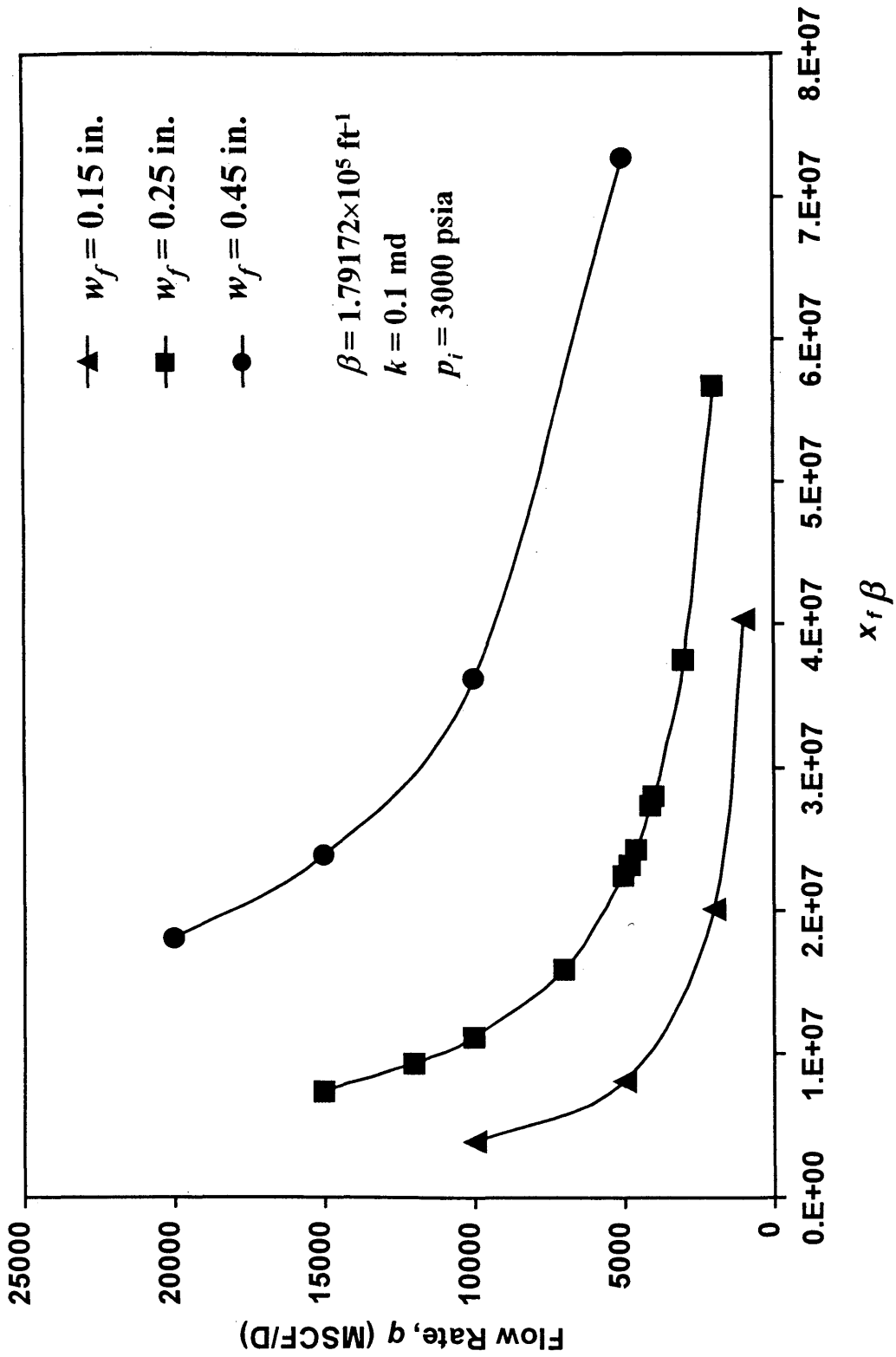


Fig. 2-11. q vs. $x_f \beta$ for different fracture widths

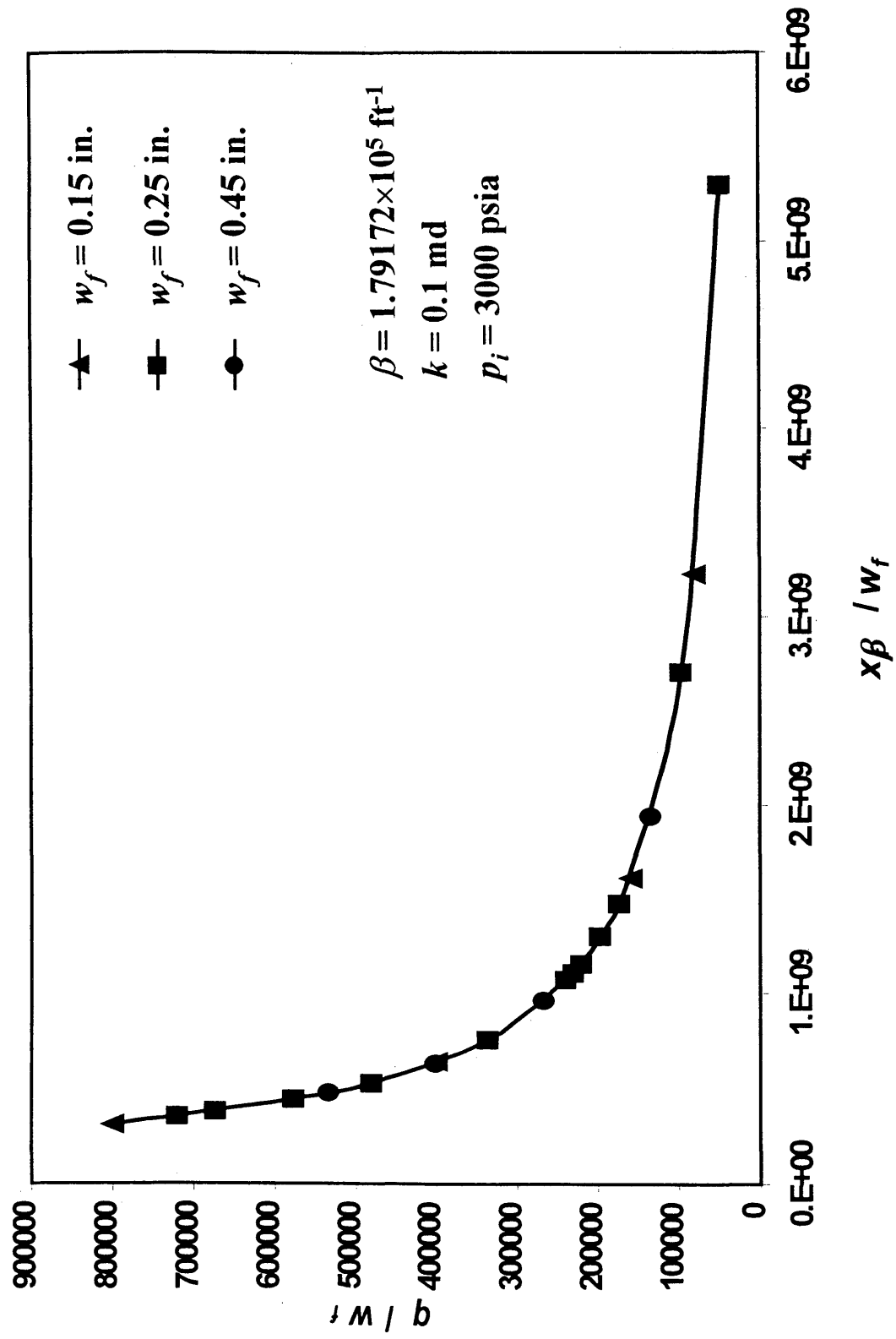


Fig. 2-12. Non-Darcy Flow correlation: q/w_f vs. $x\beta/w_f$

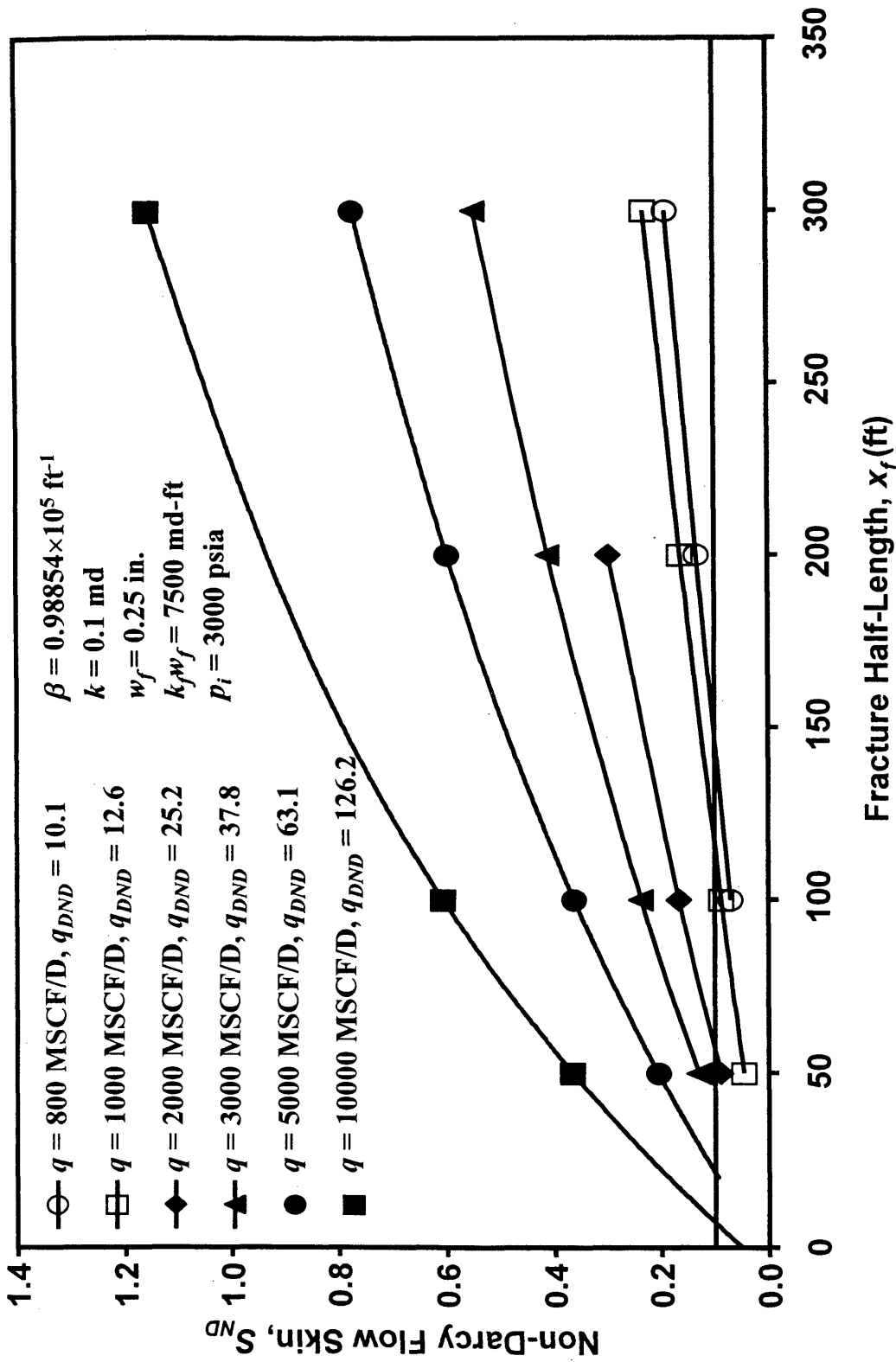


Fig. 2-13. Non-Darcy flow skin vs. fracture half-length for $k = 1 \text{ md}$

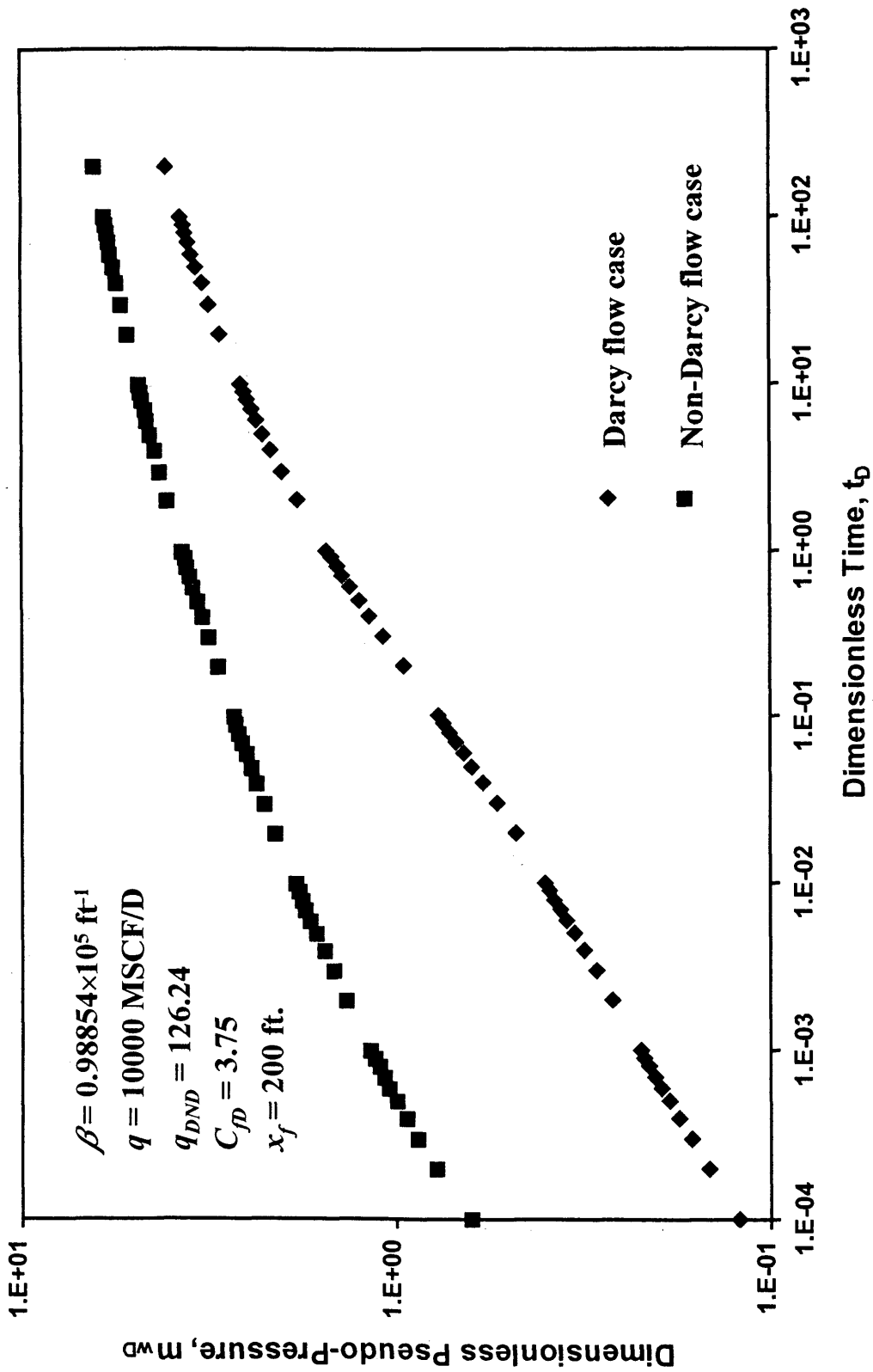


Fig. 2-14. Non-Darcy flow skin for $k = 10 \text{ md}$

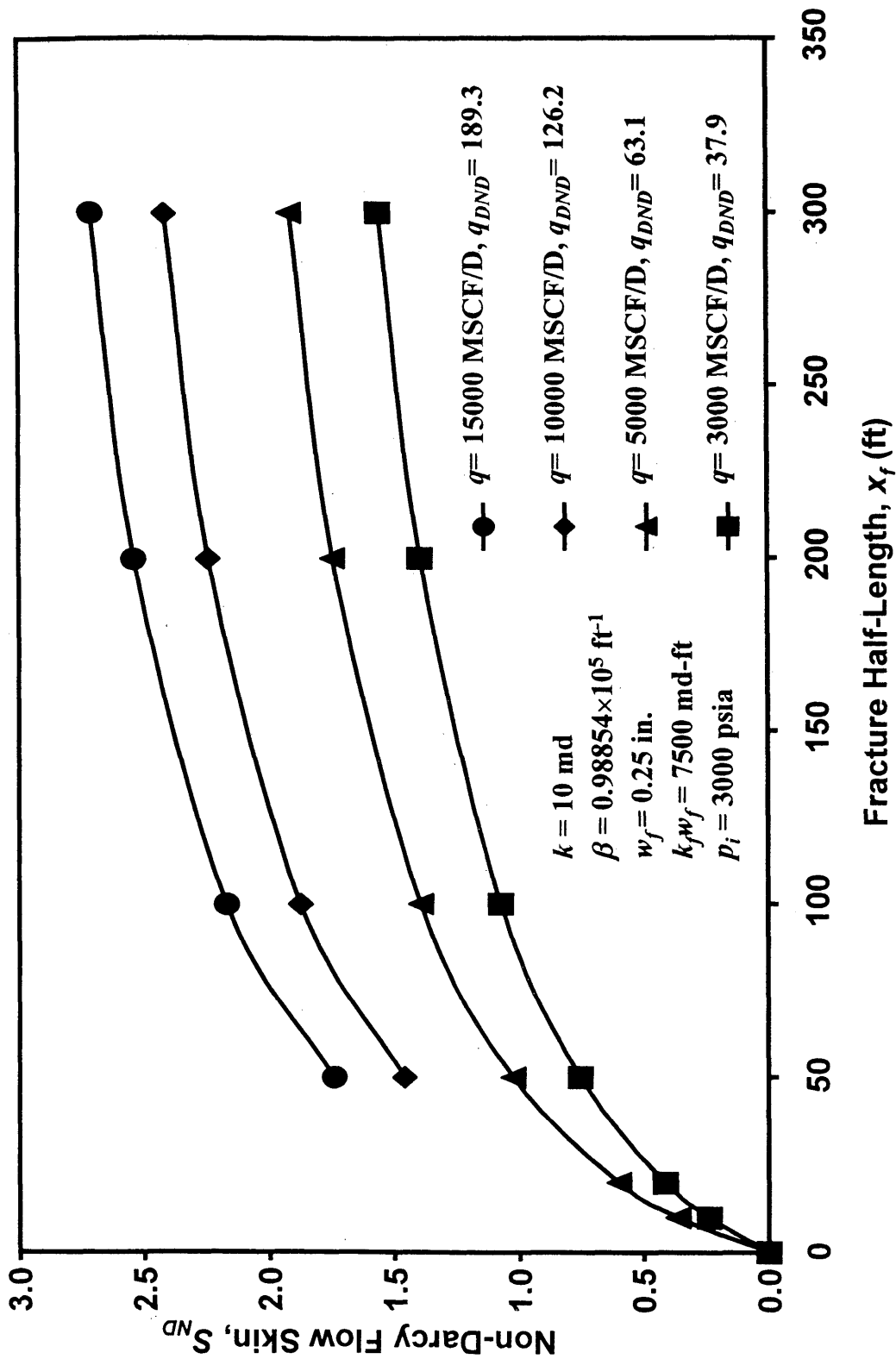


Fig. 2-15. Non-Darcy flow skin vs. fracture half-length for $k = 10 \text{ md}$

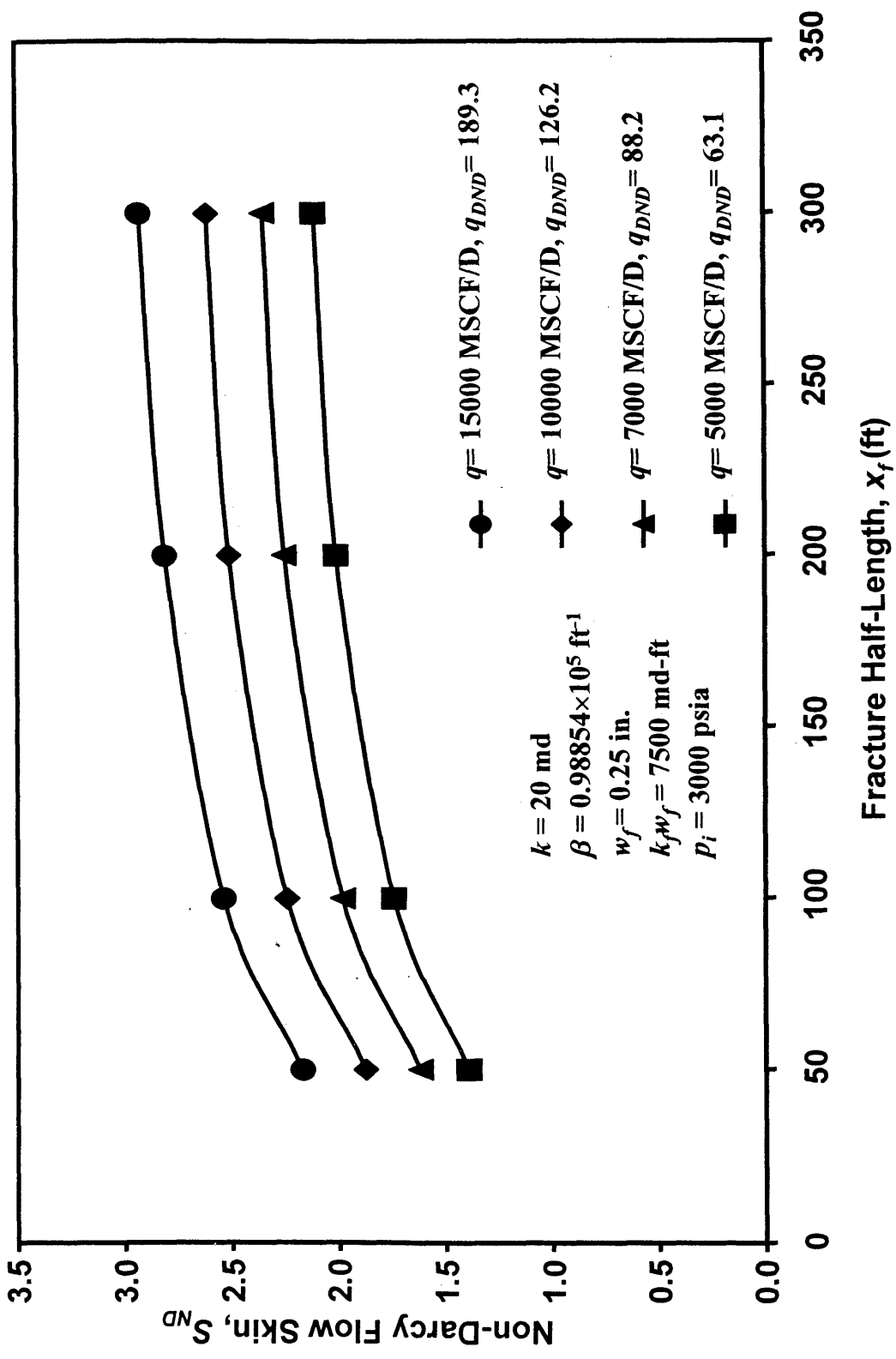


Fig. 2-16. Non-Darcy flow skin vs. fracture half-length for $k = 20 \text{ md}$

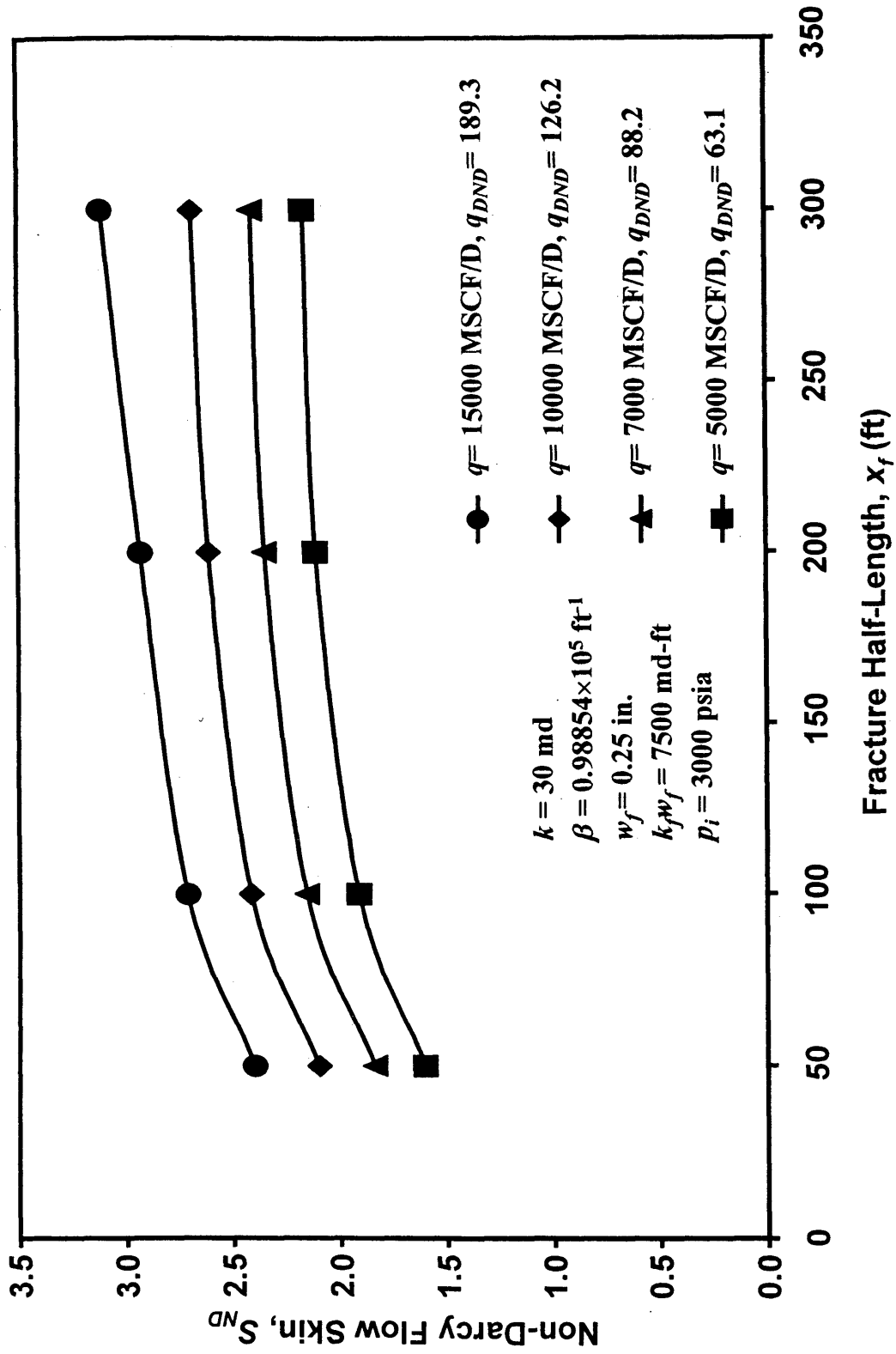


Fig. 2-17. Non-Darcy flow skin vs. fracture half-length for $k = 30 \text{ md}$

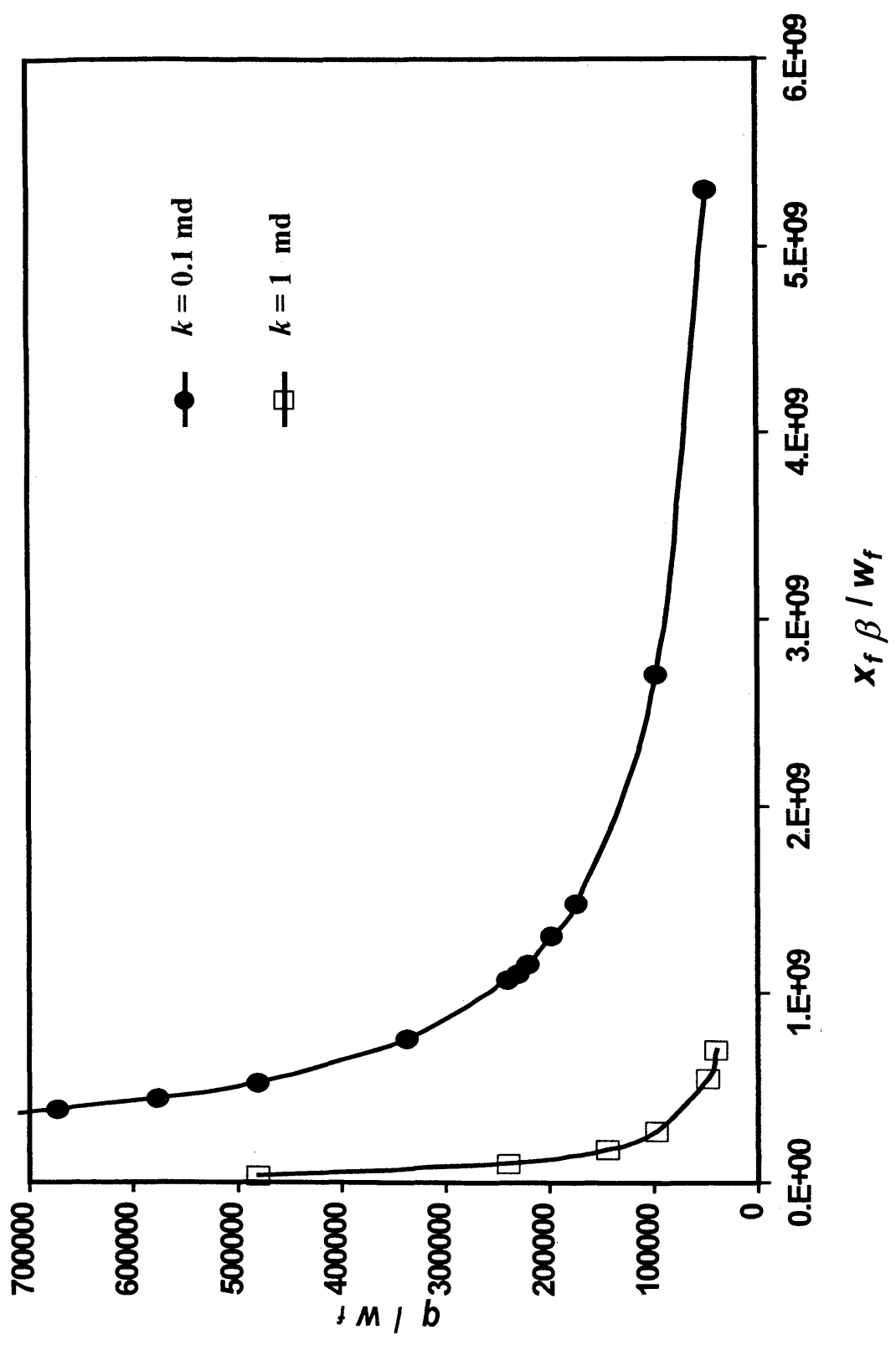


Fig. 2-18. q/w_f vs. $x_f \beta / w_f$ for different k values

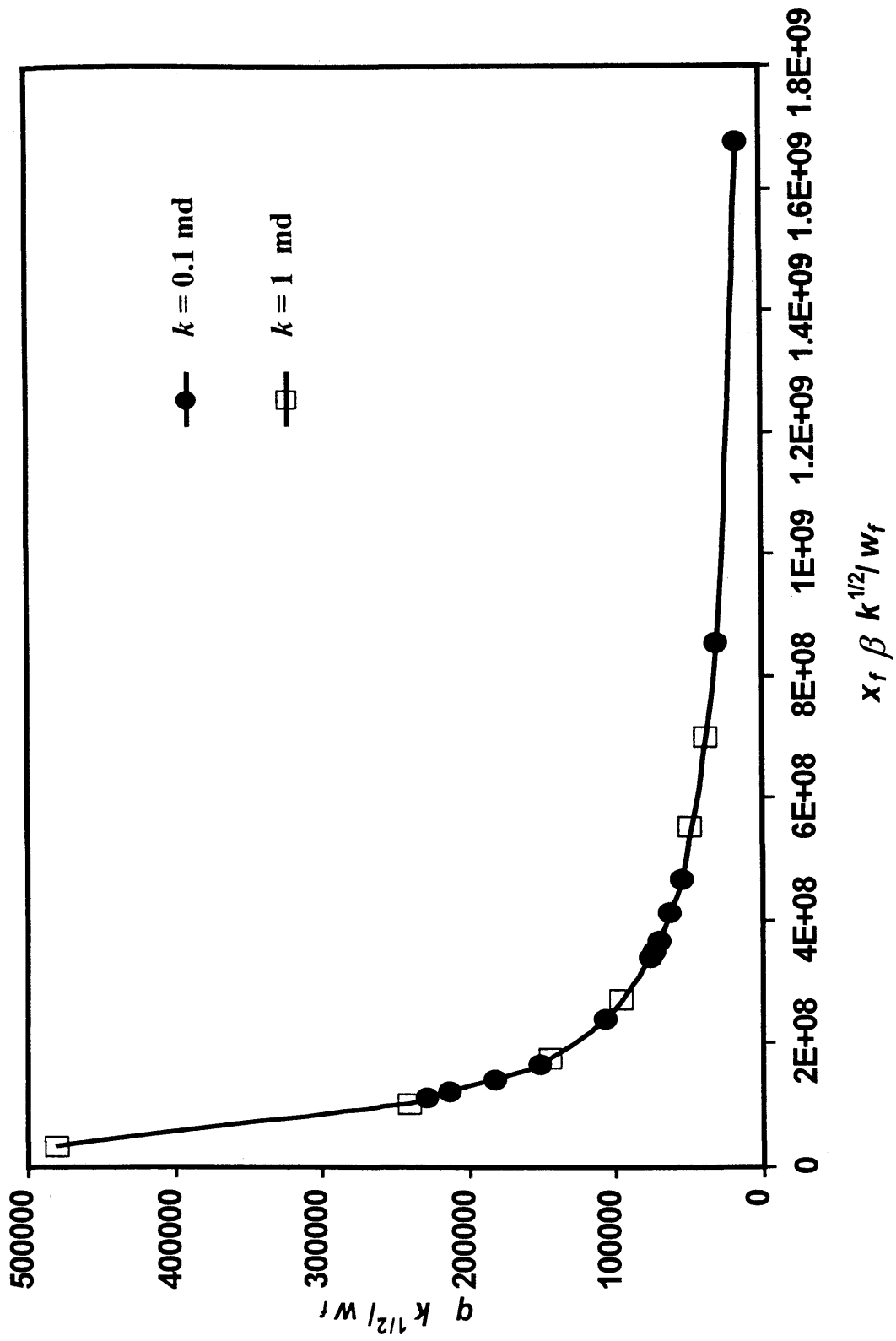


Fig. 2-19. Non-Darcy flow correlation: $(q k^{1/2})/w_f$ vs. $(x_f \beta k^{1/2})/w_f$

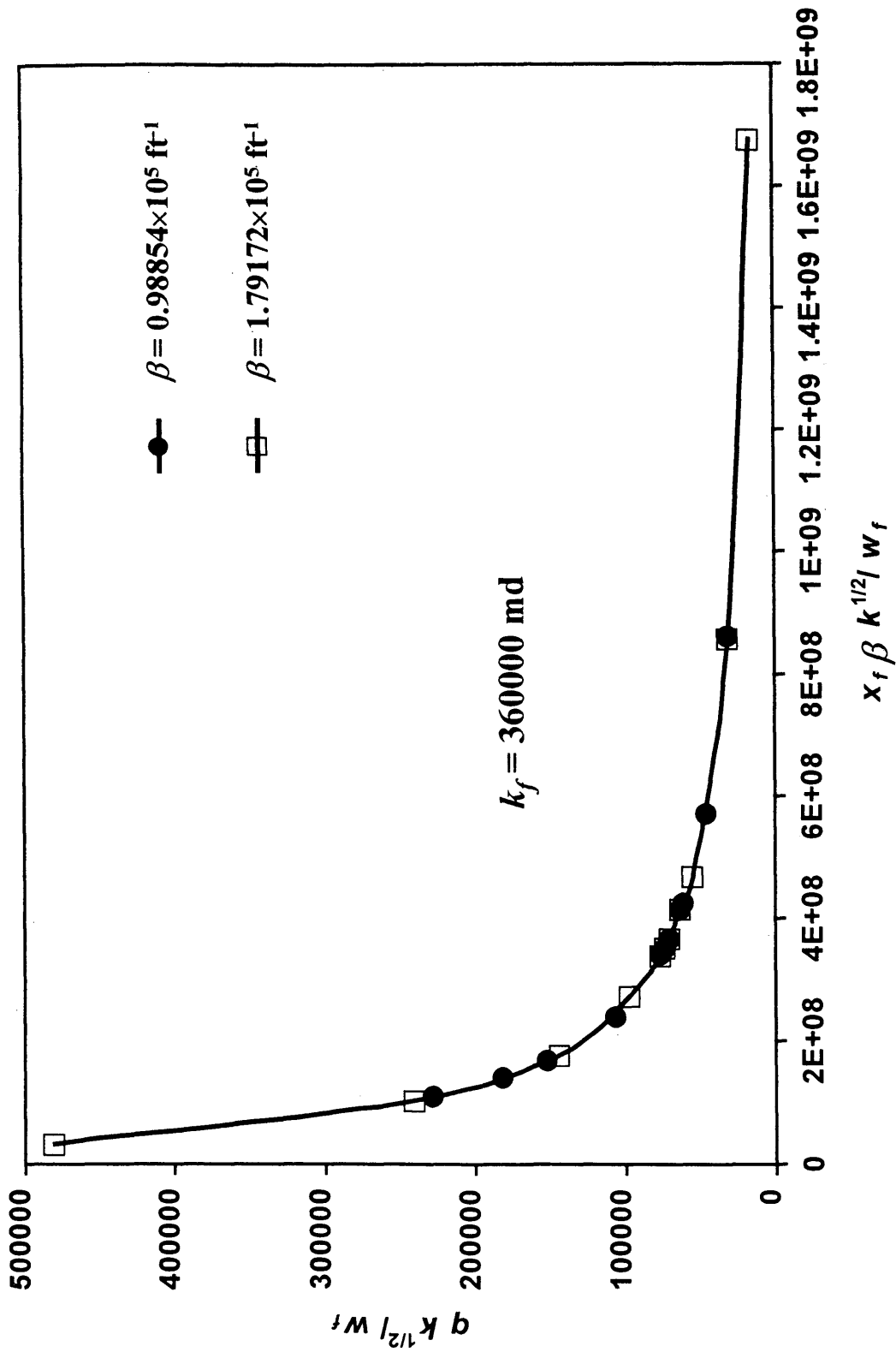


Fig. 2-20. $(q k^{1/2})/w_f$ vs. $(x_f \beta k^{1/2})/w_f$ for $k_f = 360000 \text{ md}$

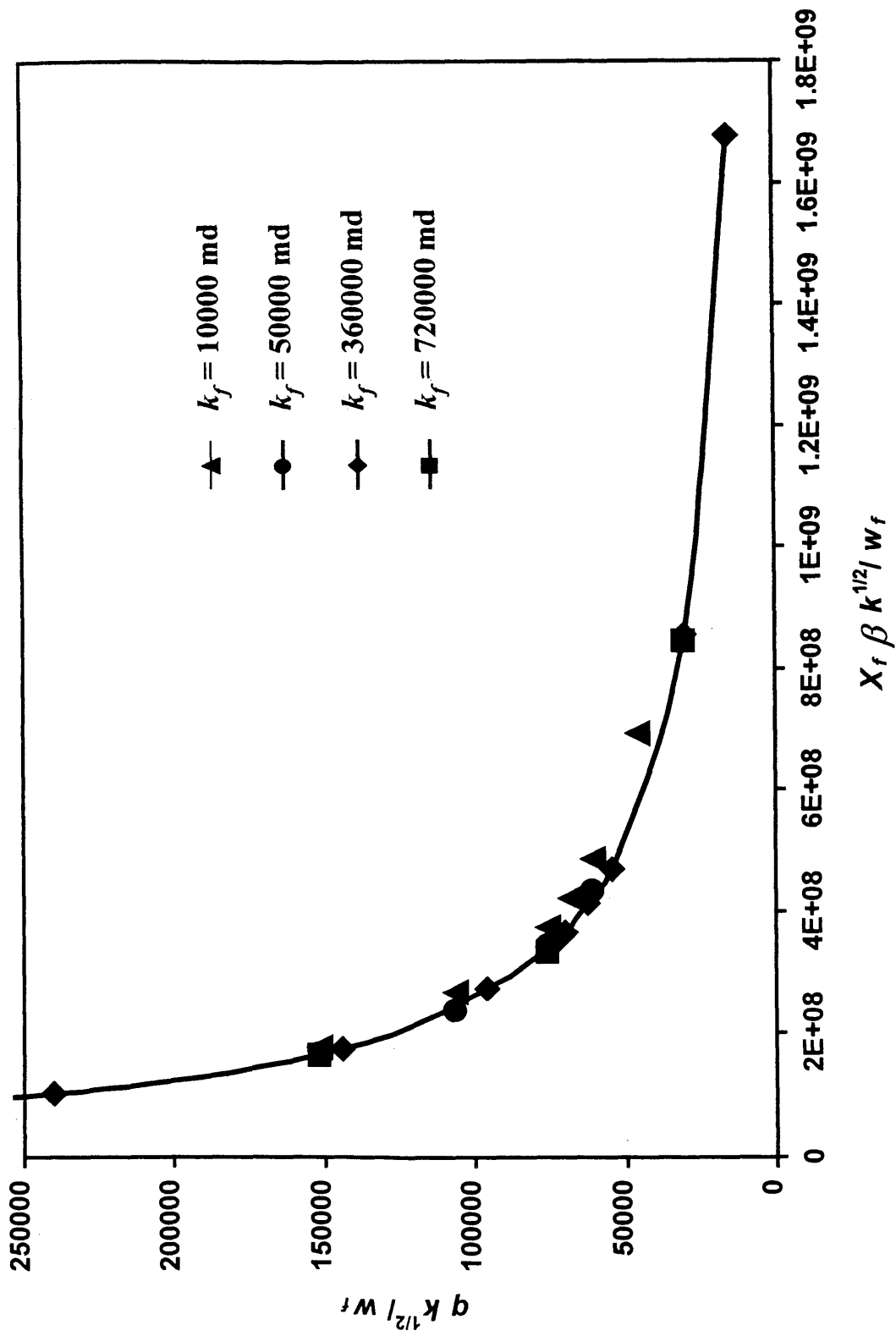


Fig. 2-21. $(q k^{1/2})/w_f$ vs. $(x_r \beta k^{1/2})/w_f$ for all k_f values

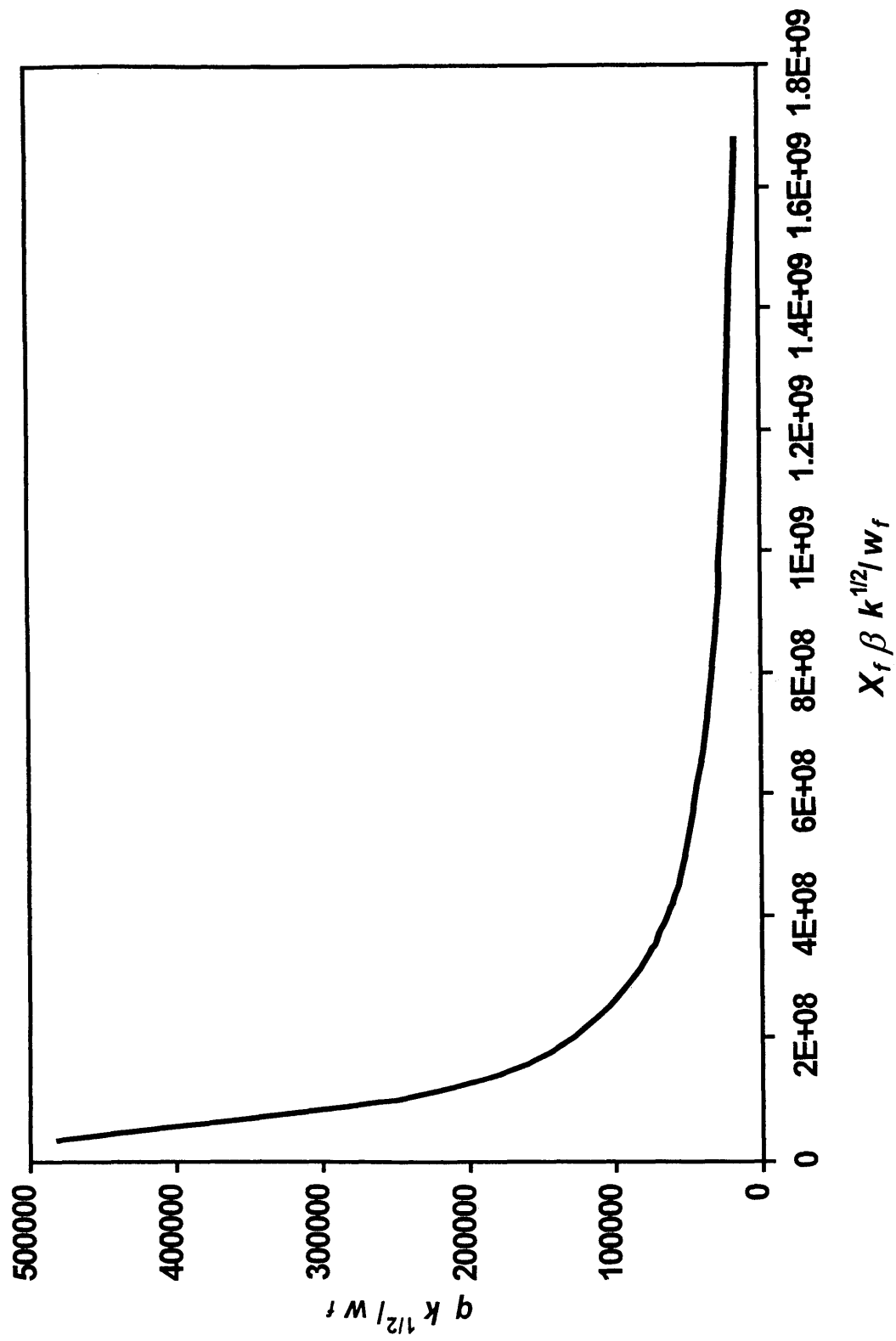


Fig. 2-22. Non-Darcy flow correlation after considering the effect of k_f ; $(q k^{1/2})/w_f$ vs. $(x_f \beta k^{1/2})/w_f$

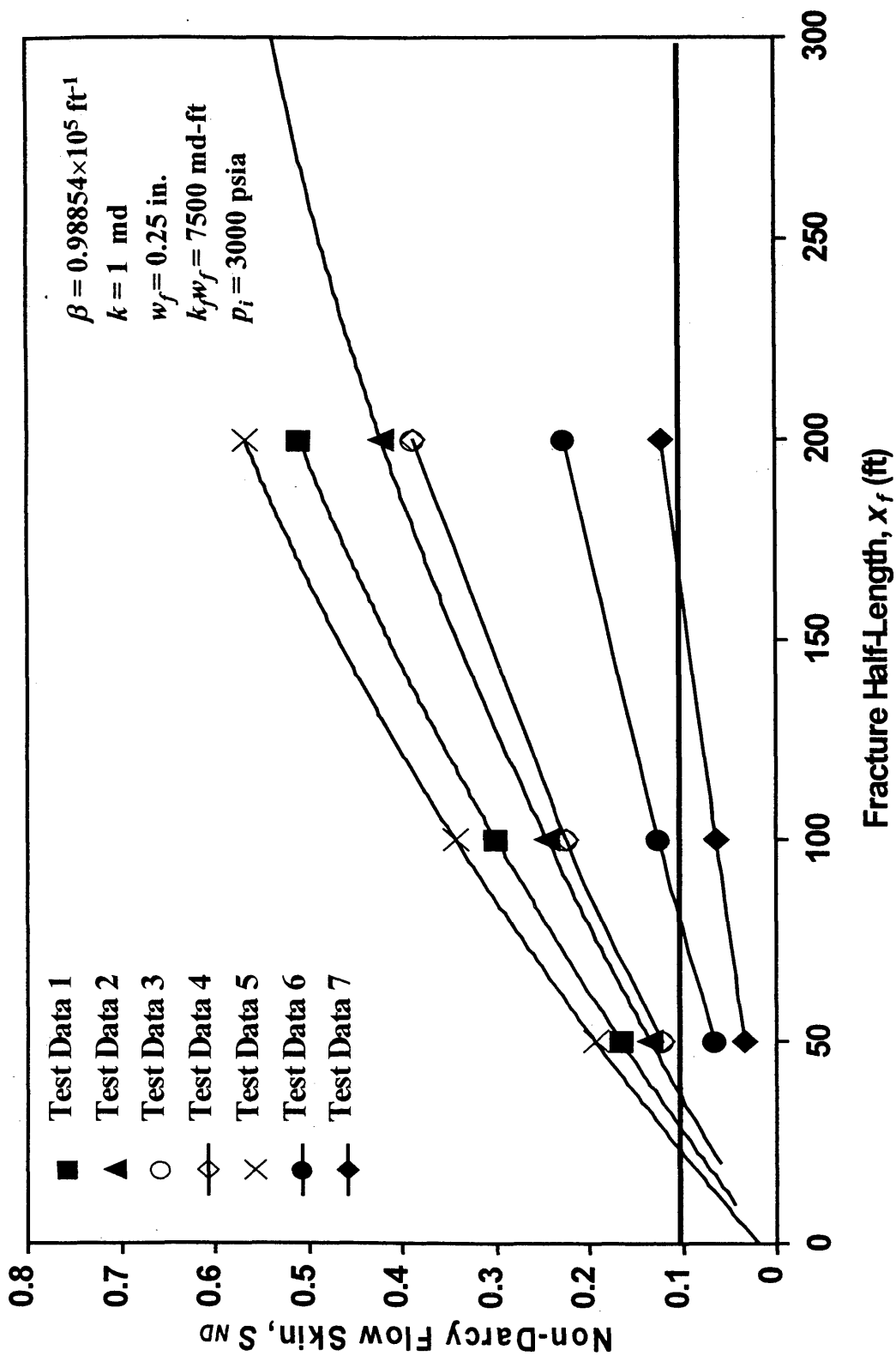


Fig. 2-23. S_{ND} vs. x_f plot for the test cases

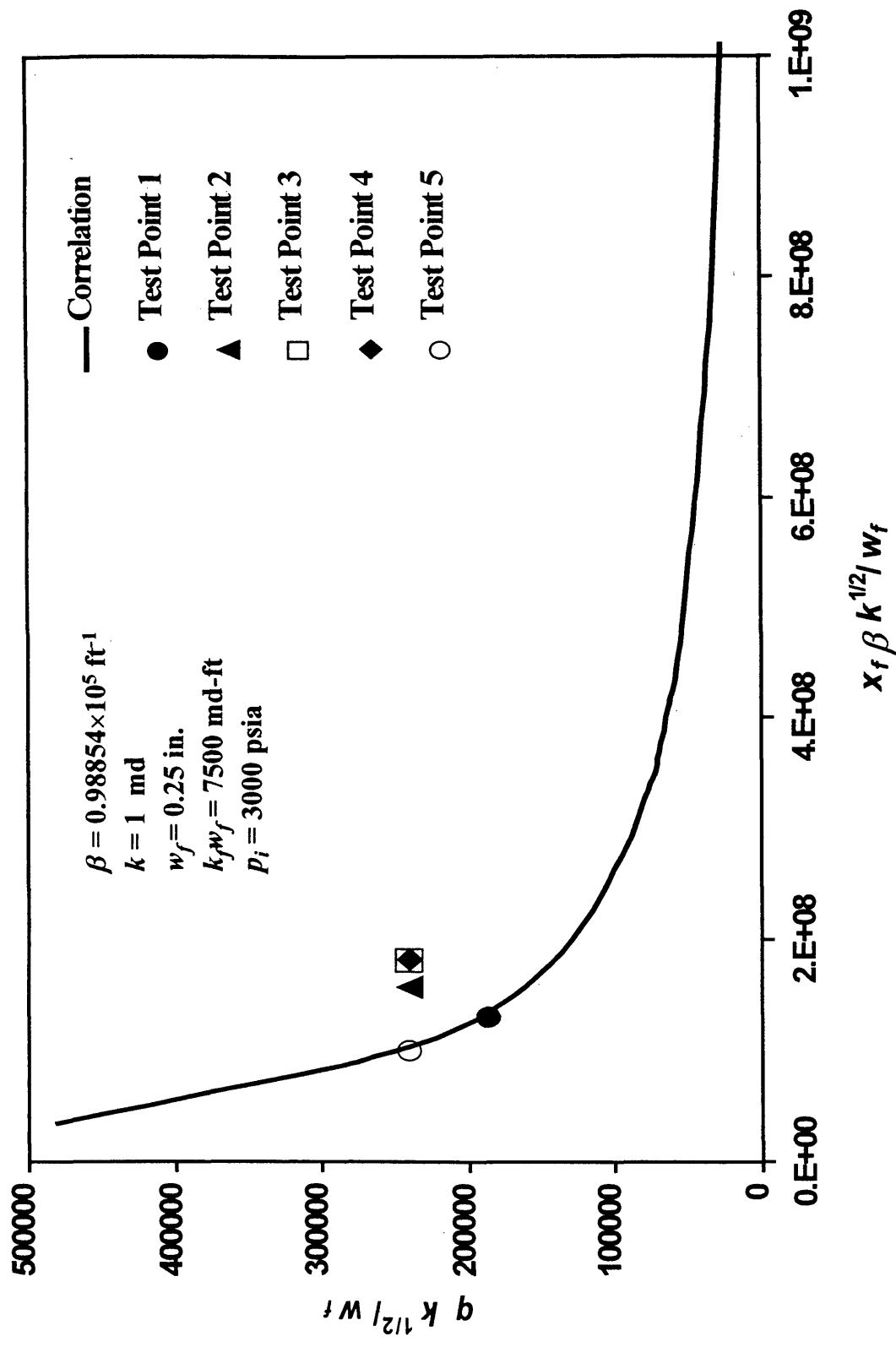


Fig. 2-24. Test points plotted on partial correlation

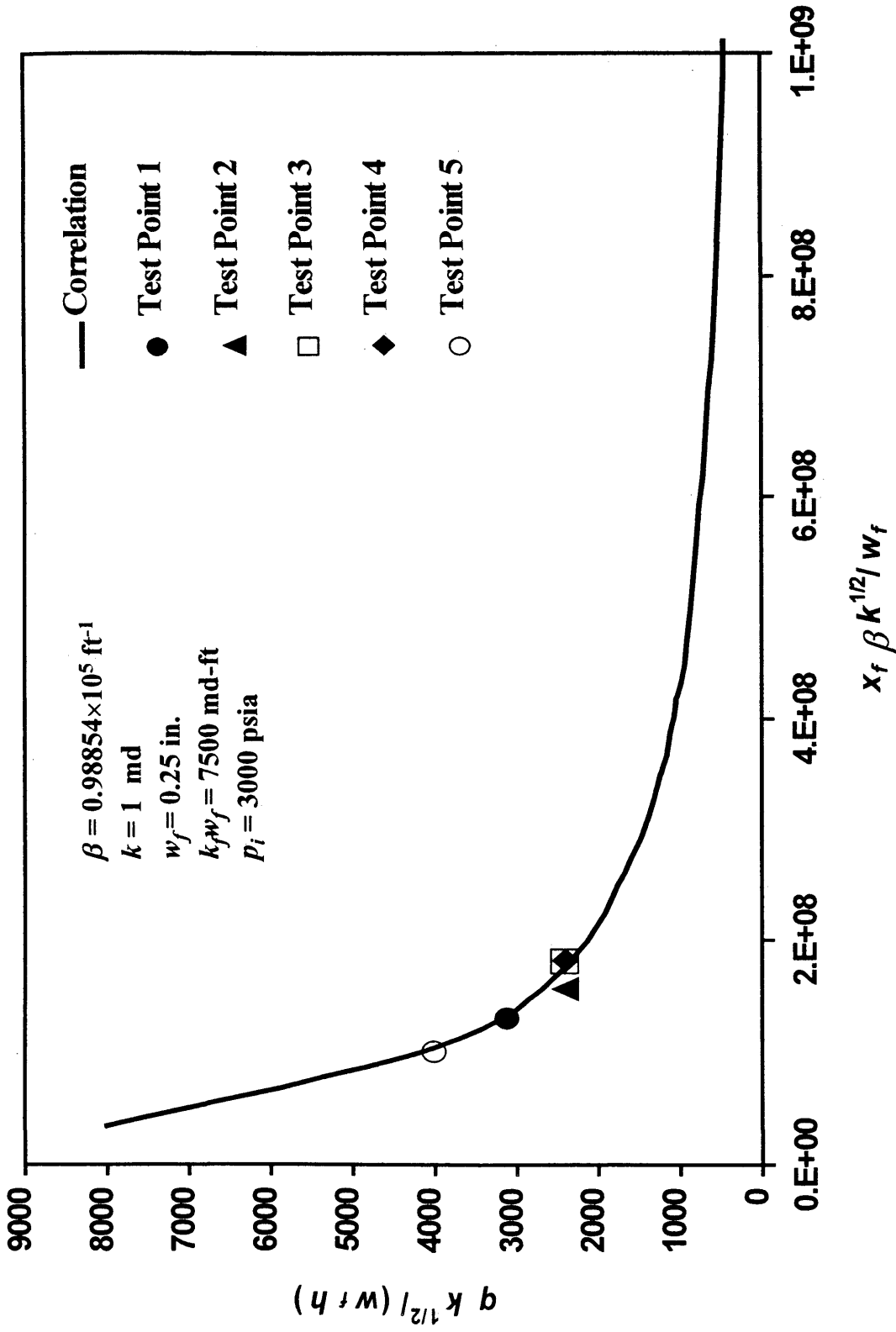


Fig. 2-25. Incorporating h to the correlation.

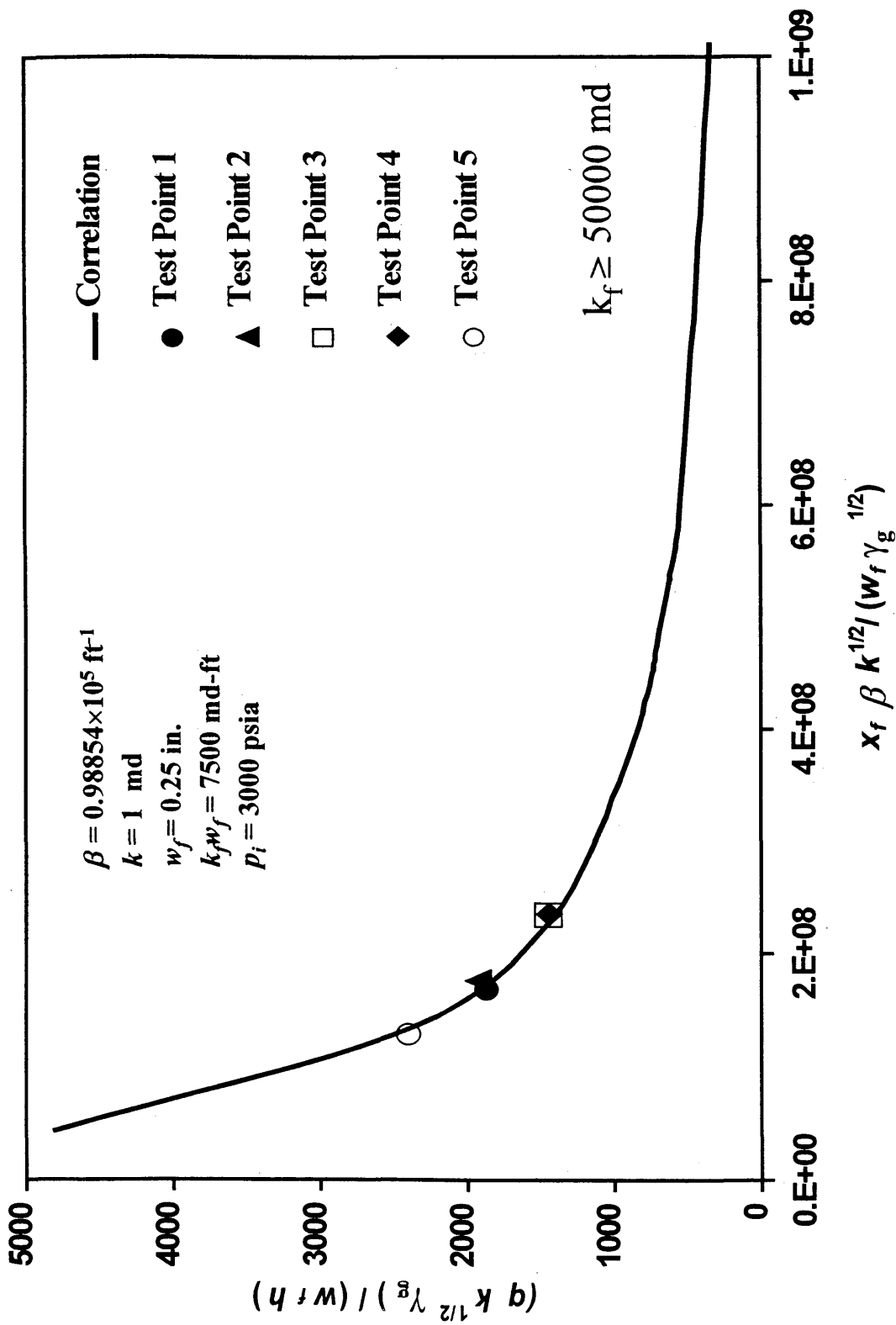


Fig. 2-26. Incorporating γ_g to the correlation

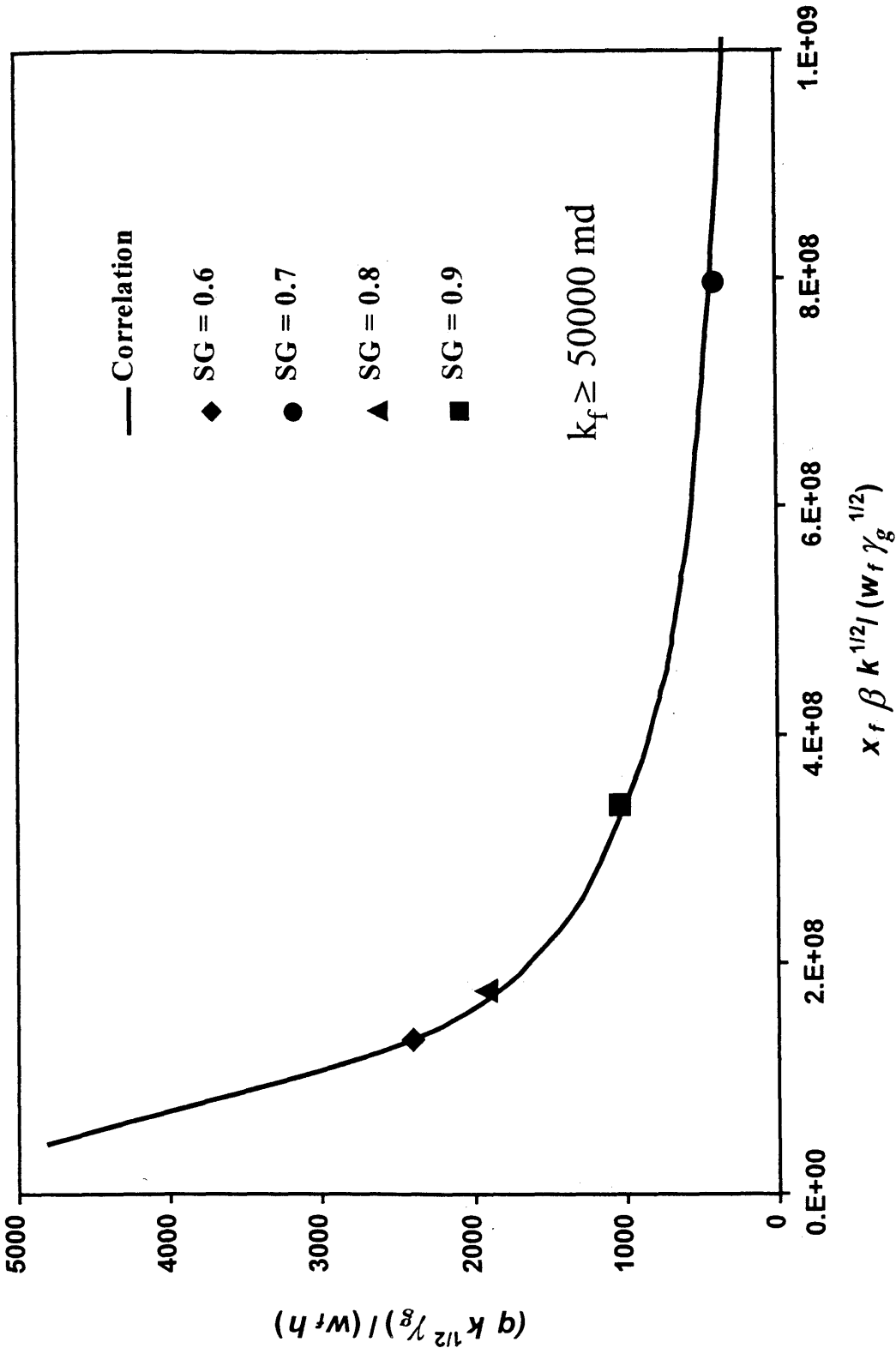


Fig. 2-27. Testing the correlation for different values of γ_g

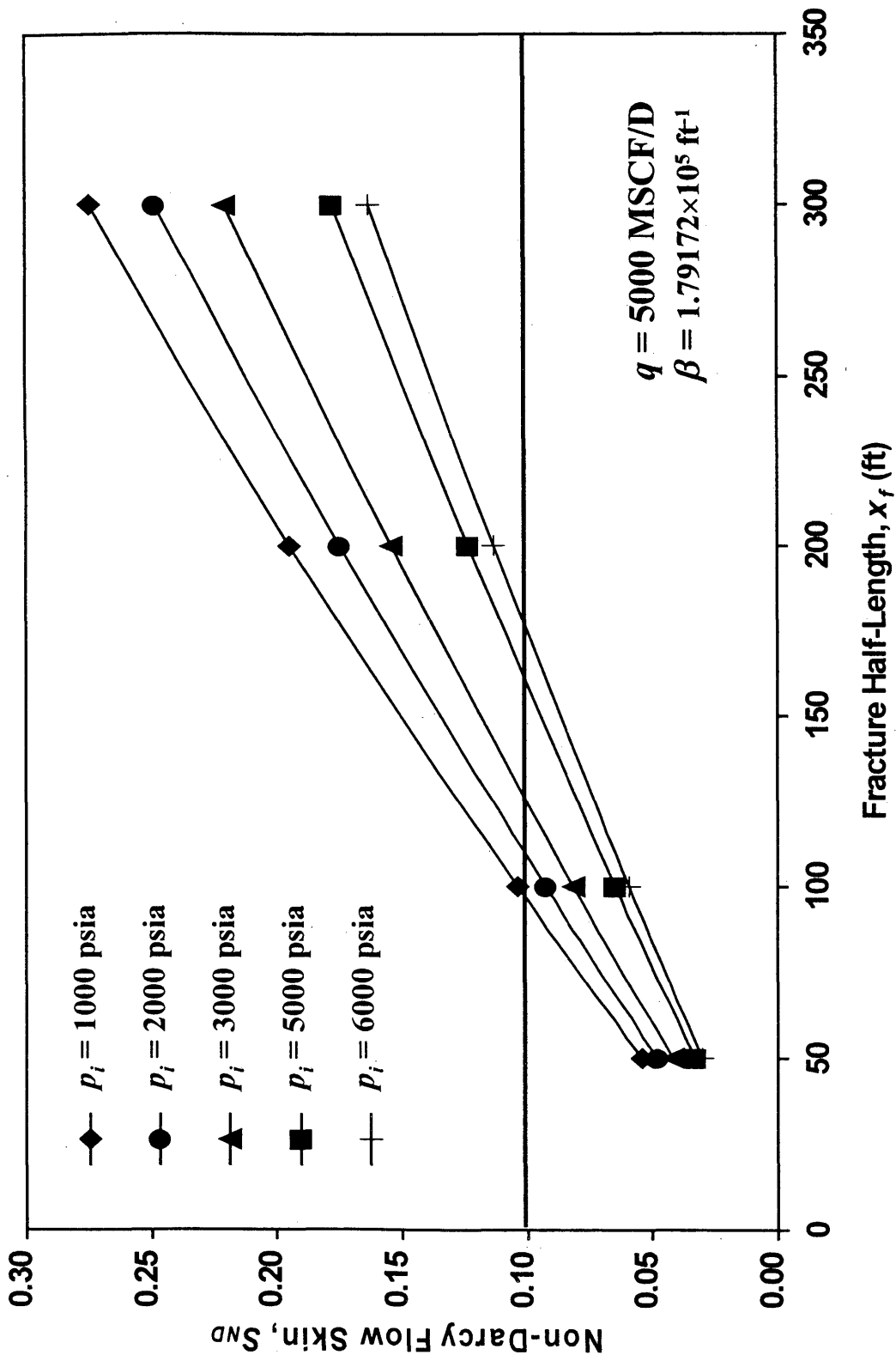


Fig. 2-28. S_{ND} vs. x_f for different p_i values

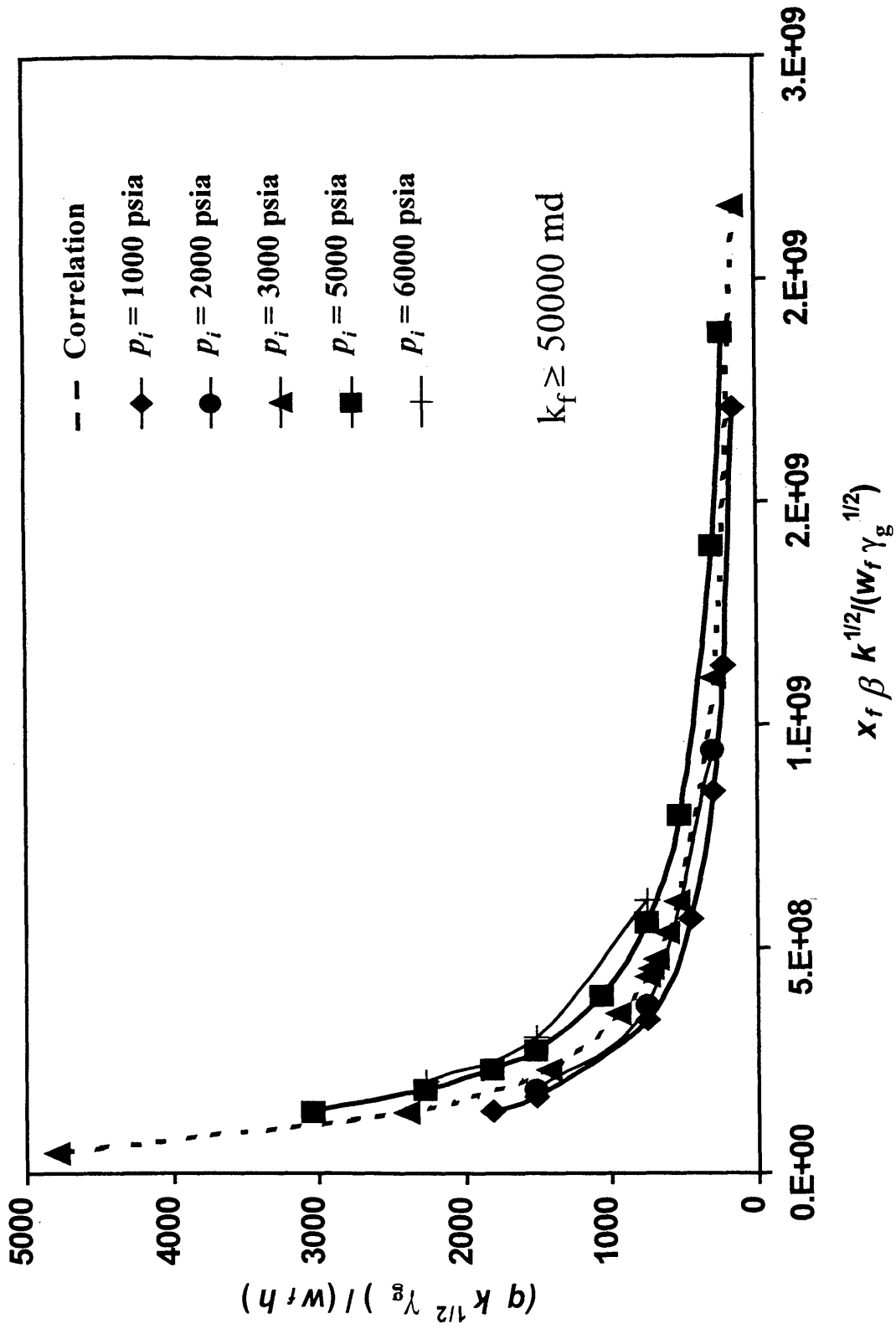


Fig. 2-29. Effect of p_i on the correlation

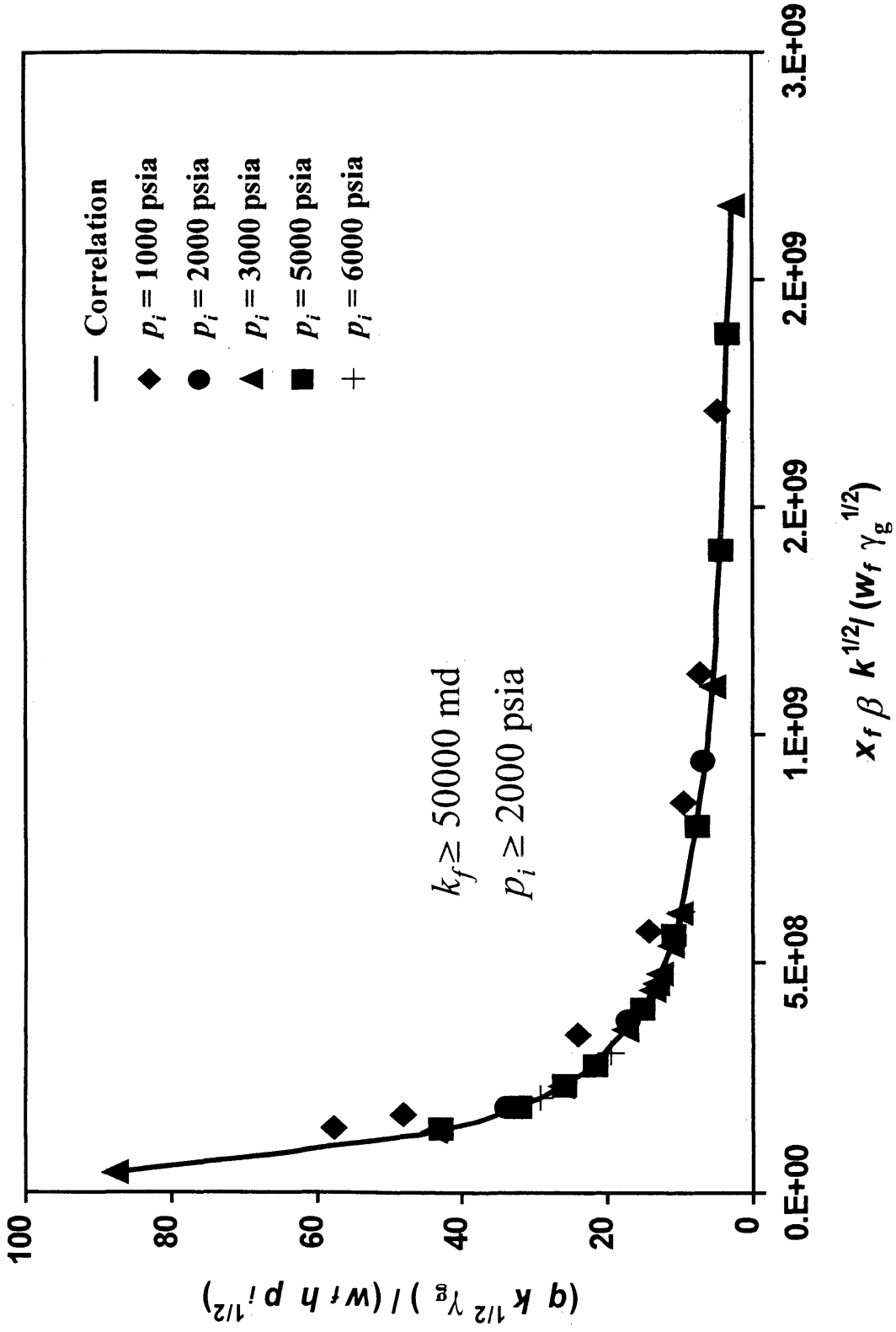


Fig. 2-30. Correlating initial reservoir pressure

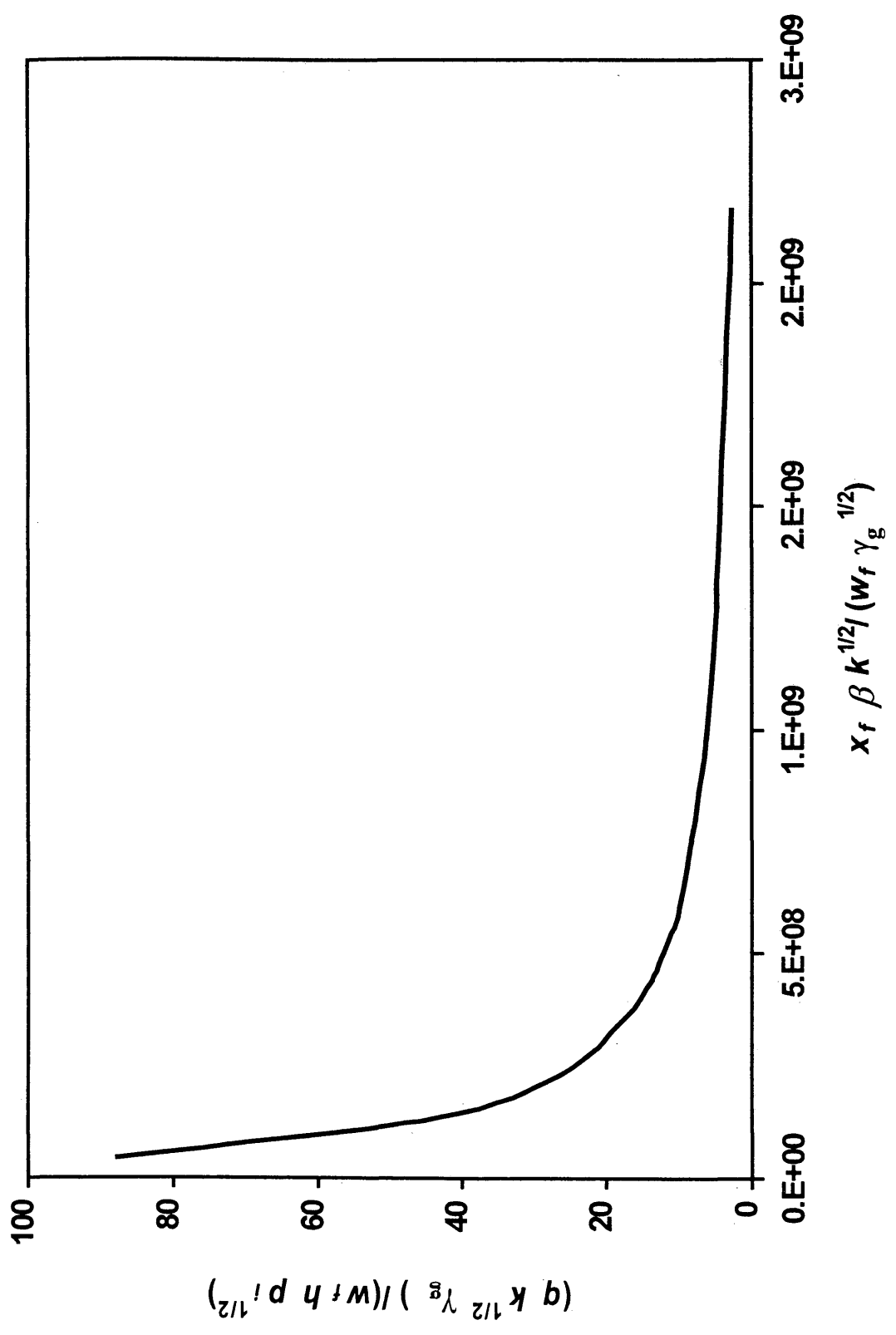


Fig. 2-31. Final correlation

CHAPTER 3

NON-DARCY FLOW AND PRODUCTIVITY

3.1 Objectives

The correlation developed in Chapter 2 is a beneficial tool to predict the conditions for which the non-Darcy flow should be of concern. This is important especially in well testing where fracture non-Darcy flow complicates the analysis and causes erroneous test interpretations. In such situations, the correlation developed in this study can be used to determine the test rates to minimize non-Darcy flow effects. For production purposes, however, non-Darcy flow may not be avoided. As explained in Chapter 2, Section 2.9.4, as the reservoir permeability increases no practical design or flow rate reduction may be able to minimize the non-Darcy flow effects. In these cases, fracture design and production decisions are simply based on the overall productivity. For example, an increase in the fracture half-length improves the reservoir performance but also increases the non-Darcy flow pressure drop in the fracture. If the net effect is still a considerable productivity increase, then the additional fracture length may be justified regardless of the magnitude of the non-Darcy flow pressure drop.

The objective of this chapter is to discuss the reduction in productivity because of fracture non-Darcy flow effects. This is accomplished by using the productivity index and productivity ratio concepts. Because the main objective of this thesis is to improve transient pressure analysis, the discussion in productivity given here is brief and is presented for completeness.

3.2 Productivity Index in Gas Wells

The pseudo-pressure equation for a radial gas reservoir under pseudo-steady state conditions is given by

$$m(\bar{p}) - m(p_{wf}) = \frac{1422qT}{kh} \left[\ln\left(\frac{r_e}{r_w}\right) - \frac{3}{4} + s \right], \quad \text{Eq. 3-1}$$

where

- s = skin factor,
- r_e = external reservoir radius, ft,
- r_w = wellbore radius, ft,
- \bar{p} = average reservoir pressure, psia,
- p_{wf} = bottomhole pressure, psia.
- q = gas flow rate, MSCF/D,
- T = reservoir temperature, °R,
- k = reservoir permeability, md,
- h = reservoir thickness, ft.

Eq. 3-1 can be also used for fractured wells by defining an effective wellbore radius. The effective wellbore radius, r'_w , is defined as the radius of an unfractured well to produce the same flow rate as the fractured well for a given drawdown. Cinco-L and Samaniego-V.¹² presented the effective wellbore radii of finite-conductivity fractures as a function of dimensionless fracture conductivity, C_{fD} . A reproduction of their effective wellbore radius vs. C_{fD} plot is shown in Fig. 3-1. Therefore, assuming that the mechanical skin, $s = 0$, the pseudo-pressure equation for a hydraulically fractured gas well under pseudo-steady state conditions is given by

$$m(\bar{p}) - m(p_{wf}) = \frac{1422qT}{kh} \left[\ln\left(\frac{r_e}{r'_w}\right) - \frac{3}{4} \right], \quad \text{Eq. 3-2}$$

If non-Darcy flow is present in the fracture, Eq. 3-2 can be modified to incorporate the non-Darcy flow skin, S_{ND} , as follows:

$$m(\bar{p}) - m(p_{wf}) = \frac{1422qT}{kh} \left[\ln\left(\frac{r_e}{r'_w}\right) - \frac{3}{4} + S_{ND} \right]. \quad \text{Eq. 3-3}$$

The above equations can now be used to define the productivity index. The productivity index, J , is defined as the drawdown, $\Delta m(p)$ (psi²/cp), required to produce at a certain flow rate, q (MSCF/D); that is,

$$J = \frac{q}{\Delta m(p)}. \quad \text{Eq. 3-4}$$

Applying this concept to Eq. 3-2, the productivity index of a fractured well with Darcy flow, J_D , is given by

$$J_D = \frac{kh}{1422T \left[\ln\left(\frac{r_e}{r'_w}\right) - \frac{3}{4} \right]}. \quad \text{Eq. 3-5}$$

Using Eqs. 3-3 and 3-4 the productivity index for a fractured well influenced by non-Darcy flow is obtained as follows:

$$J_{ND} = \frac{kh}{1422T \left[\ln\left(\frac{r_e}{r'_w}\right) - \frac{3}{4} + S_{ND} \right]}. \quad \text{Eq. 3-6}$$

To analyze the productivity behavior when non-Darcy flow is of concern, it is useful to introduce the concept of productivity ratio, PR . This can be defined as the ratio of the productivity indices for the non-Darcy and Darcy flow cases as follows:

$$PR = \frac{J_{ND}}{J_D}. \quad \text{Eq. 3-7}$$

Thus, substituting Eqs. 3-5 and 3-6 into Eq. 3-7, we obtain

$$PR = \frac{\ln\left(\frac{r_e}{r'_w}\right) - \frac{3}{4}}{\ln\left(\frac{r_e}{r'_w}\right) - \frac{3}{4} + S_{ND}} . \quad \text{Eq. 3-8}$$

3.3 Discussion of Productivity Ratio, PR

Here we considered some examples to discuss the productivity ratio as defined in Eq. 3-8. To calculate the productivity ratio, an 80-acre spacing was considered (the reservoir radius, r_e , is 1053 ft). The properties used in these analyses are given in Table 2-3 and correspond to the base case, except for those shown on the plots. The non-Darcy flow skin values were obtained from the semi-analytical model discussed in Chapter 2 and the effective wellbore radius, r'_w , was obtained from the work of Cinco-L and Samaniego-V¹² (Fig. 3-1). The productivity ratio (or productivity reduction due to non-Darcy flow) was examined as a function of fracture half-length, x_f , for different cases. The analyses of the results are discussed below.

Fig. 3-2 represents the effect of reservoir permeability, k , on the productivity ratio. Note that PR decreases as x_f increases. This is easy to understand by recalling Eq. 2-3, repeated below for convenience

$$C_{fD} = \frac{k_f w_f}{k x_f} \quad \text{Eq. 2-3}$$

It can be seen from this equation that if x_f increases, the dimensionless conductivity, C_{fD} , decreases causing a reduction in the efficiency of the fracture. Also, as x_f increases, fluid travels a longer distance within the fracture under non-Darcy flow conditions and this increases the non-Darcy flow pressure drop. Therefore, the non-Darcy flow skin, S_{ND} , is high and from Eq. 3-6, the non-Darcy productivity index becomes smaller and the productivity ratio decreases. (It should be emphasized that this work only considers non-

Darcy flow in the fracture. In general, reservoir non-Darcy flow effects are expected to decrease as the fracture length increases, which is contrary to the observations here for the case with non-Darcy flow in the fracture only.)

Another point to discuss is the decrease in PR as the reservoir permeability, k , increases. It has been shown that in moderate to high permeability reservoirs, the non-Darcy flow effects may be difficult to avoid. In these cases, even for relatively low permeabilities, the reduction in productivity may be considerable. Fig. 3-2 shows that for a fracture half-length of $x_f = 300$ ft, changing the reservoir permeability from 0.1 to 1 md the additional reduction in PR approaches 32%.

Fig. 3-3 shows, as expected, that PR decreases as the flow rate, q , increases for a fixed value of β . This effect is due to the increase in fracture flow velocities and thus non-Darcy flow pressure drop.

The effect of non-Darcy flow coefficient, β , on PR , can be seen on Fig. 3-4. Note that the $PR = 1$ curve corresponds to the Darcy flow case and is plotted for reference. As β increases, the non-Darcy flow pressure drop increases, causing the decrease in production. Even $\beta = 0.98854 \times 10^5 \text{ ft}^{-1}$, which is the lowest value considered in this study, is responsible for a productivity decrease of 16% for $x_f = 300$ ft.

As displayed on Fig. 3-5, an increase in fracture width, w_f , decreases the flow velocities in the fracture and reduces the non-Darcy flow effects, causing an increase on PR .

In Chapter 2 it was concluded that an increase in p_i causes the non-Darcy flow skin, S_{ND} , to decrease. This leads to an increase in the productivity ratio as illustrated in Fig. 3-6.

The fracture permeability was the last parameter studied. Fig. 3-7 shows that the decrease in the productivity ratio is almost constant for $k_f = 50000$, 360000 , and 720000 md. The productivity reduction resulting from a permeability change from 50000 to 720000 md does not reach 1% for $x_f = 300$ ft. However, a slightly different behavior is observed for $k_f = 10000$ md. The difference in PR between $k_f = 10000$ and $k_f = 50000$ md is 3.2%. This behavior should be expected from our earlier observation on Chapter 2 that the $k_f = 10000$ md case did not follow the general correlation for the non-Darcy flow effects.

The brief discussion presented above concludes the investigation of the productivity reduction in this study. Because the basic objective of this work is to improve the analysis of well test data under the influence of fracture non-Darcy flow, the detailed investigation of productivity reduction is left for further research.

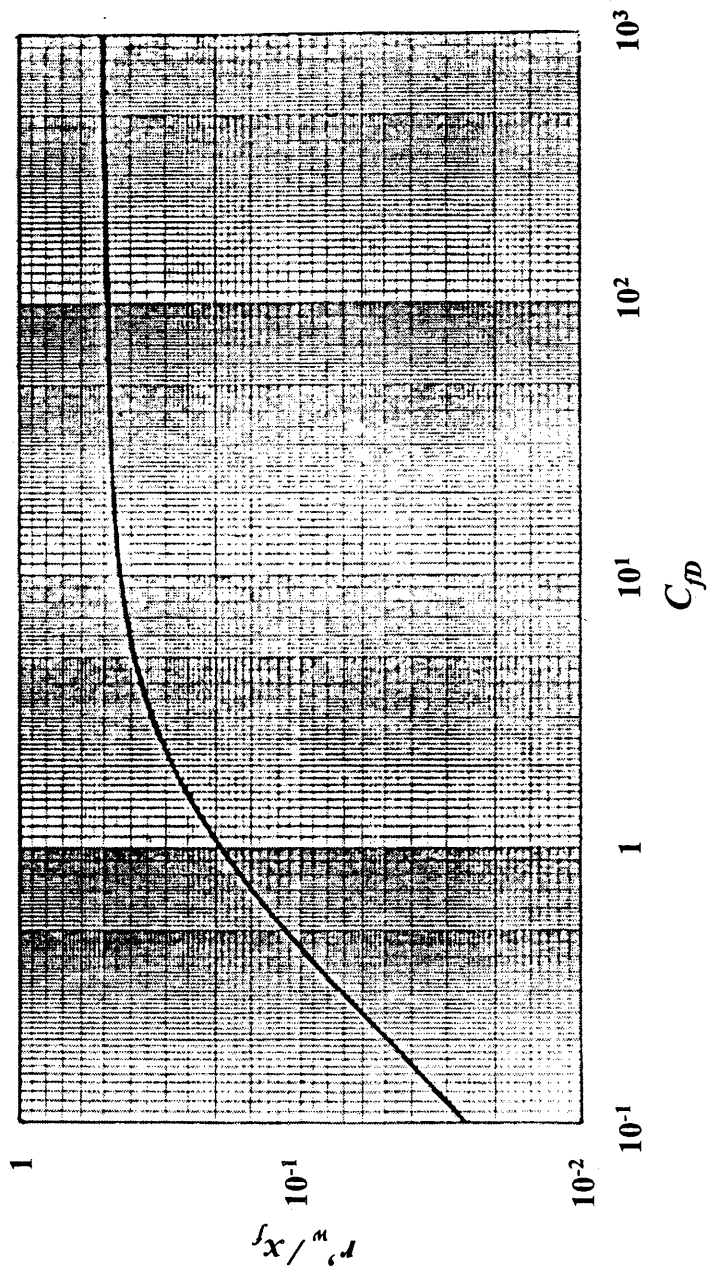


Fig. 3.1. Effective wellbore radius as a function of dimensionless conductivity
 (After Cinco-L and Samaniego-V "Transient Pressure Analysis for Fractured Wells," *JPT* (Sept. 1981) 1749.)

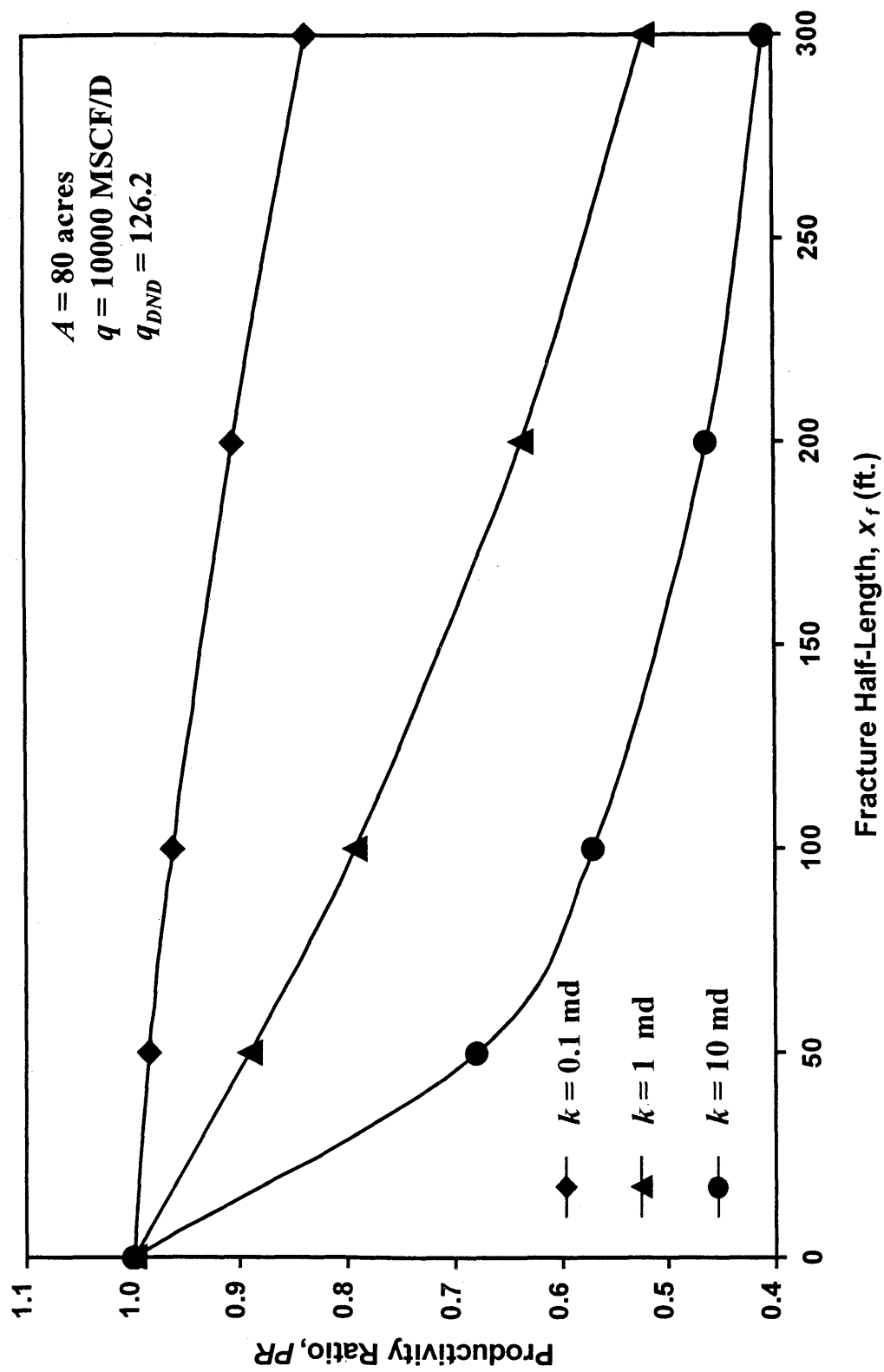


Fig. 3-2. Effect of reservoir permeability on the productivity ratio

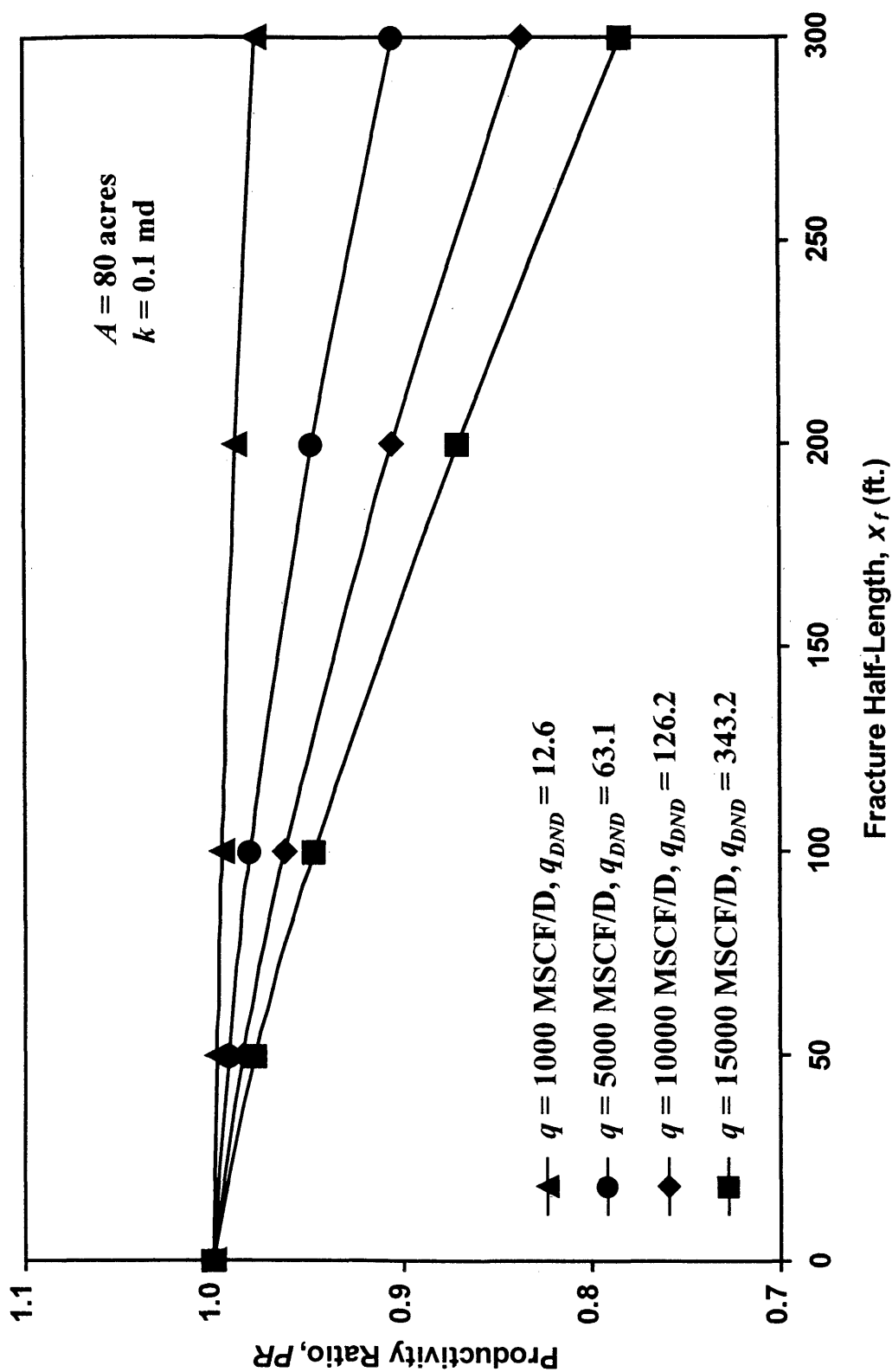


Fig. 3-3. Effect of flow rate on the productivity ratio

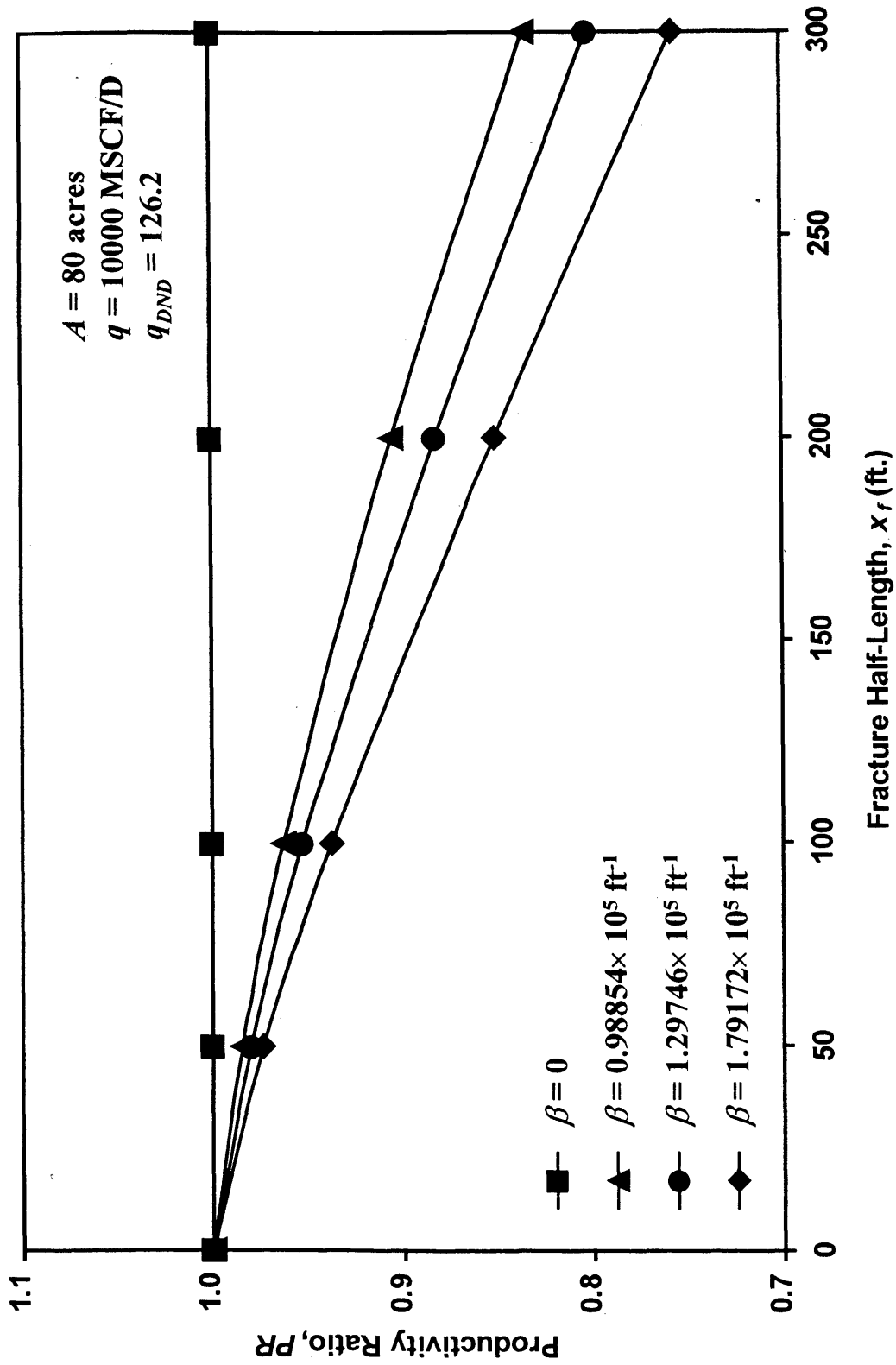


Fig. 3-4. Effect of non-Darcy flow coefficient on the productivity ratio

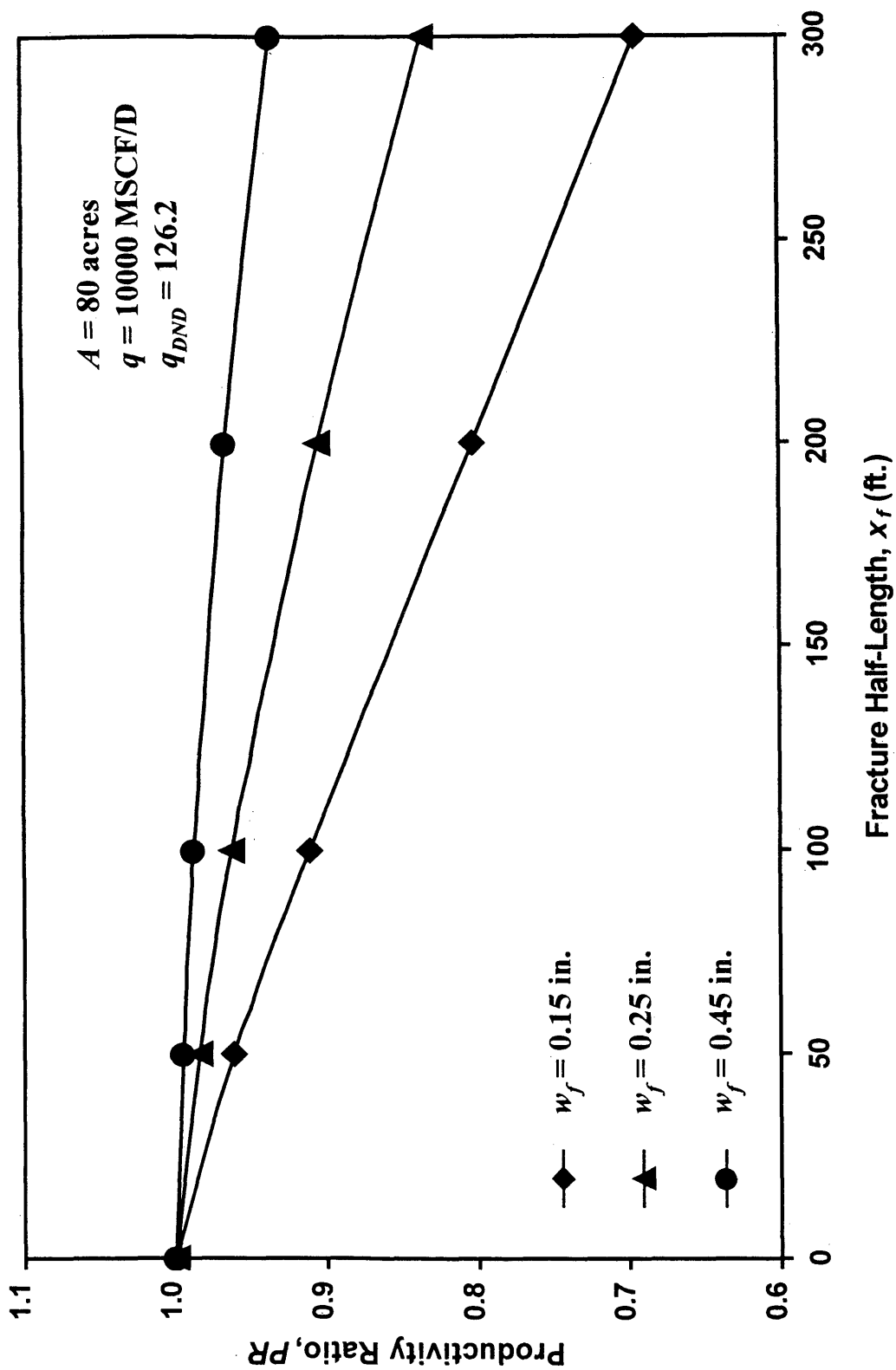


Fig. 3-5. Effect of fracture width on the productivity ratio

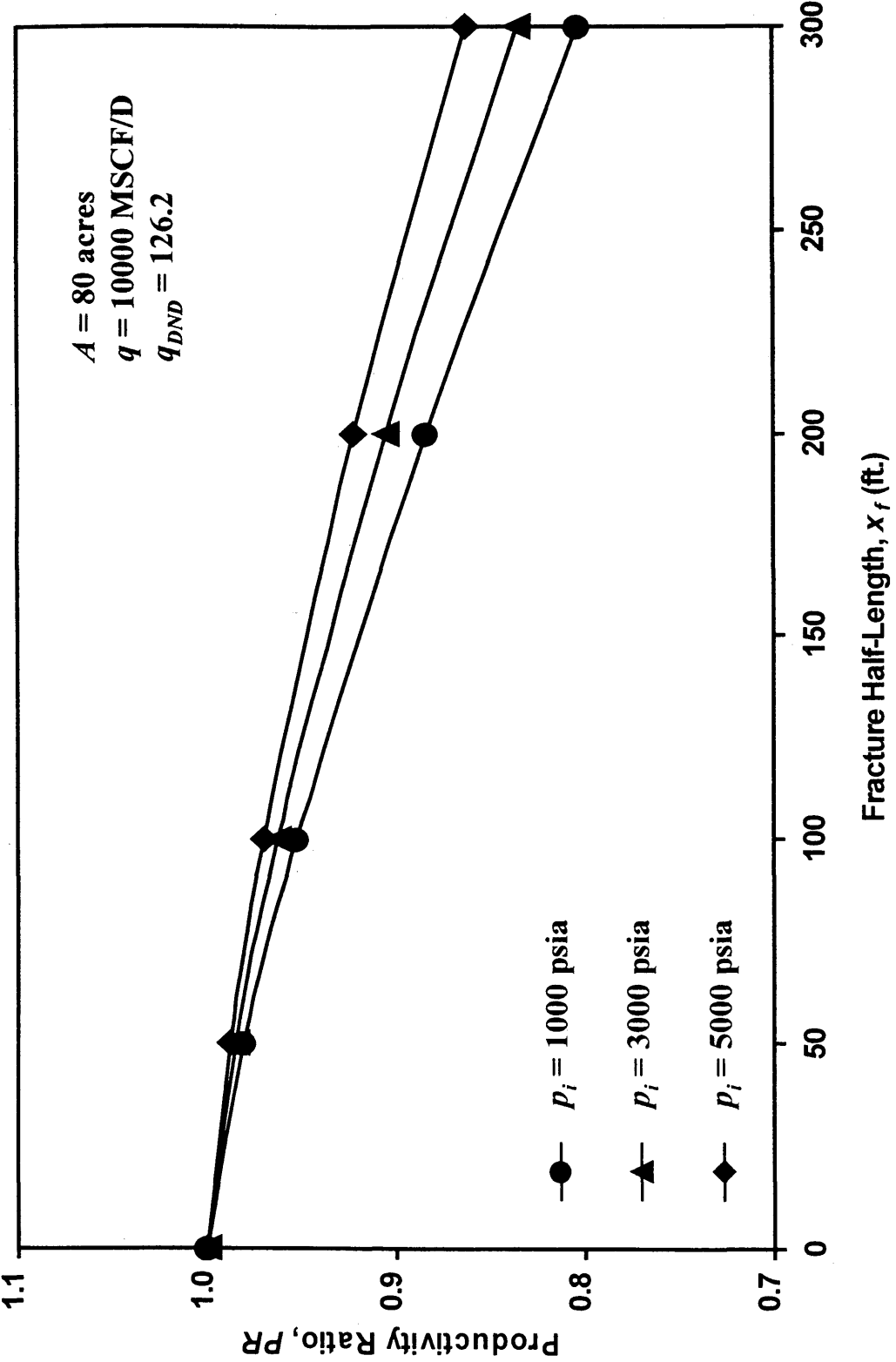


Fig. 3-6. Effect of initial reservoir pressure on the productivity ratio

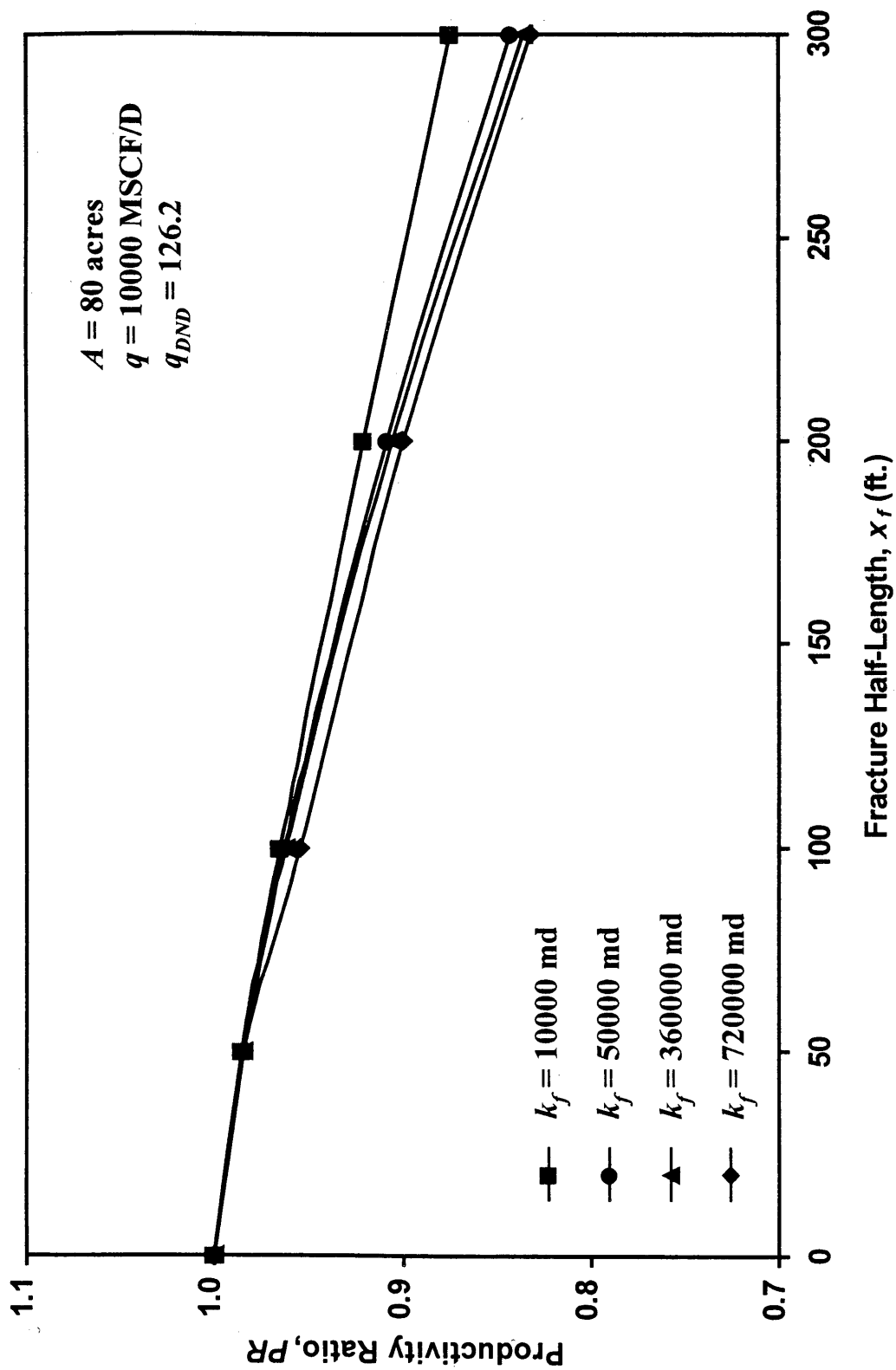


Fig. 3-7. Effect of fracture permeability on the productivity ratio

CHAPTER 4

ANALYSIS OF FRACTURED WELL TEST DATA IN THE PRESENCE OF NON-DARCY FLOW

4.1 Objectives

The analysis of fractured-well-tests in the presence of non-Darcy flow has been of interest since Millheim and Cichowicz¹ first investigated the subject in 1968. The conventional recommendation of conducting two well tests at two different flow rates⁴ is usually an unpractical proposition. Not only does it imply a higher investment, but also the delay of production. This chapter proposes an analysis technique in which only one test (with one flow rate) is sufficient, provided that bilinear and formation linear flow regimes are both present.

Guppy *et al.*⁴ and Umnuyayponwiwat *et al.*⁶, observed that under non-Darcy flow the transient pressure responses may be matched with the fracture type curves for the Darcy flow case for a lower apparent fracture conductivity. The apparent conductivity, C_{fDapp} , is a function of the non-Darcy dimensionless flow rate, q_{DND} , and the true conductivity, C_{fD} . Therefore, infinitely many combinations of q_{DND} and C_{fD} can be found to match the type curve, as long as they yield the same C_{fDapp} . The technique proposed in this study provides a unique solution so that the correct fracture and formation parameters can be computed from the analysis of the test. The analysis method is applicable even when wellbore storage masks part of the flow regimes.

4.2 Theoretical Basis

This section explains the theoretical basis of the new analysis technique. The technique is based on the use of the analytical expressions for bilinear and linear flow regimes in finite-conductivity fractures. For the bilinear flow period, two different analytical models

are presented, one is based on the combination of Guppy *et al.*⁴ and Cinco-L. *et al.*¹² works, and the second is based on the work of Gidley¹³, Guppy *et al.*⁴, and Cinco-L. *et al.*¹². The linear flow regime utilizes the results of Camacho-V.¹⁴ and Cinco-L. *et al.*¹². This analysis technique uses the concept of apparent fracture conductivity, C_{fDapp} , to derive the working expressions.

4.2.1 Bilinear Flow Regime

At early times, two flow regimes are characteristic in fractured wells: fracture linear and bilinear flow. During fracture linear flow, the real time is usually so small that this flow regime cannot be identified in well tests. Because the bilinear flow occurs relatively later, the possibility to identify this second flow regime is higher. Therefore, following Guppy *et al.*⁴, bilinear flow regime is used to develop a new technique to analyze well tests influenced by non-Darcy flow in the fracture.

4.2.1.1 Combination of Guppy *et al.*⁴ and Cinco-L. *et al.*¹² Theories

As explained at the beginning of this chapter, it has been observed that the non-Darcy flow responses could be matched with the Darcy flow responses for a lower, or apparent, conductivity, C_{fDapp} . This can be expressed as:

$$m_{wD}(C_{fD}, q_{DND}, t_D)_{non-Darcy} = m_{wD}(C_{fDapp}, t_D)_{Darcy} \quad \text{Eq. 4-1}$$

where

- m_{wD} = dimensionless pseudo-pressure,
- C_{fD} = dimensionless fracture conductivity,
- t_D = dimensionless time (based on fracture half-length),
- C_{fDapp} = dimensionless apparent fracture conductivity.

The apparent conductivity, C_{fDapp} , is a function of the non-Darcy dimensionless flow rate, q_{DND} , and the true conductivity, C_{fD} . Guppy *et al.*⁴ worked with a semi-analytical model to develop the following correlation that relates these three parameters:

$$\frac{C_{fD}}{C_{fDapp}} = 1 + 0.31q_{DND} \cdot \quad \text{Eq. 4-2}$$

The correlation presented on Eq. 4-2 is applicable for the following ranges:

1. For all values of q_{DND} that yield: $C_{fDapp} \geq 2$ and $C_{fD} < 10$.
2. For: $1 \leq q_{DND} \leq 20$ and $10 \leq C_{fD} \leq 100$.
3. For: $q_{DND} \leq 10$ and $100 \leq C_{fD} \leq 500$.

Cinco-L. and Samaniego-V.¹² proposed the following dimensionless pseudo-pressure equation for Darcy flow, $m_{wD,D}$, during the bilinear period:

$$m_{wD,D} = \frac{\pi}{\Gamma(5/4)\sqrt{2C_{fD}}} t_D^{1/4} \cdot \quad \text{Eq. 4-3}$$

As suggested in Refs. 4 and 13, Eq. 4-3 can be extended to fracture non-Darcy flow, provided that the true conductivity, C_{fD} , is replaced by the apparent conductivity, C_{fDapp} , as follows:

$$m_{wD,ND} = \frac{\pi}{\Gamma(5/4)\sqrt{2C_{fDapp}}} t_D^{1/4} \cdot, \quad \text{Eq. 4-4}$$

where $m_{wD,ND}$ stands for the dimensionless pseudo-pressure with non-Darcy flow in the fracture.

Substituting Eq. 4-2 into Eq. 4-4 yields:

$$m_{wD,ND} = \frac{\pi \sqrt{1+0.31q_{DND}}}{\Gamma(5/4)\sqrt{2C'_{fD}}} t_D^{1/4} . \quad \text{Eq. 4-5}$$

Comparing Eqs. 4-3 and 4-5 it can be established that:

$$m_{wD,ND} = m_{wD,D} \sqrt{1+0.31q_{DND}}$$

or solving for $m_{wD,D}$:

$$m_{wD,D} = \frac{m_{wD,ND}}{\sqrt{1+0.31q_{DND}}} = m_{wD,ND}(\text{Corrected, BL}) = m_{wD,D}(\text{BL}), \quad \text{Eq. 4-6}$$

where BL stands for bilinear flow.

Eq. 4-6 is one of the bases of the new technique presented in this work. It indicates that if the non-Darcy dimensionless flow rate, q_{DND} , is known, then the corrected response, $m_{wD,ND}(\text{Corrected, BL})$, must match the fracture type curve (Darcy flow) for the true dimensionless fracture conductivity during the bilinear flow period. It is important to recall here that to know q_{DND} , the value of β must be known (see Eq. 2-4).

4.2.1.2 Combination of Gidley¹³, Guppy *et al.*⁴ and Cinco-L. *et al.*¹² Theories

Gidley¹³ proposed the following relationship to correct the dimensionless fracture conductivity for non-Darcy flow effects:

$$C'_{fD} (1 + N_{RE}) = C^*_{fD} \quad \text{Eq. 4-7}$$

where C^*_{fD} = effective dimensionless fracture conductivity corrected for non-Darcy flow effects,
 C'_{fD} = dimensionless fracture conductivity for Darcy flow as described by Cinco-L. *et al.*,

N_{RE} = Reynolds number.

and
$$N_{RE} = 2.59 \times 10^{-6} \frac{\beta k_f q \gamma_g}{\mu w_f h} . \quad \text{Eq. 4-8}$$

If C_{fd}^* corrects the conductivity for non-Darcy flow effects, then this must be taken as the true conductivity C_{fd} , and C'_{fd} as described by Cinco-L. *et al.* must be recognized as the apparent conductivity C_{fdapp} . Then, Eq. 4-7 can be written as:

$$C_{fdapp} = C_{fd}(1 + N_{RE}) \quad \text{Eq. 4-9}$$

The Reynolds number can be computed from Eq. 4-8 where β is in atm-s²/g (the conversion to ft⁻¹ is given in Section 2.6 of Chapter 2), k_f in millidarcies, q in MSCF/D, γ_g relative to air, μ in centipoises, w_f in inches, and h in feet.

As explained in section 4.2.1.1, during bilinear flow the dimensionless pseudo-pressure equation proposed by Cinco-L. *et al.*¹² for Darcy flow, can be extended to fracture non-Darcy flow by using Eq. 4-4. Substituting Eq. 4-9 into Eq. 4-4:

$$m_{wD,ND} \sqrt{1 + N_{RE}} = \frac{\pi}{\Gamma(5/4) \sqrt{2C_{fd}}} t_D^{1/4} = m_{wD,D} \quad \text{Eq. 4-10}$$

The correction suggested in Eq. 4-10 was found to yield responses that are above the type curve. The following correction factor was found to multiply the left hand side of Eq. 4-10:

$$F = 0.82 \frac{C_{fdapp}}{C_{fd}} , \quad \text{Eq. 4-11}$$

or using Guppy *et al.*⁴'s definition presented in Eq. 4-2:

$$F = \frac{0.82}{1 + 0.31q_{DND}}, \quad \text{Eq. 4-12}$$

This yields the following expression:

$$m_{wD,ND} \sqrt{1 + N_{RE}} \left[\frac{0.82}{1 + 0.31q_{DND}} \right] = m_{wD,ND} (\text{Corrected, BL}) = m_{wD,D} (\text{BL}) \quad \text{Eq. 4-13}$$

The ranges of applicability of this equation are the same as those given in section 4.2.1.1 following Eq. 4-2.

4.2.2 Reservoir Linear Flow Regime

At intermediate times, the formation linear flow is the characteristic flow regime for fractured wells. This flow regime may be identified if wellbore storage is not present or if it ends early enough. Along with bilinear flow, the reservoir linear flow regime was selected for the new analysis technique. Camacho-V.¹⁴ showed that for Darcy flow, the pseudo-pressure response of a finite-conductivity fracture during linear flow may be calculated using the following equation:

$$m_{wD,D} = \sqrt{\pi t_D} + \frac{a}{C_{fD}} \quad \text{Eq. 4-14}$$

where the constant a is given by:

$$a = \begin{cases} \pi/3 & \text{for } C_{fD} \geq 25 \\ 0.944 & \text{for } C_{fD} = 10 \\ 0.902 & \text{for } C_{fD} = 5 \end{cases} \quad \text{Eq. 4-15}$$

Using the concept of apparent conductivity, C_{fDapp} , Eq. 4-14 can be extended to non-Darcy flow conditions as follows:

$$m_{wD,ND} = \sqrt{\pi t_D} + \frac{a}{C_{fDapp}} \quad \text{Eq. 4-16}$$

Assuming that Eq. 4-2 holds during reservoir linear flow period and substituting into Eq. 4-16, we obtain:

$$m_{wD,ND} = \sqrt{\pi t_D} + \frac{a}{C_{fD}} + \frac{0.31 a q_{DND}}{C_{fD}} \quad \text{Eq. 4-17}$$

Comparing Eqs. 4-14 and 4-17 yields

$$m_{wD,ND} = m_{wD,D} + \frac{0.31 a q_{DND}}{C_{fD}} \quad \text{Eq. 4-18}$$

Solving Eq. 4-18 for $m_{wD,D}$ we obtain

$$m_{wD,D} = m_{wD,ND} - \frac{0.31 a q_{DND}}{C_{fD}} = m_{wD,ND} (\text{Corrected}, L) = m_{wD,D} (L), \quad \text{Eq. 4-19}$$

where L stands for reservoir linear flow regime.

Eq. 4-19 represents the correction suggested for the reservoir linear period. As in the case of bilinear flow, if q_{DND} and C_{fD} are known, the pseudo-pressure response can be matched with the Darcy flow response during the linear flow period.

4.3 Summary of the New Analysis Technique

In light of the corrections developed for pseudo-pressure responses, the new analysis technique requires iterating on the values of q_{DND} and C_{fD} until a match is obtained with

the Darcy flow type curve. In these iterations Eqs. 4-6 (or 4-14) and 4-19 are used to correct the non-Darcy flow responses during bilinear and linear flow periods, respectively.

This procedure represents an advantage over the conventional regression analysis, since it overcomes the non-uniqueness problem. The second benefit of this technique is the requirement of only one well test, while the conventional technique requires two tests at two different flow rates. The new technique, however, requires the existence of two flow regimes and bilinear flow must be one of them. Although wellbore storage effects may mask part of the bilinear flow in some cases, it is shown in Example 2 below that the proposed analysis can still be applied.

An interesting point to note here is the observation that the correction for linear flow also works for pseudo-radial and late-time transitional flow periods. However, no analytical justification was found yet for this observation.

4.4 Application Examples

This section presents two examples. The first example is intended to show the applicability of the new analysis technique and the second example illustrates the effect of wellbore storage and skin. The properties used in these analyses are those presented in Table 2-3 corresponding to the base case, except when indicated.

Example 1

For this example, the transient pressure responses were generated for both Darcy and non-Darcy flow cases by using the semi-analytical model. For the non-Darcy flow data, Guppy⁴'s condition 2 (see section 4.2.2.1) was true: $1 \leq q_{DND} \leq 20$ and $10 \leq C_D \leq 100$. Fig. 4-1 shows the log-log plot of the pressure responses. The bilinear and linear flow

periods are both present. Note that because of the use of dimensionless variables, the Darcy flow case (solid line) corresponds to the type curve for $C_{fD} = 74.98$. The non-Darcy flow case (dashed line) does not follow the Darcy flow behavior for $C_{fD} = 74.98$ as expected. It can, however, be matched with another Darcy flow type curve for $C_{fD} = 18.16$. Because this is not the true conductivity but rather an apparent conductivity because of non-Darcy flow effects, it is denoted as C_{fDapp} . (Note that the definition of C_{fD} is not a function of non-Darcy flow and should be the same for both Darcy and non-Darcy flow).

Fig. 4-2 shows the corrections made on the non-Darcy flow pseudo-pressure data to match the type curve. For the bilinear and linear flow corrections, Eqs. 4-6 and 4-19 were used respectively. The circular and triangular data points correspond to the corrections for bilinear and linear flow, respectively. Note that they match very well the type curve for the corresponding flow regimes. The match parameters for β and C_{fD} presented on the figure are consistent with the data used to generate the pressure responses and this indicates the success of the match.

Fig. 4-3 presents the same data as in Fig. 4-2, but this time, different values for β and C_{fD} have been used on the corrections. Note that although the value of C_{fDapp} is the same (computed using Eq. 4-2), it is not possible to match both flow periods with the Darcy type curve at the same time. For example, the linear flow correction overlaps the type curve, but the bilinear flow correction does not. This means that the chosen combination of β and C_{fD} was not adequate and unless the right values are selected, none or at least one of the corrections does not match the type curve. This example demonstrates the uniqueness of the analysis claimed before.

As mentioned earlier, an important observation from Fig. 4-2 is that the linear flow correction (triangles) matches the non-Darcy flow data with the Darcy type curve for all times after the beginning of the linear flow, i.e., during the linear, pseudo-radial or late-time transitional flow periods. However, no analytical justification has been found for this behavior.

Example 2

This example demonstrates the application of the new analysis technique under the influence of wellbore storage. The transient pressure responses used here were again generated by using the properties in Table 2-3, except for the following parameters: $k = 10$ md, $q = 700$ MSCF/D, $q_{DND} = 8.83$, $x_f = 80$ ft. The input data fall in the range of Guppy⁴'s condition 1 (see section 4.2.2.1).

For convenience, Fig. 4-4 first presents the new data set without wellbore storage. Note that the bilinear flow is fully developed. However, no apparent linear flow is observed at later times. The corrections suggested in this work were applied and the bilinear and intermediate time transitional flow regimes matched with the Darcy flow type curve for the true fracture conductivity, $C_{fD} = 9.37$.

Fig. 4-5 shows the example data with wellbore storage effects. The wellbore storage coefficient is $C_D = 0.01$. Comparing Figs. 4-4 and 4-5 it can be noted that the bilinear flow period is completely masked by the wellbore storage effects. However, the new analysis technique was applied again, obtaining good results. Fig. 4-6 presents the perfect match of the corrected responses with the type curve for the bilinear and late-time flow periods. This shows that the wellbore storage does not preclude the application of the new technique and again, as long as the right combination of β and C_{fD} are selected, both flow periods should match the Darcy flow curve. In Fig. 4-7 the derivative type curve has

been included for completeness and it shows that the corrections can also be performed on derivative responses.

An important remark is that, following Lingen¹⁵, sandface flow rates were used to obtain q_{DND} in this study. Although this approach provided good results, the computation of the sandface rates, q_{sf} , from the following equation was not an easy task because of the pressure derivative term.

$$\frac{q_{sf}}{q} = 1 - C_D \frac{dm_{wD}}{dt_D}, \quad \text{Eq. 4-20}$$

where q_{sf} = sandface flow rate, MSCF/D,
 q = constant surface production rate, MSCF/D,
 dm_{wD}/dt_D = dimensionless pseudo-pressure derivative with respect to dimensionless time.

It is known that the derivative data is inaccurate in most cases due to typical oscillations. Eq. 4-21 given below provides a means to compute q_{sf} without involving the pressure derivative.

$$\frac{q_{sf}}{q} = 1 - \exp(-at_D). \quad \text{Eq. 4-21}$$

In this work, q_{sf}/q was first computed from Eq. 4-20 and then was matched with Eq. 4-21. This required an iterative process to determine the best value of the constant a in Eq. 4-21. After determining the constant a , Eq. 4-21 was used to generate a smooth curve for q_{sf}/q .

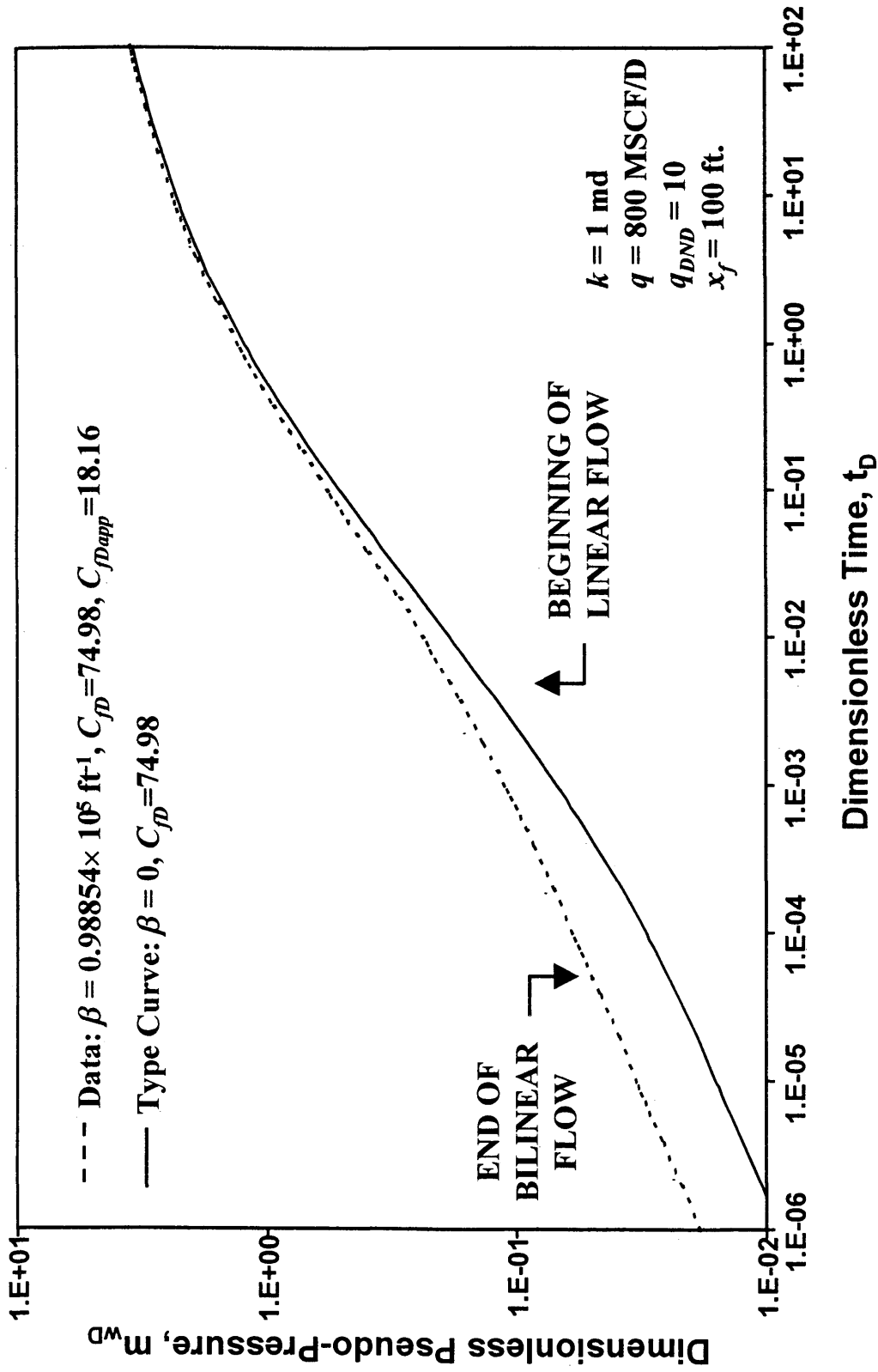


Fig. 4-1. Non-Darcy flow response and type curve

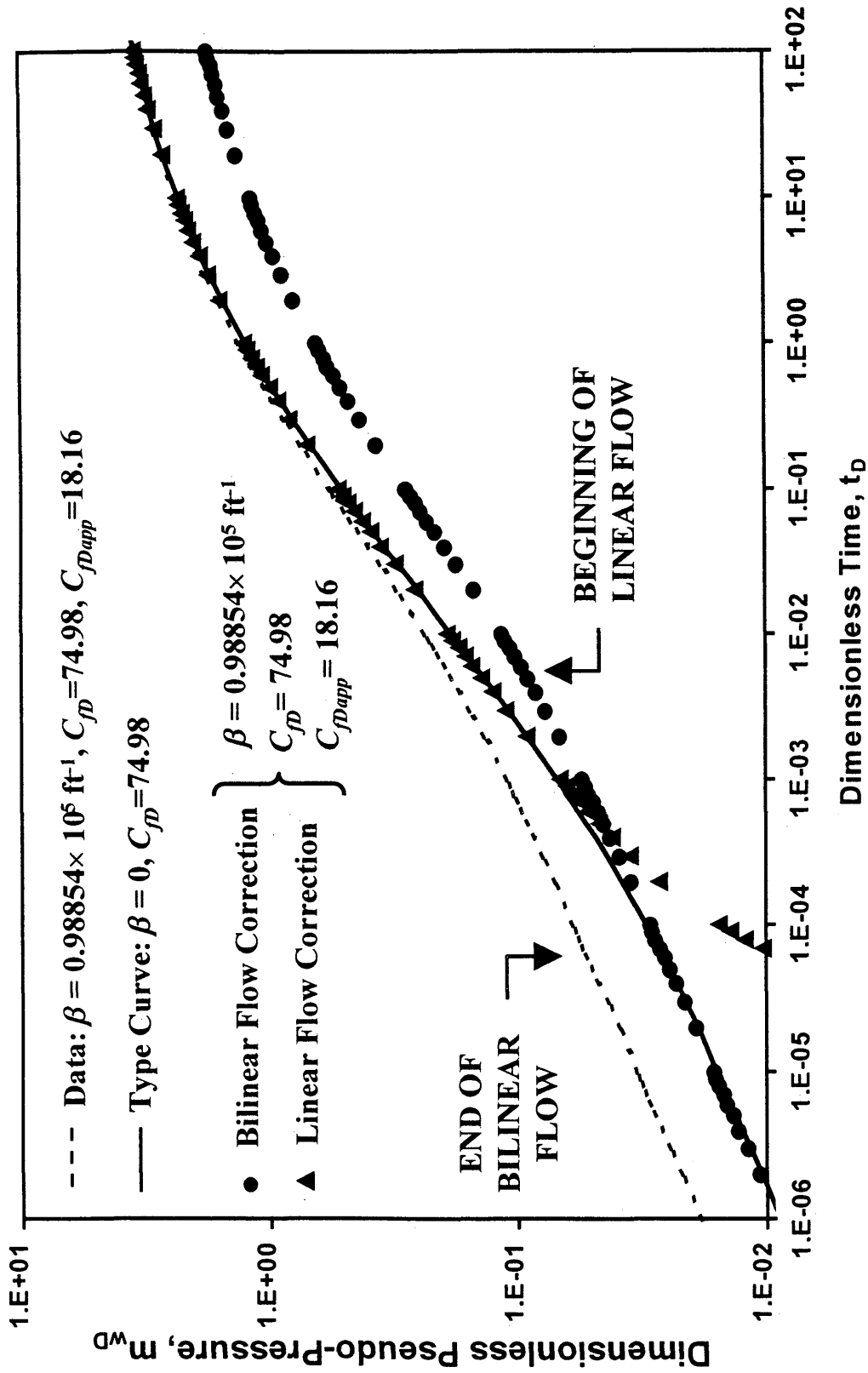


Fig. 4-2. Bilinear and linear flow corrections

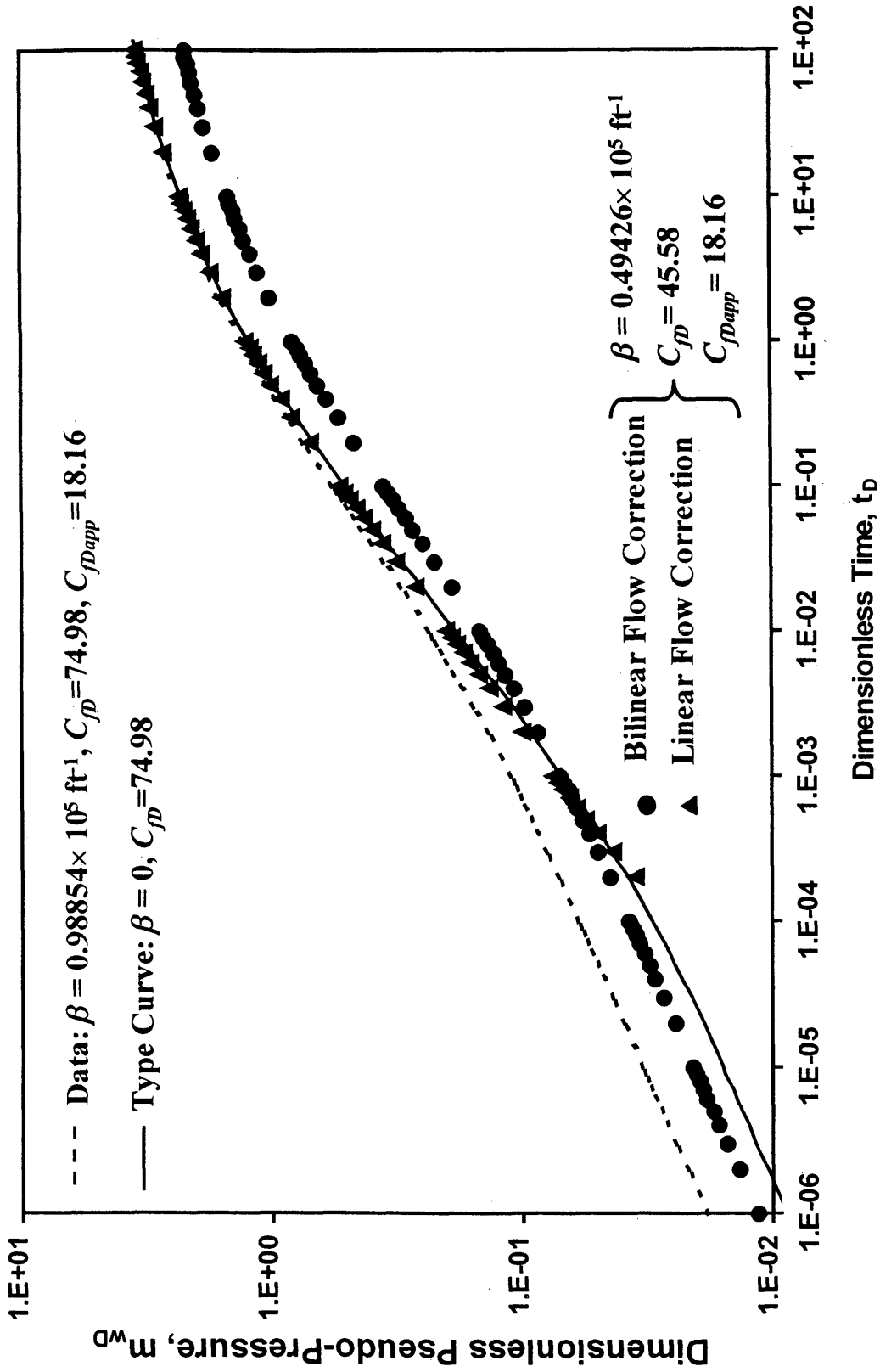


Fig. 4-3. Demonstration of the uniqueness of the results

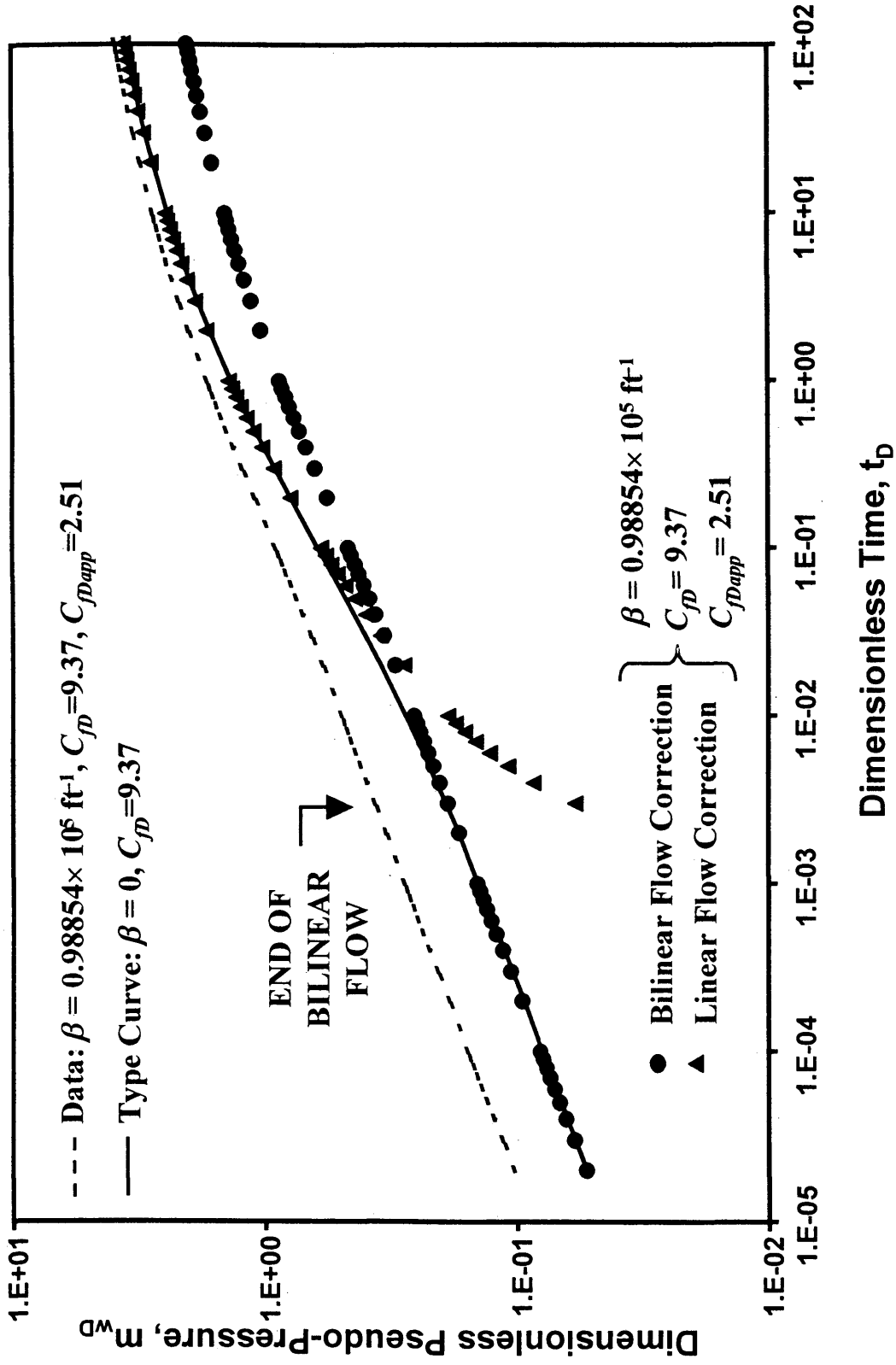


Fig. 4-4. Data for Example 2 without wellbore storage effects

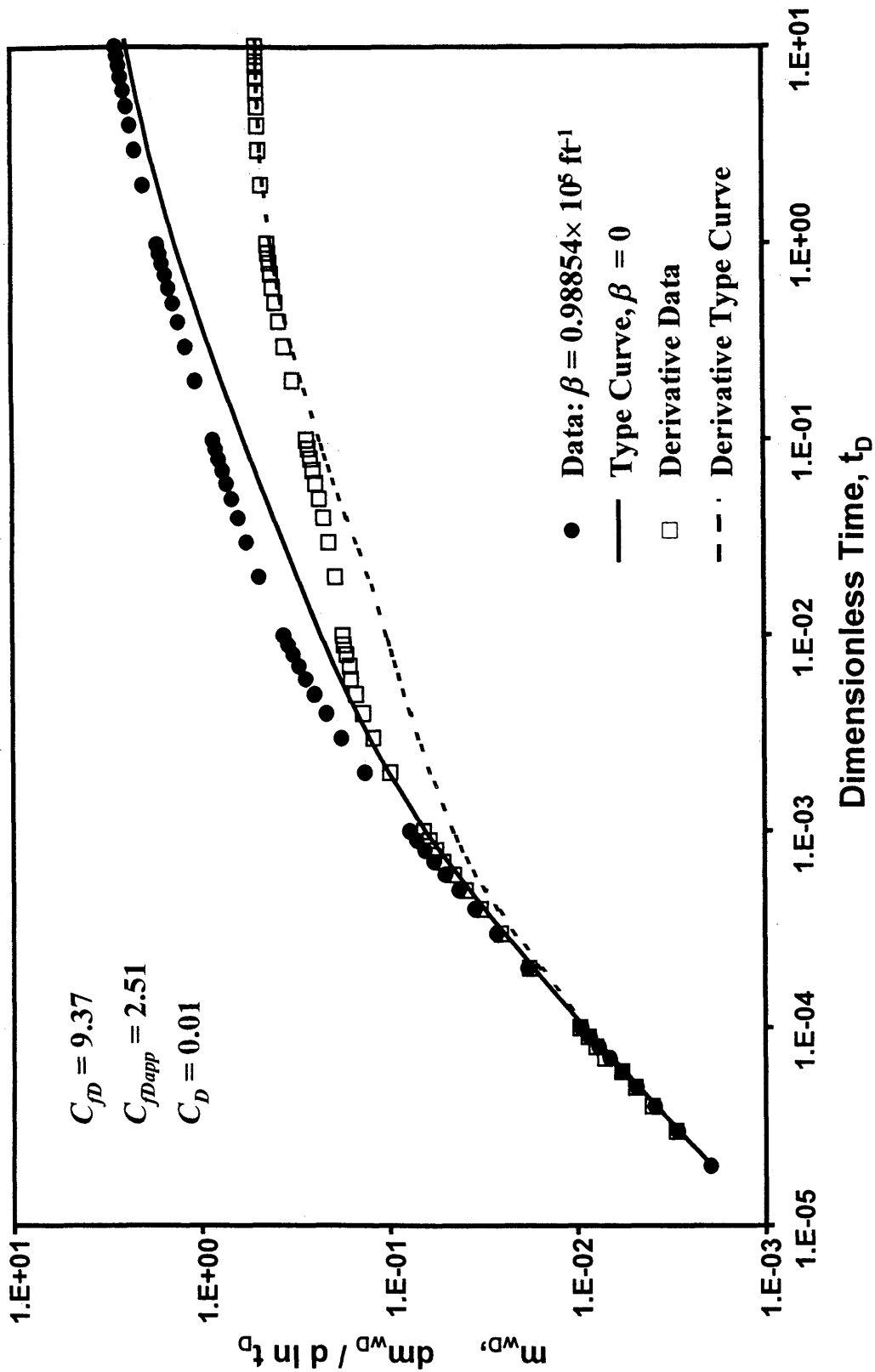


Fig. 4-5. Data for Example 2 with wellbore storage effects

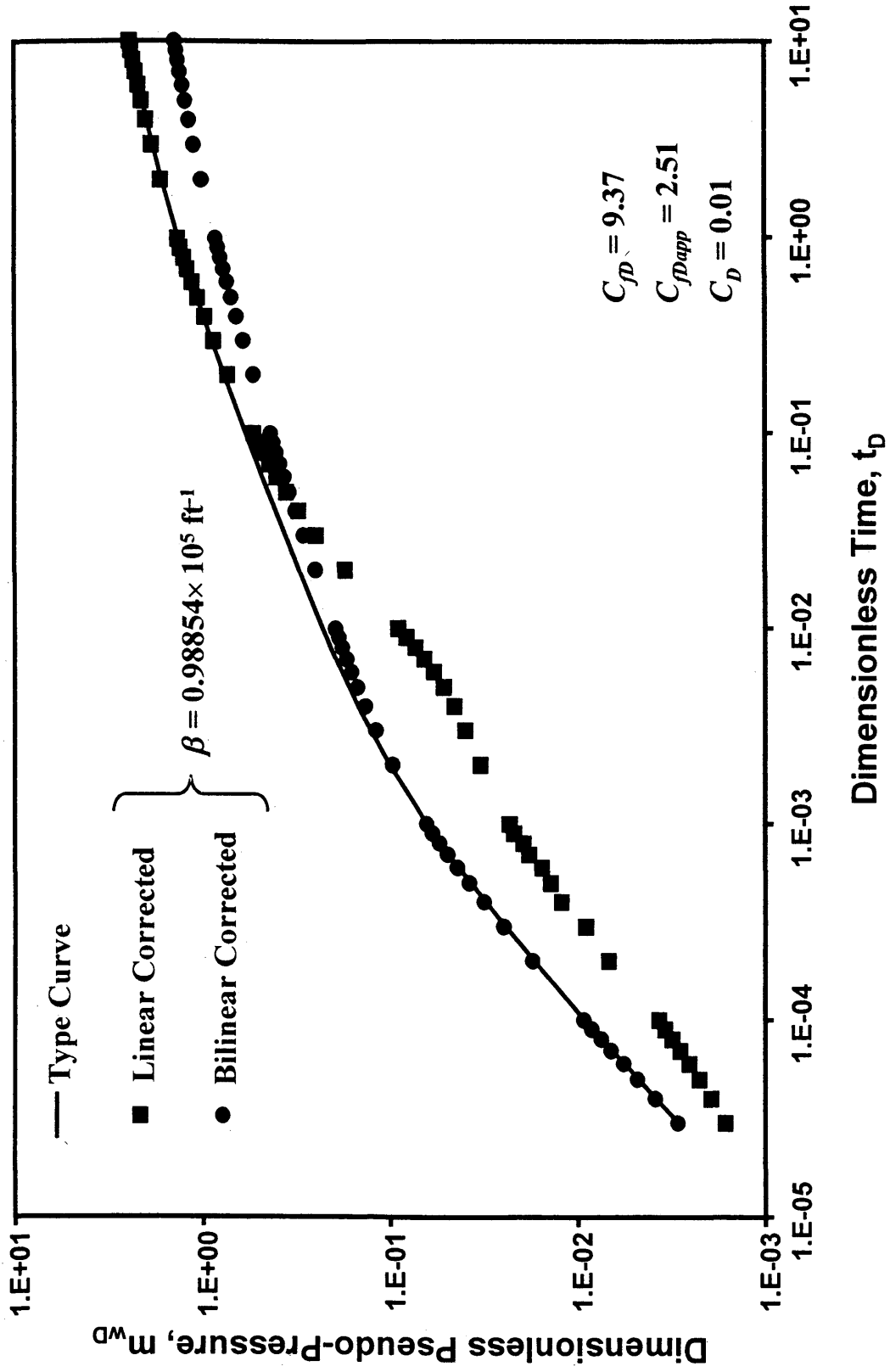


Fig. 4-6. Match of the corrected responses with the type curve under wellbore storage effects

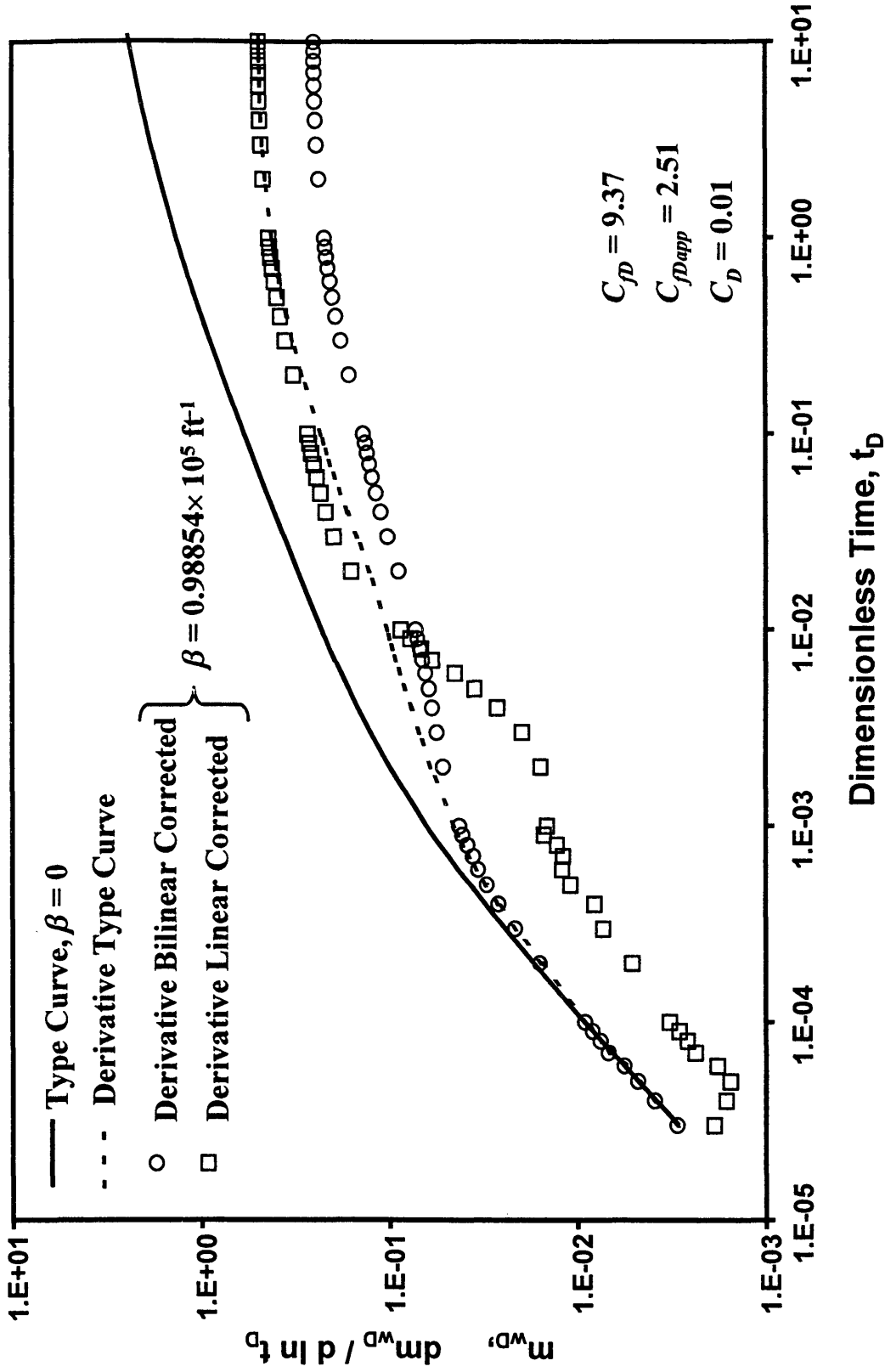


Fig. 4-7. Match with the derivative type curve under wellbore storage effects

CHAPTER 5

CONCLUSIONS

The objective of this study was to contribute to the understanding of the effects of non-Darcy flow in finite-conductivity vertical fractures. The study led to the development of a correlation to improve the design of fractured well tests and a new analysis technique to better interpret the pressure transient responses. The adverse effects of non-Darcy flow on the productivity of the wells were also highlighted. The specific conclusions drawn from this work are as follows:

1. The correlation developed in this work is a convenient tool to design well tests for finite-conductivity fractures when non-Darcy flow is of concern.
2. The correlation is restricted by two conditions: initial pressures lower than 2000 psia and fracture permeabilities less than 50000 md. In either case, the correlation can still be used and it provides conservative estimates of the properties responsible for non-Darcy flow effects in fractures.
3. It was demonstrated that it is not always possible to minimize the non-Darcy flow effects, especially in moderate to high permeability reservoirs. As the reservoir permeability increases, the fracture non-Darcy flow effects become too severe to be reduced by simple design considerations.
4. The new analysis technique for the interpretation of fractured well tests in the presence of non-Darcy flow is a very useful tool. It requires the presence of two flow

regimes: bilinear and reservoir linear flow, and it works even in the presence of wellbore storage.

5. Contrary to the existing techniques, in which two tests at different flow rates are necessary, the new analysis technique requires one test at one flow rate. This represents a significant advantage over the existing techniques.
6. The new analysis technique provides a unique solution, which contributes to the estimation of the correct values for the fracture conductivity, C_{fD} , and fracture half-length, x_f . The value of the non-Darcy flow parameter, β , can also be estimated.

REFERENCES

1. Millheim, K. K. and Cichowicz, L.: "Testing and Analyzing Low-Permeability Fractured Gas Wells," *JPT* (Feb. 1968) 193.
2. Wattenbarger, R. A. and Ramey, Jr., H. J.: "Well Test Interpretation of Vertically Fractured Gas Wells," *JPT* (May 1969) 625.
3. Holditch, S. A. and Morse, R. A.: "The Effects of Non-Darcy Flow on the Behavior of Hydraulically Fractured Gas Wells," *JPT* (Oct. 1976) 1169.
4. Guppy, K.H., Cinco-Ley, H., Ramey, Jr. H. J., and Samaniego V., F.: "Non-Darcy Flow in Wells with Finite-Conductivity vertical Fractures" *SPEJ* (Oct. 1982) 681.
5. Guppy, K. H., Cinco-Ley, H., and Ramey, Jr. H. J.: "Pressure Buildup Analysis of Fractured Wells Producing at High Flow Rates," *JPT* (Nov. 1982) 2656.
6. Umnuayponwiwat, S., Ozkan, E., Pearson, C. M., and Vincent, M.: "Effect of Non-Darcy Flow on the Interpretation of Transient Pressure Responses of Hydraulically Fractured Wells," paper SPE 63176 presented at the SPE 2000 Annual Technical Conference and Exhibition, Dallas, TX, Oct. 1-4, 2000.
7. Settari, A., Stark, A. J., and Jones, J. R.: "Analysis of Hydraulic Fracturing of High Permeability Gas Wells to Reduce Non-Darcy Skin Effects," *JCPT* (May 2000) Vol. 39, No. 5, 56.
8. Vincent, M. C., Pearson, C. M., and Kullman, J.: "Non-Darcy and Multiphase Flow in Propped Fractures: Case Studies Illustrate the Dramatic Effect on Well Productivity," paper SPE 54630 presented at the 1999 SPE Western Regional Meeting, Anchorage, Alaska, May 26-28, 1999.
9. Geertsma, J.: "Estimating the Coefficient of Inertial Resistance in Fluid Flow through Porous Media," *SPEJ* (Oct. 1974) 445.

10. Gil, J. A., Ozkan, E., Raghavan, R.: "Fractured-Well-Test Design and Analysis in the Presence of Non-Darcy Flow" paper SPE 71573 to be presented at the SPE 2001 Annual Technical Conference and Exhibition, New Orleans, Sept. 30 – Oct. 3, 2001.
11. Cinco L., H., Samaniego V., F., and Dominguez A., N.: "Transient Pressure Behavior for a Well with a Finite-Conductivity Vertical Fracture," *SPEJ* (Aug. 1978) 253.
12. Cinco-Ley, H. and Samaniego-V., F.: "Transient Pressure Analysis for Fractured Wells," *JPT* (Sept. 1981) 1749.
13. Gidley, J. L.: "A Method for Correcting Dimensionless Fracture Conductivity for Non-Darcy Flow Effects," *SPEPE* (Nov. 1991), 391.
14. Camacho-V., R. G.: "Response of Wells Producing Commingled Reservoirs: Unequal Fracture Length", MS Thesis, The University of Tulsa, Tulsa, OK (1984).
15. Lingen, P. L.: "Rate-Dependent Skin from Afterflow," paper SPE 28832 presented at the SPE 1994 European Petroleum Conference, London, U.K., Oct. 25-27, 1994.

LIST OF SYMBOLS

a	:	constant for computing q_{sf} (Eq. 4-22), constant used in Eq. 4-15
BL	:	bilinear flow period
C_D	:	wellbore storage coefficient
C_{fD}	:	dimensionless fracture conductivity
C_{fDapp}	:	dimensionless apparent fracture conductivity
C_{fD}^*	:	effective dimensionless fracture conductivity as defined by Gidley ¹³
c_t	:	total compressibility, psi^{-1}
F	:	correction factor for Eq. 4-10
h	:	formation thickness, ft
J	:	productivity index, $(\text{MSCF/D})/(\text{psi}^2/\text{cp})$
J_D	:	productivity index of a well in the presence of Darcy flow, $(\text{MSCF/D})/(\text{psi}^2/\text{cp})$
J_{ND}	:	productivity index of a well in the presence of non-Darcy flow, $(\text{MSCF/D})/(\text{psi}^2/\text{cp})$
k	:	formation permeability, md
k_f	:	fracture permeability, md
L	:	length (cm), linear flow period
M	:	gas molecular weight, lbm/lbmole
$m(p)$:	pseudo-pressure function, psi^2/cp
m_{wD}	:	dimensionless pseudo-pressure
N_{RE}	:	Reynolds number
p	:	reservoir pressure, psia
\bar{p}	:	average pressure, psia

PR	:	productivity ratio
p_{wf}	:	flowing bottomhole pressure, psia
q	:	constant surface flow rate, MSCF/D
q_{DND}	:	dimensionless non-Darcy flow rate
q_{sf}	:	sand face flow rate, MSCF/D
r_e	:	external reservoir radius, ft
r_w	:	wellbore radius, ft
r'_w	:	effective wellbore radius, ft
s	:	skin factor
S_{ND}	:	non-Darcy flow skin
T	:	reservoir temperature, °R
t_D	:	dimensionless time (referred to fracture half-length)
\vec{U}	:	superficial fluid velocity vector, cm/s
w_f	:	fracture width, ft, in
x_f	:	fracture half-length, ft
Z	:	gas compressibility factor

Greek symbols

β	:	non-Darcy flow coefficient, ft^{-1} , $\text{atm}\cdot\text{s}^2/\text{g}$
ϕ	:	formation porosity
γ_g	:	gas gravity (relative to air)
μ_i	:	initial gas viscosity, cp
ρ	:	fluid density, lbm/ft^3

Subscripts

<i>i</i>	:	initial
<i>g</i>	:	gas
<i>t</i>	:	total
<i>f</i>	:	fracture
<i>D</i>	:	dimensionless, Darcy
<i>ND</i>	:	non-Darcy